AD-A054 281 PRINCETON UNIV N J DEPT OF AEROSPACE AND MECHANICAL--ETC F/G 1/3
A STUDY OF THE PRECISION HOVER CAPABILITIES OF THE AEROCRANE HY--ETC(U)
FEB 78 H C CURTISS, W F PUTMAN, R M MCKILLIP N62269-77-C-0074
UNCLASSIFIED AMS-TR-1363 NADC-76341-30 NL

1 OF 2
AD
A054281

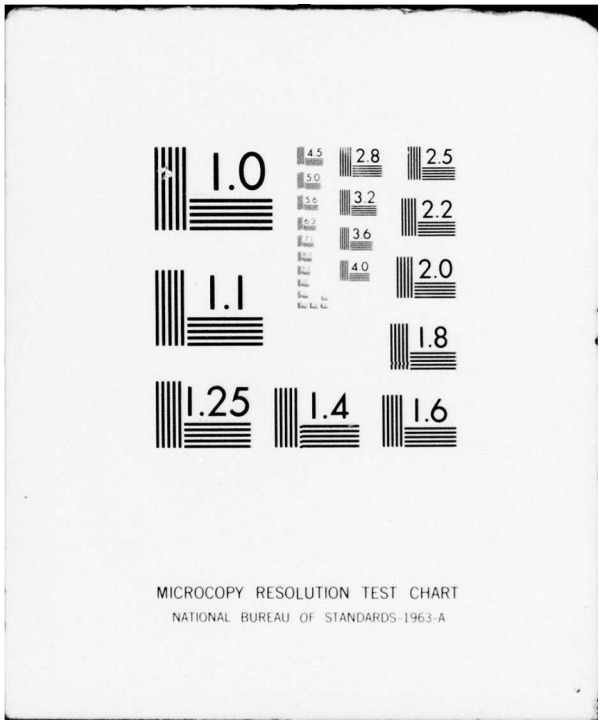
1.0
1.1
1.25
1.4
1.6
1.8
2.0
2.2
2.5
2.8
3.2
3.6
4.0
4.5
5.0
5.6
6.3
MICROCOPY RESOLUTION TEST CHART
NATIONAL BUREAU OF STANDARDS-1963-A

(12)

REPORT NADC 76341-30

A STUDY OF THE PRECISION HOVER CAPABILITIES OF THE AEROCRANE HYBRID HEAVY LIFT VEHICLE

H. C. Curtiss, Jr.
W. F. Putman
R. M. McKillip, Jr.

Department of Aerospace and Mechanical Sciences
Princeton University
Princeton, N. J. 08540

February 1978

FINAL REPORT

Approved for Public Release; Distribution Unlimited

Prepared for:

Naval Air Development Center
Code 6096
Warminster, Pa. 18974

UNCLASSIFIED

SECURITY CLASSIFICATION OF THIS PAGE (When Data Entered)

REPORT DOCUMENTATION PAGE

READ INSTRUCTIONS BEFORE COMPLETING FORM

1. REPORT NUMBER: NADC 76341-30	2. GOVT ACCESSION NO.
3. RECIPIENT'S CATALOG NUMBER	
4. TITLE (and Subtitle): A STUDY OF THE PRECISION HOVER CAPABILITIES OF THE AEROCRANE HYBRID HEAVY LIFT VEHICLE	5. TYPE OF REPORT & PERIOD COVERED: FINAL REPORT.
6. PERFORMING ORG. REPORT NUMBER: AMS-TR-1363	
7. AUTHOR(s): H. C. Curtiss, Jr. W. F. Putman R. M. McKillip, Jr.	8. CONTRACT OR GRANT NUMBER(s): N62269-77-C-0074
9. PERFORMING ORGANIZATION NAME AND ADDRESS: Princeton University Department of Aerospace and Mechanical Sciences Princeton, N. J. 08540	10. PROGRAM ELEMENT, PROJECT, TASK AREA & WORK UNIT NUMBERS: AIRTASK No. A03P-03PA/001B/8WF41411000 Work Unit Number DH816
11. CONTROLLING OFFICE NAME AND ADDRESS: Naval Air Development Center Code 6096 Warminster, PA 18974	12. REPORT DATE: Feb 1978
	13. NUMBER OF PAGES: 145 (146 p.)
14. MONITORING AGENCY NAME & ADDRESS(if different from Controlling Office)	15. SECURITY CLASS. (of this report): UNCLASSIFIED
	15a. DECLASSIFICATION/DOWNGRADING SCHEDULE

16. DISTRIBUTION STATEMENT (of this Report)

Approved for Public Release; Distribution Unlimited

16 F41411 17 WF41411000

17. DISTRIBUTION STATEMENT (of the abstract entered in Block 20, if different from Report)

PE 62241N WUDH816

18. SUPPLEMENTARY NOTES

WU 03P03PA001B

19. KEY WORDS (Continue on reverse side if necessary and identify by block number)

AEROCRANE	Cyclic control
Precision hover	Winglet control
Sling load	Gust response
Heavy lift	Rotor

20. ABSTRACT (Continue on reverse side if necessary and identify by block number)

An analytical study of the precision hover capabilities of the AEROCRANE, based on equations of motion verified by flight tests of a dynamic model, is described. Two methods of control (cyclic pitch and winglets) are examined. A real time simulation of the tasks of hovering a proposed large AEROCRANE in gusts and translating from point to point was conducted to evaluate the two control methods and to compare the AEROCRANE with proposed large helicopters. The stability and control characteristics of large AEROCRANES are compared with those of proposed large helicopters and the helicopter handling qualities

DD FORM 1 JAN 73 1473 EDITION OF 1 NOV 65 IS OBSOLETE
S/N 0102-LF-014-6601

UNCLASSIFIED

SECURITY CLASSIFICATION OF THIS PAGE (When Data Entered)

288 475

Block 20: Abstract Continued.

specifications. The results of the study indicate that winglets provide a very effective means of hover control. With cyclic control, the precision hover capabilities of the AEROCRANE are similar to helicopters of equivalent gross weight. Extrapolation of helicopter handling qualities specifications to large gross weights characteristic of proposed large AEROCRANES indicates that the configurations studied can meet these specifications. Certain aspects of hovering control which are characteristic of any vehicle which derives an appreciable portion of its lift from buoyancy and carries a heavy sling load are examined.

TABLE OF CONTENTS

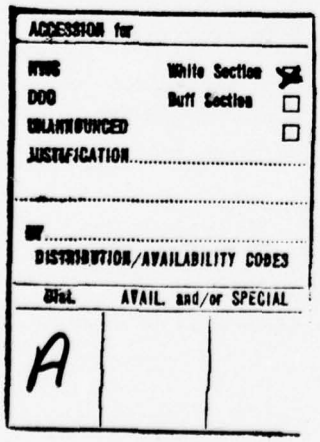

LIST OF ILLUSTRATIONS

NOMENCLATURE

A	aerodynamic moment factor, $A = \frac{\rho \pi R^5}{I'}$
a	rotor blade lift curve slope, per rad.
a_W	winglet lift curve slope, per rad.
$\bar{a}$	acceleration vector
A_{1s}	longitudinal cyclic pitch, deg or rad.
b	number of blades
b_W	winglet span, ft.
$\bar{\bar{b}}_W$	winglet span nondimensionalized by rotor radius
B_{1s}	lateral cyclic pitch, deg or rad.
c	blade chord, ft.
C	*damping matrix*
C_D	drag coefficient of centerbody, $C_D = \frac{D}{\frac{1}{2} \rho V^2 \pi R_B^2}$
C_H	rotor in-plane force coefficient, $C_H = \frac{H}{\rho \pi R^2 (\Omega R)^2}$
C_L	rolling moment coefficient, $C_L = \frac{L}{\rho \pi R^2 (\Omega R)^2 R}$
C_{LM}	Magnus force coefficient of centerbody, $C_{LM} = \frac{F_M}{\frac{1}{2} \rho V^2 \pi R_B^2}$
C_M	pitching moment coefficient, $C_M = \frac{M}{\rho \pi R^2 (\Omega R)^2 R}$

C_T thrust coefficient, $C_T = \dfrac{T}{\rho\, \pi R^2\, (\Omega R)^2}$

C_{W_o} weight coefficient, $C_{W_o} = \dfrac{W_o}{\rho\, \pi R^2\, (\Omega R)^2}$

C_Y rotor lateral force coefficient, $C_Y = \dfrac{Y}{\rho\, \pi R^2\, (\Omega R)^2}$

D sphere drag force, lbs.

F control matrix

F_B buoyant force, lbs.

F_M Magnus force, lbs.

F_R Froude number based on tip speed and rotor radius, $F_R = \dfrac{\Omega^2 R}{g}$

f_N rotor radial station factors, $f_N = 1 - \chi^n$

H rotor in-plane force, rotor axis system, positive to the rear, lb.

H_u, M_u stability derivatives divided by m' and I' respectively

I' vehicle moment of inertia about x_B and y_B axes, including apparent mass contribution, slug ft^2

I_z vehicle moment of inertia about z_B axis, slug ft^2

I_1 blade flapping moment of inertia, slug ft^2

j proportionality constant between harmonic inflow and rotor aerodynamic moment $\{j = \dfrac{a\sigma}{2|\lambda_o|}\}$

k_y radius of gyration of vehicle in pitch or roll, ft, $k_y = \sqrt{\frac{I'}{m_o}}$

K spring matrix, feedback gain

K_A attitude feedback gain, rad/rad/ or deg/deg

K_{cw} gearing between cyclic and winglet required to eliminate winglet pitching moment, degrees cyclic per degree winglet deflection

ℓ horizontal distance between center of gravity and rotor hub on tandem helicopter, ft.

L rotor hub rolling moment, positive right side down, ft-lb.

m' sum of mass of vehicle and apparent mass, slugs

m_A apparent mass of vehicle, estimated for centerbody only. For a spherical centerbody filled with lifting gas, $m_A = \frac{\beta}{2} m_o$, slugs

m_L sling load mass, slugs

m_o vehicle mass, slugs

M rotor hub pitching moment, positive nose up, ft-lb., mass matrix

p roll rate, positive right side down, rad/sec

q pitch rate, positive nose up, rad/sec

$\hat{q}$ pitch rate nondimensionalized by rotor angular velocity

r_o distance between center of buoyancy and center of gravity, positive for center of gravity below center of buoyancy, ft.

R	rotor radius, ft.
R_B	centerbody radius, ft.
s	Laplace operator, dimensionless quantity, $s = \frac{C_D \pi R_B^2}{4 S_W a_W}$
$\tilde{s}$	Laplace operator nondimensionalized by sling load frequency, $\tilde{s} = \frac{s}{\omega_{SL}}$
S_W	area of one winglet. The winglet chord is taken equal to the blade chord, $S_W = b_W c$
SAS	stability augmentation system
t	time
T	rotor thrust, positive up, lbs.
u	vehicle longitudinal velocity, ft/sec
u_G	longitudinal gust velocity, ft/sec
v	vehicle lateral velocity, ft/sec, or induced velocity, ft/sec.
v_G	lateral gust velocity, ft/sec.
V_T	tip speed, ft/sec. $V_T = \Omega R$
$\forall$	volume of centerbody, ft^3
w	gross weight ratio
W_O	vehicle weight, lbs.
x	vehicle longitudinal displacement, ft.
X	rotor wake angle measured from line normal to rotor plane
y	vehicle lateral displacement, ft.
Y	rotor side force, rotor axis system, positive right
Z_A	distance from load attachment point to vehicle center of gravity, positive for attachment point below the center of gravity, ft.

β buoyancy ratio, ratio of buoyant force to vehicle weight, $\beta = \frac{F_B}{W_o}$

γ Lock number, $\gamma = \frac{\rho a c R^4}{I_1}$

δ_c cosine component of winglet deflection, deg or rad.

δ_s sine component of winglet deflection, deg or rad.

δ_w total winglet deflection angle, $\delta_w = \delta_c \cos \psi + \delta_s \sin \psi$

ϵ' drag damping nondimensionalized by rotor angular velocity, $\epsilon' = -\frac{X}{\Omega u}$

η rotor thrust to apparent mass ratio, ft/sec^2, $\eta = \frac{T}{m'}$

θ rotor blade pitch angle. Referenced to body axes $\theta = \theta_o - A_{1s} \cos \psi - B_{1s} \sin \psi$

θ_L sling load angular deflection in pitch measured relative to vehicle axis of rotation, positive forward, rad.

θ_{LA} sling load deflection in pitch measured relative to space, positive forward, rad.

θ_o rotor collective pitch rad.

λ_s rotor inflow ratio, positive for flow up through rotor ($\lambda_s = \lambda_o$ in hover flight)

λ_B cosine component of dimensionless induced velocity due to blow back, $\lambda_B = \lambda_1 x$

λ_m, λ_L — harmonic inflow components due to rotor aerodynamic pitching and rolling moments, $\lambda_m = j\frac{2C_M}{a\sigma}$, $\lambda_L = -j\frac{2C_L}{a\sigma}$

λ_o — hovering induced velocity nondimensionalized by rotor tip speed, positive upwards

λ_1 — rate of change of cosine component of induced velocity with radius due to "blow back", dimensionless

μ — rotor advance ratio, sling load weight ratio

ζ_{SL} — sling load damping ratio

ρ — density of air, slugs/ft^3

σ — rotor solidity, $\sigma = \frac{bc}{\pi R}$

ϕ — vehicle roll angle, positive right side down, rad.

ϕ_L — sling load angular deflection in roll measured relative to the vehicle axis of rotation, positive for sling load to the left, rad.

ψ — blade azimuth angle, ψ is measured from vehicle reference axes, positive in direction of rotor rotation

ω_G — nutation frequency, $\omega_G = \frac{I_Z}{I'}\Omega$, rad/sec

ω_R — reference frequency, $\omega_R = \sqrt{\frac{W_o R_B}{I'}}$, rad/sec

ω_{SL} — uncoupled sling load pendulous frequency, $\omega_{SL} = \sqrt{\frac{g}{Z_L}}$, rad/sec

$\tilde{\omega}$ — frequency non-dimensionalized by sling load frequency

$\hat{\omega}$ — frequency non-dimensionalized by rotor angular velocity

Ω	rotor/centerbody angular velocity, RPM or rad/sec
χ	ratio of centerbody radius to rotor radius, $\chi = \frac{R_s}{R}$

Subscripts

$(\tilde{\ })$	quantity nondimensionalized by sling load frequency
$(\cdot)$	differentiation with respect to time
$(\ )'$	differentiation with respect to nondimensional time, $(\ )' = \frac{d}{d(\Omega t)} = \frac{1}{\Omega}(\cdot)$
$(\bar{\ })$	length nondimensionalized by centerbody radius, velocity nondimensionalized by tip speed
$(\ )_c$	cyclic control
$(\ )_w$	winglet control
$(\hat{\ })$	quantity nondimensionalized by rotor angular velocity

INTRODUCTION

The AEROCRANE is a hybrid heavy lift vehicle which shows considerable potential for accomplishing a variety of low speed heavy lift missions. An extensive experimental and analytical study of the trim and dynamic stability characteristics of the AEROCRANE is reported in Reference 1. The experimental investigations described in Reference 1 were designed to provide verification of equations of motion to predict the dynamic stability and control characteristics of AEROCRANE vehicles. Excellent agreement between an analytical model of the flight behavior and the experimentally measured characteristics of a free-flight dynamic model of the AEROCRANE was obtained.

This report employs the analytical model of Reference 1 to study various aspects associated with the precision hover capabilities of this vehicle.

The vehicle configuration of Reference 1 employed conventional helicopter type controls, i.e., cyclic and collective pitch. It has been proposed that vertical surfaces or winglets could be mounted on the tips of the rotating wings of the AEROCRANE to provide effective hover control. This report compares these two methods of control in hovering flight and in addition examines other questions associated with precision hover of the AEROCRANE, including a comparison with large helicopters.

First, the basic features of cyclic and winglet control are examined and compared. Then using a simplified dynamic model, the impact of these two control methods on the precision hovering task is discussed.

Since the basic mission of an AEROCRANE vehicle is to lift and move heavy loads, various features of the dynamic motion of a sling load and

its influence on the vehicle is considered.

The hovering equations of motion for the AEROCRANE with a sling load are presented in nondimensional form, such that, the important parameters are evident and the influence of vehicle size can be readily determined.

The basic hovering dynamic stability characteristics of the AEROCRANE are discussed with particular reference to the influence of vehicle center of gravity position, sling load attachment point, and sling load length.

Then a series of simulation studies are described which employed an analog computer operating in real time to examine the problem of hovering over a spot in gusts and point to point translation. The use of cyclic pitch and winglets for control is examined and the results compared to results of a Heavy Lift Helicopter simulation.

Finally the hovering control and stability characteristics of the AEROCRANE are compared with conventional helicopters.

CONTROL METHODS

Two control systems are examined in this report for maneuvering the AEROCRANE. One is a cyclic pitch system similar to that used on a conventional helicopter and in fact was the system employed to control the dynamic model of Reference 1. A second control system involves the use of winglets or vertical aerodynamic surfaces mounted on the tips of the rotor blades. The winglet control characteristics are developed in Appendix A. The cyclic control primarily produces moments on the vehicle as a result of a control deflection. The winglet control primarily produces a translational force. It should be noted that one of these control systems cannot be substituted for the other. That is, the vehicle can be flown by a cyclic system only. However, it does not appear likely that the vehicle could be controlled by the winglet system only. While it is expected that the translational force control would be effective in maneuvering the vehicle, it would not be capable of countering gusts effectively since gust inputs will produce pitching and rolling moments as well as translational forces. In this section the nature of the control forces and moments are discussed and then a simplified model of the dynamics is examined in order to obtain some insight into the relative advantages and disadvantages of these two control systems.

A. Cyclic Pitch

The cyclic system involves imposing a once per revolution pitch variation on the rotor to produce primarily a moment. The parameters

of the rotor system and vehicle are such that the rotor blades can be assumed to be rigid (the lowest natural frequency of the rotor blades in flapping is considerably larger than the rotor RPM) so that a cyclic input with its maximum and minimum along the fore and aft axis of the vehicle will produce a pitching moment. In addition to the moment produced, a small inplane force is produced. This inplane force produces as well a small moment about the other axis of the vehicle since the center of gravity of the vehicle is located below the rotor plane. That is, a longitudinal cyclic (A_{1s}) input produces a pitching moment and a side force. The side force acting about the center of gravity produces a rolling moment. In order to examine the size of this coupling effect consider the theoretical expressions for the pitching moment and side force produced by longitudinal cyclic (Appendix B).

$$\frac{2}{a\sigma} C_{M_{A_{1s}}} = \frac{\frac{1}{8} f_4}{1 + \frac{j}{6} f_3}$$

$$\frac{2}{a\sigma} C_{Y_{A_{1s}}} \approx \frac{1}{4} \lambda_s f_2$$

If the center of gravity is located a distance r_o below the rotor plane (the center of buoyancy is assumed to lie in the rotor plane) then the ratio of the rolling acceleration to pitching acceleration produced by longitudinal cyclic is

$$\frac{L_{A_{1s}}}{M_{A_{1s}}} = \lambda_s \{2\ \bar{r}_o\ \chi\ \frac{f_2}{f_4}\ (1 + \frac{j}{6}\ f_3)\}$$

For typical AEROCRANE parameters

$$\frac{L_{A_{1s}}}{M_{A_{1s}}} \cong 3\ \bar{r}_o\ \lambda_s$$

and

$$\lambda_s = -\sqrt{\frac{C_T}{2(1 - \chi^2)}} = -\ 0.062$$

Therefore

$$\frac{L_{A_{1s}}}{M_{A_{1s}}} \cong -\ 0.2\ \bar{r}_o$$

and for a typical $\bar{r}_o$ of 0.1 the rolling moment produced by longitudinal cyclic is about 2 percent of the pitching moment.

The ratio of the lateral translational acceleration to the angular acceleration in pitch is given by

$$\frac{\dot{v}}{\dot{q}} = \frac{I'}{m'R}\ \frac{\frac{2}{a\sigma}\ C_{Y_{A_{1s}}}}{\frac{2}{a\sigma}\ C_{M_{A_{1s}}}} = R\ \frac{\bar{k}_y^2\ \chi^2}{(1 + \frac{\beta}{2})}\ \{2\ \frac{f_2}{f_4}\ (1 + \frac{j}{6}\ f_3)\}\ \lambda_s$$

Note that this dimensional quantity depends upon the size of the vehicle as it is directly proportional to rotor radius. Non dimensionalizing,

$$\frac{\bar{v}'}{\hat{q}'} = \frac{\bar{k}_y^2\ \chi^2}{(1 + \frac{\beta}{2})}\ \{2\ \frac{f_2}{f_4}\ (1 + \frac{j}{6}\ f_3)\}\ \lambda_s$$

Taking $\bar{k}_y \cong 1$

$$\beta = 1.42$$

$$\chi = 0.43$$

$$\frac{\bar{v}'}{\hat{q}'} = 0.32\,\lambda_s = -\,0.02$$

This ratio will be compared with the winglet characteristics below. It can be seen that this ratio will always be small since it is proportional to the ratio of the induced velocity to the tip speed (λ_s). Note that this is a side force in conjunction with a pitching moment. Owing to symmetry it can also be seen that a rolling moment will produce a horizontal force and the relative magnitude of the coupling terms due to the horizontal force arising from a lateral cyclic input, will be identical to the side force terms due to longitudinal cyclic.

B. Winglets

The winglet is thought of as a control that primarily produces a translational force. In addition, winglet deflection will produce a moment owing to the fact that the center of gravity lies below the rotor plane. Appendix A derives expressions for the winglet control effectiveness. The winglet control is azimuthally uncoupled in the sense that a longitudinal force produces only a pitching moment and no rolling moment.

The ratio of the translational acceleration to the pitching acceleration can be obtained from the expressions given in Appendix A as,

$$\frac{\dot{u}}{\dot{q}} = \frac{\frac{1}{m'}\frac{\partial X_{BW}}{\partial \delta_c}}{\frac{1}{I'}\frac{\partial M_{BW}}{\partial \delta_c}} = R_B \frac{\bar{k}_y^2}{(1 + \frac{\beta}{2})\bar{r}_o}$$

Again it may be noticed that the dimensional quantity depends upon the size of the vehicle. Essentially, if a series of Froude scaled vehicles is considered, as the vehicle size is increased the translation acceleration produced by an angular control deflection is invariant with size, however, the angular acceleration decreases with size.

Non dimensionalizing the above expression

$$\frac{\bar{u}'}{\hat{q}'} = \frac{\chi \bar{k}_y^2}{\bar{r}_o(1 + \frac{\beta}{2})}$$

Placing the typical values used above

$$\frac{\bar{u}'}{\hat{q}'} = \frac{.25}{\bar{r}_o} \quad .$$

For a typical $\bar{r}_o = 0.1$

$$\frac{\bar{u}'}{\hat{q}'} = 2.5 \quad .$$

Thus the winglet control emphasizes the translational acceleration, producing only a relatively small angular acceleration and essentially gives an effect on the vehicle which is the inverse of the cyclic control.

One further comparison is of interest. That is, the question of how much cyclic is required to cancel the angular acceleration of the winglet such that the winglet control produces translational acceleration only. The angular acceleration produced per unit cyclic is

$$\dot{q}_c = \frac{1}{I'} \frac{\partial M_c}{\partial A_{1s}} (\Delta A_{1s}) = \frac{a\sigma \rho \pi R^2 (\Omega R)^2 R}{2I'} \left(\frac{2}{a\sigma} C_{M_{A_{1s}}}\right) (\Delta A_{1s})$$

The angular acceleration produced by the winglets is given in Appendix A as

$$\dot{q}_W = \frac{1}{I'} \frac{\partial M_{BW}}{\partial \delta_c} \Delta\delta_c = \left(\frac{1}{I'} \rho (\Omega R)^2 S_W r_o a_W\right) \Delta\delta_c$$

Taking the ratio of these two terms

$$\frac{\dot{q}_W}{\dot{q}_c} = \left(\frac{2 S_W r_o a_W}{\pi R^3 a\sigma}\right) \frac{1}{\left(\frac{2}{a\sigma} C_{M_{A_{1s}}}\right)} \left(\frac{\Delta\delta_c}{\Delta A_{1s}}\right)$$

Introducing the definition of $\sigma = \frac{bc}{\pi R}$, and assuming that the winglet is of rectangular planform with a chord equal to the blade chord, and taking the number of blades as four, this ratio can be expressed as

$$\frac{\dot{q}_W}{\dot{q}_c} = \frac{1}{2} \bar{b}_W \bar{r}_o \chi \left(\frac{a_W}{a}\right) \frac{1}{\left(\frac{2C_{M_{A_{1s}}}}{a\sigma}\right)} \left(\frac{\Delta\delta_c}{\Delta A_{1s}}\right)$$

Inserting numbers into this expression, assuming that $\bar{b}_W = 0.25$ (a value shown in Appendix A as suitable for trimming the AEROCRANE in forward flight), and

$$\frac{a_W}{a} = 0.8$$

(to account for the finite aspect ratio of the winglet) and using the value of $\frac{2C_{M_{A_{1s}}}}{a\sigma} = 0.062$ corresponding to a $C_T = 0.0064$ from Appendix B,

$$\frac{\dot{q}_W}{\dot{q}_c} = 0.7 \bar{r}_o \frac{\Delta\delta_c}{\Delta A_{1s}} \quad .$$

Thus for a typical $\bar{r}_o = 0.1$, the angular acceleration produced by winglet deflection is roughly 7 percent of the angular acceleration produced by cyclic deflection.

The total angular acceleration produced by the winglet can be expressed as

$$\frac{\dot{q}}{\dot{q}_w} = 1 + \frac{\dot{q}_c}{\dot{q}_w} = 1 + \frac{1}{0.7\,\bar{r}_o}\,\frac{\Delta A_{1s}}{\Delta \delta_w}$$

It is possible to eliminate the angular acceleration produced by the winglet control by mixing cyclic into the winglet control stick. The amount required is obtained by taking

$$\Delta A_{1s} = K_{\dot{c}w}\,\Delta\delta_w$$

Again for a typical center of gravity location $\bar{r}_o = 0.1$, the coupling required is

$$K_{\dot{c}w} = -\,0.07\,\frac{{}^{o}\text{cyclic}}{{}^{o}\text{winglet}}$$

indicating that the cyclic control produces large moments compared to the winglet. This gearing would of course also result in a translational force along the other axis, that is, use of a coupling of longitudinal cyclic to eliminate the pitching moment produced by cosine or translational force winglet deflection will result in a side force.

Above we have developed expressions for the ratio of translational acceleration to angular acceleration of the two controls. For typical parameters, for cyclic control

$$\frac{\bar{v}_c'}{\hat{q}_c'} = 0.32\,\lambda_s$$

For winglet control

$$\frac{\bar{u}_w'}{\hat{q}_w'} = \frac{.25}{\bar{r}_o}$$

Now with the cyclic control coupled to the winglet control to eliminate the angular acceleration produced by the winglet, it is implied that $\hat{q}_w' = -\hat{q}_c'$ and therefore the ratio of lateral acceleration produced by cyclic deflection to translational acceleration produced by winglet deflection is

$$\frac{\bar{v}_c'}{\bar{u}_w'} = -1.28\,\lambda_s\,\bar{r}_o$$

Again inserting typical values of $\bar{r}_o = 0.1$ and $\lambda_s = -0.06$

$$\frac{\bar{v}_c'}{\bar{u}_w'} = 0.0077$$

Thus, while mixing cyclic with winglet deflection to eliminate the angular acceleration produced by winglet deflection does produce a control coupling in the sense that a lateral force is produced in addition to the longitudinal force arising from winglet deflection, the effect is essentially negligible. In effect, the above ratio is equivalent to shifting the phase of the winglet control by 0.0077 radians (.44 degrees) to obtain a translational force only with the cyclic mixing to eliminate the pitching moment. Precisely speaking, there is still a small

moment remaining about the other axis (roll in the case of this example) owing to the fact that the cyclic has been mixed with the winglet deflection, however, this effect should be very small.

C. Summary

Thus to summarize the results of this section, a cyclic control input primarily produces a moment on the vehicle and secondarily produces a small translational force. A winglet control primarily produces a translational force and secondarily produces a small moment. For typical AEROCRANE parameters only a small level of cyclic mixing with winglet deflection is required (less than 0.1 deg cyclic per deg winglet) to eliminate the moment produced by winglet deflection. This ratio is of course dependent upon the center of gravity location on the vehicle and would be of the order of 1 if the center of gravity of the vehicle was located on the gondola as a limiting case.

HOVERING CONTROL CONSIDERATIONS

In order to obtain some insight into the basic mechanics of hovering control of the AEROCRANE a simplified model of the hovering dynamics is examined. In this model, to bring out the central features of hovering control, the long time dynamics and the sling load dynamics are neglected. That is, it has been shown in Reference 1 that the basic modes of motion of the AEROCRANE include a rapid angular mode whose characteristics depend primarily on the rotor angular damping and the gyroscopic effects of vehicle and rotor rotation. In addition, two long period oscillatory modes exist with frequencies primarily determined by the velocity stability (M_u), dihedral effect (L_v) and the aerodynamic coupling terms M_v and L_u. Typical periods for these motions as shown in a later section of this report, are of the order of $\frac{60}{\Omega}$ seconds and $\frac{40}{\Omega}$ seconds. For a large AEROCRANE with a rotor angular velocity of the order of one radian per second, the corresponding periods of these slow motions are 60 and 40 seconds. Consequently, it would not be expected that these longer period modes would be particularly significant in precision hover control. Thus, in the following analysis the speed dependent derivatives are neglected with respect to their influence on the vehicle dynamics. Only the translational gust response can be examined with this simplified model. The rapid angular response mode, primarily determined by the terms M_q and ω_a, is retained. This mode, characterized by a period of the order $\frac{5}{\Omega}$, or 5 seconds for Ω = 1.0 rad/sec., is the one primarily involved in maneuvering near hover.

Thus the following equations of motion are employed in this section

to examine the hovering dynamics and control of the AEROCRANE.

$$\begin{bmatrix} (s) & (s - M_q) & \omega_G s & 0 & 0 \\ -\omega_G s & & (s)(s - M_q) & 0 & 0 \\ 0 & & \eta & (s - X_u) & 0 \\ -\eta & & 0 & 0 & (s - X_u) \end{bmatrix} \begin{Bmatrix} \phi \\ \theta \\ u \\ v \end{Bmatrix} = \begin{bmatrix} 0 & -M_{A_{1s}} \\ M_{A_{1s}} & 0 \\ 0 & 0 \\ 0 & 0 \end{bmatrix} \begin{Bmatrix} A_{1s} \\ B_{1s} \end{Bmatrix}$$

$$+ \begin{bmatrix} M_{\delta_c} & 0 \\ 0 & M_{\delta_c} \\ 0 & X_{\delta_c} \\ -X_{\delta_c} & 0 \end{bmatrix} \begin{Bmatrix} \delta_s \\ \delta_c \end{Bmatrix} + \begin{bmatrix} 0 & 0 \\ 0 & 0 \\ 0 & X_u \\ X_u & 0 \end{bmatrix} \begin{Bmatrix} v_G \\ u_G \end{Bmatrix}$$

where $\eta = \frac{T}{m'}$. The symmetry of the vehicle has been employed to express the lateral derivatives in terms of the longitudinal derivatives. Note that the derivative X_u is entirely due to the winglets. That is, the centerbody drag is assumed to be proportional to the square of the velocity and therefore does not contribute to the linearized model when hovering is the equilibrium condition. It was shown in a previous section that the translational forces due to cyclic are small and therefore the terms are neglected.

The characteristic equation for the dynamic motion of the vehicle described by this simplified model is

$$\Delta_c = s^2 (s - X_u)^2 [(s - M_q)^2 + \omega_G^2]$$

The short term dynamics are described by the quadratic factor in the square brackets and the long term dynamics are given by the first two factors which

correspond to two roots at the origin and two real roots at X_u. Without winglets, $X_u = 0$ and the long term approximation to the dynamics consists of four roots at the origin.

The transfer functions describing the translational response of the vehicle can be written as

$$u = \frac{(s)(s - X_u)\left[s\,\Delta X\left\{(s - M_q)^2 + \omega_G^2\right\} - \Delta M \eta\,(s - M_q)\right]}{\Delta_c}$$

$$v = \frac{(s)(s - X_u)\left[-\Delta M\,\omega_G\,\eta\right]}{\Delta_c}$$

where the influence of various inputs is shown by the following expressions:

$$\Delta X = X_{\delta_c}\,\delta_c + X_u u_G$$

$$\Delta M = M_{A_{1s}}\,A_{1s} + M_{\delta_c}\,\delta_c$$

Only longitudinal inputs have been included at this point. Owing to symmetry the lateral response problem will be similar so only the longitudinal is discussed.

First we contrast the basic features of winglet control to cyclic control for hovering position control. In the first instance it is assumed that for the winglet control case the cyclic is coupled to the winglet such that no pitching moment is applied to the vehicle as a result of a winglet input. That is, the cyclic is geared to winglet motion such that

$$M_{A_{1s}}\,A_{1s} + M_{\delta_c}\,\delta_c = 0$$

resulting in a gearing

$$A_{1s} = -\frac{M_{\delta_c}}{M_{A_{1s}}}\,\delta_c$$

This is a low level of gearing as noted in an earlier section.

The longitudinal velocity response to winglet input becomes, after inserting the expression for the characteristic equation into the transfer function

$$\frac{u}{\delta_c} = \frac{X_{\delta_c}}{(s - X_u)}$$

Consequently the expression for longitudinal position response is

$$\frac{x}{\delta_c} = \frac{X_{\delta_c}}{(s)(s - X_u)}$$

If it is assumed that the pilot attempts to control longitudinal position by moving the winglet control proportional to longitudinal displacement, a closed loop system which is stable with a closed loop frequency dependent upon gain is obtained as shown in Figure 1a.

Before considering this situation in more detail, consider the contrast with cyclic control of position. From the transfer functions given above the longitudinal velocity response to cyclic is given by

$$\frac{u}{A_{1s}} = \frac{- M_{A_{1s}} \eta (s - M_q)}{s^2 [(s - M_q)^2 + \omega_G^2]}$$

X_u has been set equal to zero since it is assumed that the vehicle is not equipped with winglets. The transfer function for longitudinal position is

$$\frac{x}{A_{1s}} = \frac{- M_{A_{1s}} \eta (s - M_q)}{s^3 [(s - M_q)^2 + \omega_G^2]}$$

Again assuming that the pilot attempts to control longitudinal position with cyclic, the closed loop dynamics shown in Figure 1b result. The closed loop system is unstable, illustrating the classical problem of controlling the translational displacement of a hovering vehicle. That is, the pilot must supply a considerable amount of lead in order to stablize the vehicle. The feedback transfer function required to to stabilize the vehicle must be of the form

$$A_{1s} = - K_p (\tau_{L1} s + 1) (\tau_{L2} s + 1) x$$

With sufficient gain and a double lead this closed loop system is stable as shown in Figure 1c. The control of translational displacement with cyclic pitch is a difficult task.

The double lead term can be interpreted in another way by noting the relationship between translational displacement and vehicle attitude from the equations of motion. The translational force equation gives the following relationship between vehicle attitude and displacement.

$$\eta\theta = - s^2 x$$

Thus the double lead term may be interpreted as a requirement that the pilot provides an attitude feedback or inner loop plus an outer loop involving translational displacement and velocity feedback.

The interest in the use of winglets relates to hovering control where, by direct control of translational force, two integrations are eliminated from the transfer function relating longitudinal displacement to control action simplifying the pilot's control task.

It should also be noted that if the winglet configuration does produce an appreciable pitching moment in addition to translational force then the winglet control problem becomes somewhat more complex as shown below. The transfer function for longitudinal displacement including the influence of winglet pitching moment is

$$\frac{x}{\delta_c} = \frac{X_{\delta_c}\left[s\left\{(s - M_q)^2 + \omega_G^2\right\} - \frac{M_{\delta_c}}{X_{\delta_c}}\eta\,(s - M_q)\right]}{(s^2)\,(s - X_u)\left[(s - M_q)^2 + \omega_G^2\right]}$$

Figure 1d shows the effect of the ratio $\frac{M_{\delta_c}}{X_{\delta_c}}$ on the location of the zeros of this transfer function. In the limit of a very large value of the ratio $\frac{M_{\delta_c}}{X_{\delta_c}}$ the zeros approach the cyclic case. Now consider the effect of translational position feedback with some significant value of the ratio $\frac{M_{\delta_c}}{X_{\delta_c}}$ as shown in Figure 1e. Thus, if the winglet produces an appreciable pitching moment as well as a translational force, the hovering control of position becomes more complex and the closed loop dynamics are marginally stable unless the pilot provides a single lead as shown in Figure 1f. If the vehicle configuration is such that a winglet input produces a significant pitching moment, then it is desirable to provide cyclic mixing such that a winglet input provides translational force only.

This simple model is now employed to examine the translational response of the vehicle to gusts. Owing to the fact that the translational velocity pitching moment derivatives have been neglected, the model is valid for translational investigations only. The gust response of the complete dynamic model is described in a later section. Thus, the transfer function relating translational displacement to gust velocity is,

$$\frac{x}{u_G} = \frac{X_u}{(s)(s - X_u) + K_x X_{\delta_c}}$$

X_u and X_{δ_c} are simply related as shown in Appendix A since both terms arise from the winglets.

Let

$$\epsilon' = \frac{3\sigma a_w \bar{\bar{b}}_w}{16 \chi^3} \left\{ \frac{\beta}{1 + \frac{\beta}{2}} \right\}$$

and noting that

$$X_u = - \frac{1}{\Omega R} X_{\delta_c}$$

Then

$$X_{\delta_c} = \frac{1}{m'} \frac{\partial X}{\partial \delta_c} = \Omega^2 R \epsilon'$$

and

$$X_u = - \Omega \epsilon'$$

The translational gust response transfer function can be written as

$$\frac{x}{u_G} = \frac{1}{\Omega} \left\{ \frac{- \epsilon'}{\hat{s}^2 + \epsilon' \hat{s} + \epsilon' \bar{K}_x} \right\}$$

where the Laplace variable has been nondimensionalized by the rotor angluar velocity

$$\hat{s} = \frac{s}{\Omega}$$

and $\bar{K}_x$ is a nondimensional gain,

$$\bar{K}_x = R\, K_x$$

K_x is the dimensional feedback gain in radians per foot.

The mean square value of the displacement response for a typical gust input spectrum is now evaluated. A reasonable model for the power spectrum of horizontal gusts at low wind velocities can be obtained by passing white noise through a low pass filter. The power spectrum of a gust with mean square gust velocity $\tilde{\tilde{u}}_G^2$ is given by

$$G_G(\omega) = \frac{2}{\omega_c \pi} \left\{ \frac{\tilde{\tilde{u}}_G^2}{1 + (\frac{\omega}{\omega_c})^2} \right\}$$

where ω_c is the cutoff frequency of the low pass filter and is usually taken to be 0.314 rad/sec as a reasonable match to experimental data on gust spectra.

The power spectrum of the translational displacement can then be calculated from the transfer function given above.

$$G_x(\omega) = \left| \frac{x}{u_G} \right|^2 G_G(\omega)$$

The mean square value of the displacement of the vehicle, $\tilde{\tilde{x}}^2$ is given by

$$\tilde{\tilde{x}}^2 = \frac{1}{2} \int_{-\infty}^{\infty} G_x(\omega)\, d\omega$$

Explicitly

$$\tilde{\bar{x}}^2 = \frac{\tilde{\bar{u}}_G}{\Omega^2} \left\{ \frac{1}{\bar{K}_x \hat{\omega}_c \left[1 + \left(\frac{\epsilon'}{\epsilon' + \hat{\omega}_c} \right) \frac{\bar{K}_x}{\hat{\omega}_c} \right]} \right\}$$

or

$$\tilde{\bar{x}}^2 = \frac{\tilde{\bar{u}}_G^2}{\Omega^2} \; f\,(\hat{\omega}_c, \epsilon', \bar{K}_x)$$

The function, f, is plotted in Figure 2, for a typical value of ϵ'. It can be seen that the critical parameter is the dimensionless feedback gain, $\bar{K}_x$, and the mean square displacement is not particularly sensitive to $\hat{\omega}_c$. Thus, the influence of size of the vehicle enters primarily through the rotor RPM. For the dynamic model of Reference 1, with Ω = 3.14 rad/sec and a root mean square gust level of 5 fps, the value of f = 0.39 yields a root mean square (RMS) displacement of 1 ft. Figure 2 indicates that a dimensionless gain of the order of 2 is required for this RMS displacement. To determine the dimensional gain,

$$K_x = \frac{\bar{K}_x}{R}$$

and for the model of Reference 1, R = 19.64 ft. and therefore the dimensional gain is

K_x^o = 5.8 degrees winglet deflection per foot displacement.

This gain corresponds to a closed loop natural frequency

$$\omega_N = \sqrt{\Omega^2 R \epsilon' K_x} = 2.42 \text{ rad/sec.}$$

or a 2.6 second period. If the 16 ton vehicle is examined, with $\Omega = 1.14$ rad/sec, for a root mean square displacement of 1 foot, $f = 0.046$ is required and this corresponds to a dimensionless gain $\bar{K}_x = 6$. The dimensional gain ($R = 136.5$ ft.) required is about one-half the value for the smaller vehicle. That is $K_x^o = 2.51$ degrees per foot. This example illustrates, as indicated also in Reference 4, that in order to maintain position in gusts a relatively high gain displacement feedback is required.

For the vehicle without winglets, the linearized model would indicate no response to gusts since the centerbody forces depend upon the square of the velocity. The analog computer model included this nonlinear effect and the complete gust response of the vehicle based on the computer model is discussed in a later section.

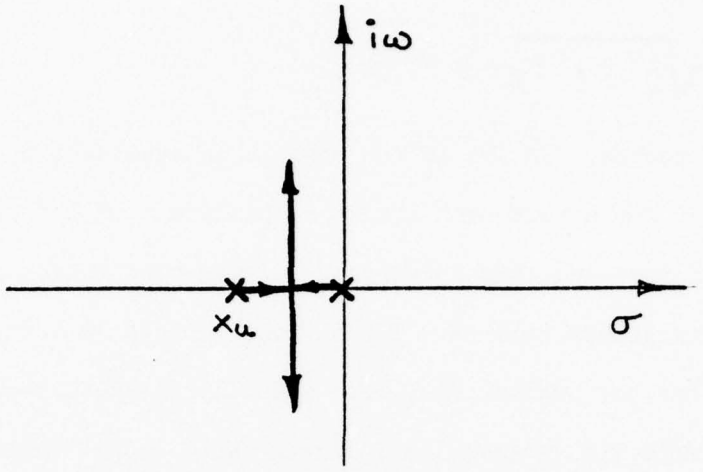

a.) Winglet Control of Displacement (No Winglet Pitching Moment)
Control Law: $\delta_c = K_w x$

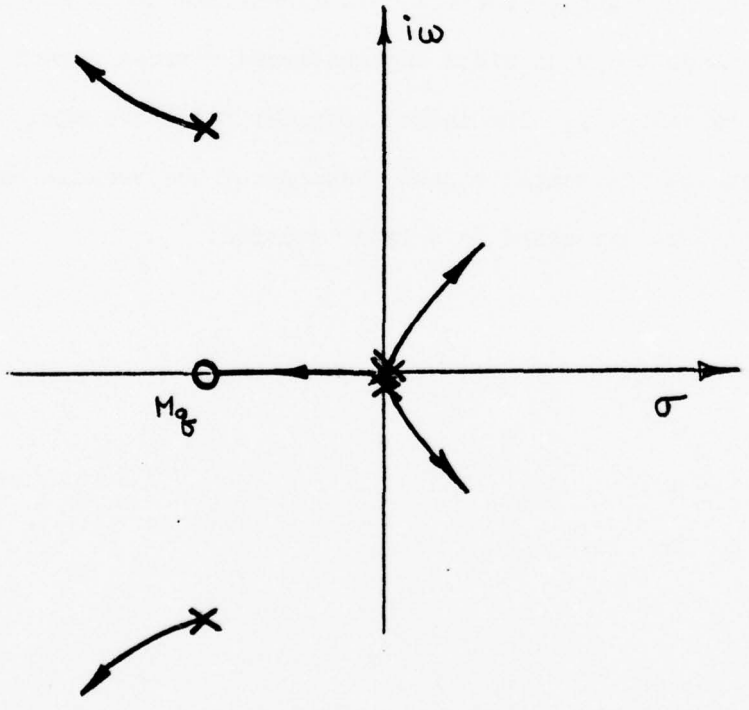

b.) Cyclic Control of Displacement
Control Law: $A_{1s} = - K_c x$

Figure 1: Comparison of Winglet and Cyclic Control in Hovering Flight. Simplified Dynamic Model.

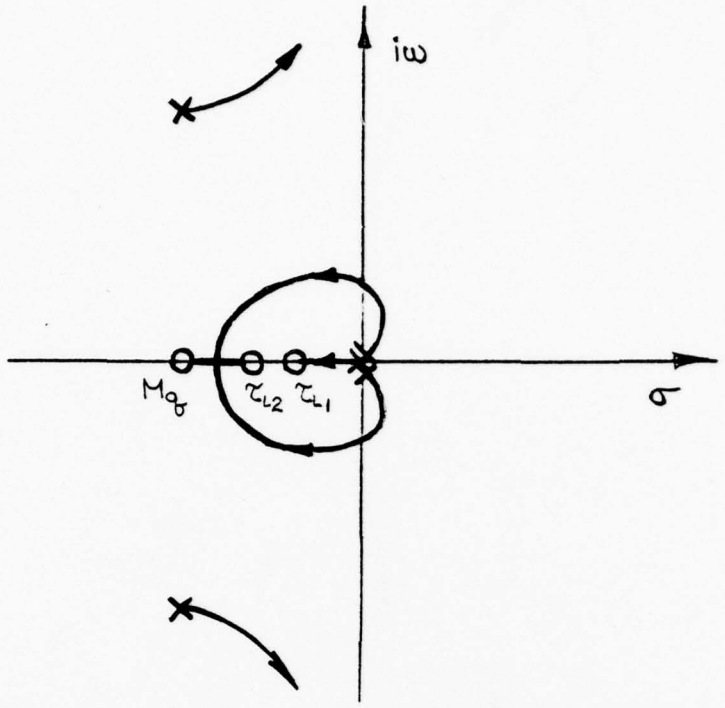

c.) Cyclic Control of Displacement with Double Lead
Control Law: $A_{1s} = - K_c (\tau_{L1} s + 1) (\tau_{L2} s + 1) x$

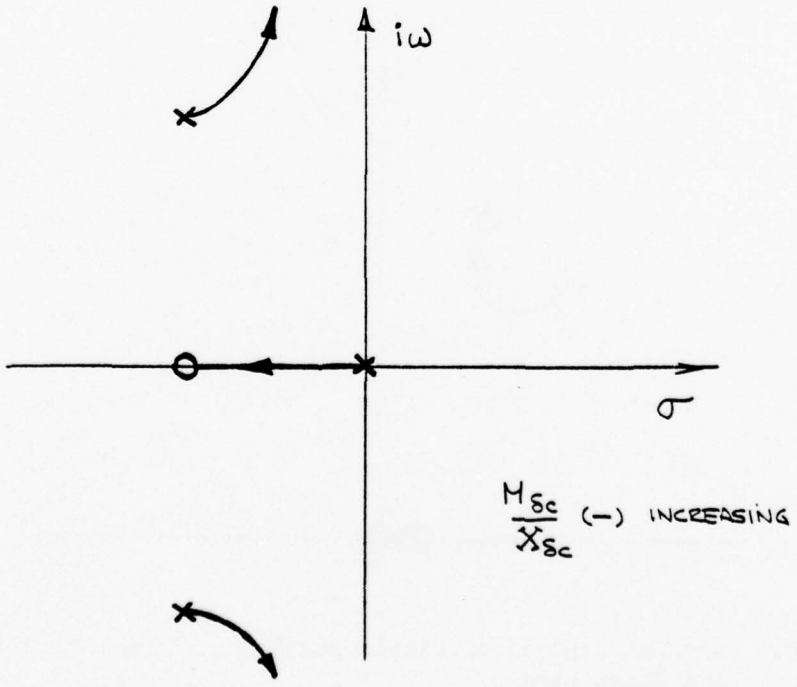

d.) Root Locus for Zeros of $\frac{x}{\delta_c}$ Transfer Function as a Function of $\frac{M_{\delta c}}{X_{\delta c}}$.

Figure 1: Continued.

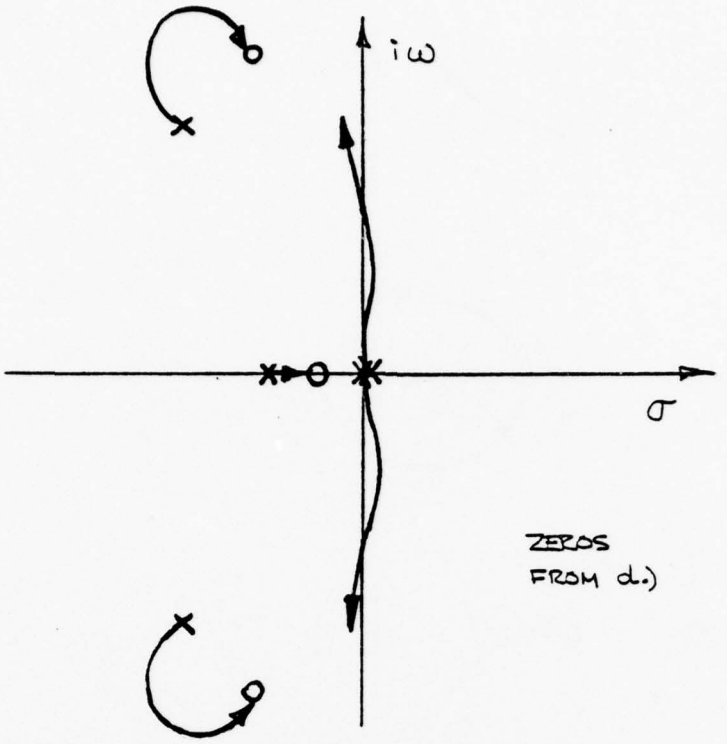

e.) Winglet Control of Displacement Including Moment Effect of Winglets

Control Law: $\delta_c = - K_c x$

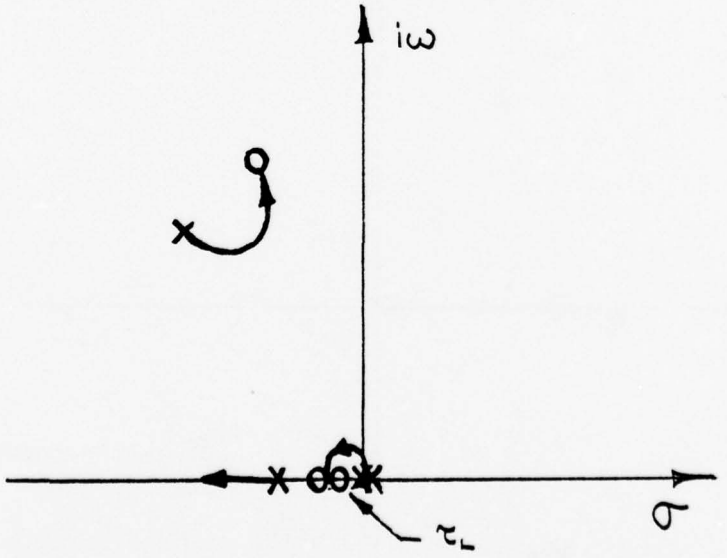

f.) Winglet Control of Displacement Including Moment Effect of Winglets and Pilot Lead

Control Law: $\delta_c = - K_c (\tau_L s + 1) x$

Figure 1: Continued.

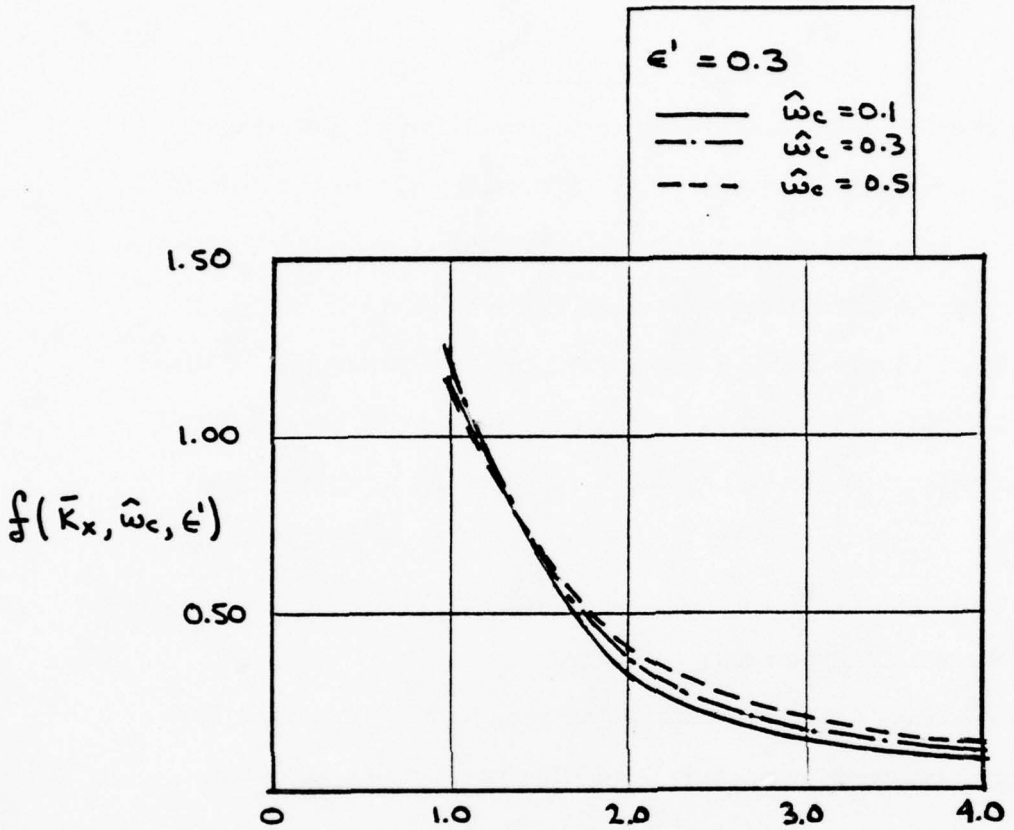

$$\overline{x^2} = \frac{\overline{\mu_\theta^2}}{\Omega^2} f(\bar{K}_x, \hat{\omega}_c, \epsilon')$$

Figure 2: Dependence of Mean Square Translational Displacement on Displacement Gain. Winglets On.

SLING LOAD DYNAMICS

In this section some basic features of the sling load motion are examined. Of particular interest is the influence of the presence of a buoyant force in addition to aerodynamic thrust. Consequently various results obtained are contrasted with a hovering helicopter for which the buoyant force equals zero ($\beta = 0$). The analysis presented is based on a simplified model, such that, it not only applies to the AEROCRANE but to any hovering vehicle which obtains part of its lifting force from buoyancy. Of particular interest therefore is the influence of the buoyant force ratio, β, and the sling load mass ratio, μ, on the sling load and vehicle dynamics.

It is shown in a later section of the report that the sling load geometry (the location of the sling load attachment point, and the sling length) has only a small influence on the dynamic stability characteristics of the vehicle (i.e., the characteristic roots), that is, in a dynamic sense, the sling load is not strongly coupled to the vehicle. Therefore, it is possible to examine the dominant effects of the sling load using an approximate model.

It is assumed that the sling load motion and its effect on vehicle motion can be estimated by considering the system in the following way. The interaction between sling load motion and vehicle motion is approximated as a forced response problem. That is, the pitch attitude of the vehicle is assumed to be the input and the sling load motion and the vehicle translation motion are assumed to be outputs. Thus, the motion of the complete dynamic system is reduced to an examination of a relatively

simple frequency response problem. Since vehicle pitch attitude is taken as the input, it has been assumed that cyclic pitch is being employed for control and the input frequency characterizes the pilot's control action. It has been shown by frequency response experiments with the complete dynamic model of the AEROCRANE that this simplified approach is valid.

With this simplified model, the following discussion applies to any heavy lift vehicle which is controlled by moments and derives an appreciable portion of its lift from buoyancy, since only the translational force and sling load equations are involved in the analysis. If X_u is neglected, the horizontal force equation as given in Appendix C is

$$m' \dot{u}_s = - (W_o - F_B) \theta + W_{s_L} \theta_L$$

The sling load equation is

$$- \dot{u}_s - g (\theta + \theta_L) - \ddot{\theta} (Z_A + Z_L) - \ddot{\theta}_L Z_L = 0$$

The horizontal acceleration is eliminated from the sling load equation, using the translational force equation to obtain an equation relating load deflection relative to the vehicle (θ_L) and vehicle attitude (θ). The geometry is shown in Figure 3. The resulting equation is,

$$\omega_{s_L}^2 \left\{ 1 - \frac{(W_o - F_B)}{m'g} \right\} \theta + \left(1 + \frac{Z_A}{Z_L} \right) \ddot{\theta} + \omega_{s_L}^2 \left(1 + \frac{m_L}{m'} \right) \theta_L + \ddot{\theta}_L = 0$$

Nondimensionalizing the time by the sling load frequency and introducing the dimensionless parameters μ and β describing the sling load weight ratio and the buoyancy ratio, the above equation becomes

$$\left(\frac{\frac{3}{2}\beta}{1 + \frac{\beta}{2}} \right) \theta + \left(1 + \frac{Z_A}{Z_L} \right) \theta'' + \left(\frac{1 + \frac{\beta}{2} + \mu}{1 + \frac{\beta}{2}} \right) \theta_L + \theta_L'' = 0$$

This equation can now be viewed as describing the response of the sling

load to vehicle attitude changes. Taking the Laplace transform and reorganizing

$$\frac{\theta_L}{\vartheta} = -\left\{ \frac{\left(1 + \frac{Z_A}{Z_L}\right)\tilde{s}^2 + \frac{\frac{3}{2}\beta}{\left(1 + \frac{\beta}{2}\right)}}{\tilde{s}^2 + \frac{\left(1 + \frac{\beta}{2} + \mu\right)}{\left(1 + \frac{\beta}{2}\right)}} \right\}$$

Consider first for reference a conventional helicopter with $\beta = 0$

$$\frac{\theta_L}{\theta} = \left\{ \frac{\left(1 + \frac{Z_A}{Z_L}\right)\tilde{s}^2}{\tilde{s}^2 + (1+\mu)} \right\}$$

If the load is attached at the center of gravity, such that $Z_A = 0$

$$\frac{\theta_L}{\theta} = -\left\{ \frac{\tilde{s}^2}{\tilde{s}^2 + (1+\mu)} \right\}$$

Now consider the frequency response of θ_L to θ inputs, i.e., let $\tilde{s} = i\tilde{\omega}$ recalling that the time has been nondimensionalized by the sling load frequency. It is clearer at this point to examine the sling load motion with respect to space. Let

$$\theta_{LA} = \theta_L + \theta$$

The transfer function for the absolute load motion is therefore

$$\frac{\theta_{LA}}{\theta} = \frac{1+\mu}{\tilde{s}^2 + (1+\mu)}$$

With $\tilde{s} = i\tilde{\omega}$

$$\frac{\theta_{LA}}{\theta} = \frac{(1 + \mu)}{-\tilde{\omega}^2 + (1 + \mu)}$$

at low frequencies as $\tilde{\omega} \rightarrow 0$,

$$\frac{\theta_{LA}}{\theta} = 1$$

indicating that the motion of the load in space is the same as the helicopter motion and at high frequencies the absolute load motion tends towards zero, that is, the load remains fixed in space. This frequency response is shown in Figure 4.

Now consider the case in which the load is attached some distance below the center of gravity. The transfer function is

$$\frac{\theta_{LA}}{\theta} = \frac{-\frac{Z_A}{Z_L}\tilde{s}^2 + (1 + \mu)}{\tilde{s}^2 + (1 + \mu)}$$

The low frequency behavior is unchanged, however there is a difference in the high frequency response

$$\frac{\theta_{LA}}{\theta}_{\omega \rightarrow \infty} = -\frac{Z_A}{Z_L}$$

and the complete frequency response is given by

$$\frac{\theta_{LA}}{\theta} = \frac{\frac{Z_A}{Z_L}\tilde{\omega}^2 + (1 + \mu)}{-\tilde{\omega}^2 + (1 + \mu)}$$

Thus for the nose up motion of the helicopter, the load moves aft of the vertical by an amount dependent upon the distance between the center of gravity and the load attachment point. Note that in the case where $\frac{Z_A}{Z_L}$ equals one, although the amplitude of the load is essentially independent of frequency, the phase shifts by 180° so that the load motion is in fact different for forcing above and below the natural frequency of the load.

Now consider the case with buoyancy. The transfer function for the absolute load motion in response to vehicle attitude is

$$\frac{\theta_{LA}}{\theta} = \frac{-\frac{Z_A}{Z_L}\tilde{s}^2 + \frac{(1 - \beta + \mu)}{(1 + \frac{\beta}{2})}}{\tilde{s}^2 + \frac{(1 + \frac{\beta}{2} + \mu)}{(1 + \frac{\beta}{2})}}$$

Letting $\tilde{s} = i\tilde{\omega}$

$$\frac{\theta_{LA}}{\theta} = \frac{\frac{Z_A}{Z_L}\tilde{\omega}^2 + \frac{(1 - \beta + \mu)}{(1 + \frac{\beta}{2})}}{-\tilde{\omega}^2 + \left(\frac{1 + \frac{\beta}{2} + \mu}{1 + \frac{\beta}{2}}\right)}$$

The high frequency response is unchanged, however, the low frequency response becomes

$$\frac{\theta_{LA}}{\theta}_{\tilde{\omega} \to 0} = \frac{(1 - \beta + \mu)}{(1 + \frac{\beta}{2} + \mu)}$$

It can be seen that in the fully buoyant case ($\beta = 1 + \mu$) the load remains vertical, that is, the absolute load motion tends towards zero. Thus, the effect of adding a buoyant force to a hovering vehicle is to tend to reduce the low frequency response of the load motion. This is, of course, a consequence of the fact that with a buoyant force there is less translational acceleration as a result of tilting. Figure 5, shows the frequency response of the load in this case.

To summarize, the high frequency (above the sling load natural frequency) maneuvering excites the motion of the load. If the load is attached at the center of gravity of the vehicle the load tends to remain vertical and with the load below the center of gravity the absolute motion of the load, with respect to space, is increased. Thus, rapid maneuvering will tend to excite the load motion which has little damping and will tend to continue to oscillate. In the slower maneuvering of the vehicle with a buoyant force present, the load tends to remain near the vertical. It should also be noted that the use of winglets will tend to excite the load as winglet deflection will produce a horizontal force and consequently the load will experience an acceleration and commence swinging.

Another important aspect of the influence of the sling load on the response of the AEROCRANE can be seen by examining the translational acceleration response to vehicle attitude. This quantity can be thought of as a measure of the translational response of the vehicle to cyclic pitch with a tight attitude loop such that it is reasonable to assume that cyclic

pitch produces attitude. The horizontal acceleration response to attitude can then be examined using only the sling load equation and the translational force equation, that is, pitch attitude is considered to be an input. It should be noted that most of the features of this response discussed below are characteristic of the response of any heavy lift vehicle which obtains an appreciable amount of its lift from buoyancy.

The translational force equation as given above is

$$\dot{u}_s = -\left(\frac{W_o - F_B}{m'}\right)\theta - \frac{W_{sL}}{m'}\,\theta_L$$

The important point to note about this equation is the fact that when there is an appreciable buoyant force F_B, the influence of vehicle attitude (θ) upon the horizontal acceleration becomes small compared to the influence of sling load deflection (θ_L). Expressing this equation in terms of dimensionless ratios,

$$\frac{\dot{u}_s}{g} = -\left(\frac{1 - \beta}{1 + \frac{\beta}{2}}\right)\theta + \frac{\mu}{1 + \frac{\beta}{2}}\,\theta_L$$

For the AEROCRANE parameters assumed here,

$$\beta = 1.42$$

$$\mu = 0.84$$

$$\frac{\dot{u}_s}{g} = +0.24\,\theta + 0.49\,\theta_L$$

The effect of sling load deflection is about twice the influence of vehicle attitude and in addition, the effect of vehicle attitude has changed sign

compared to a helicopter. Thus, the translational acceleration response to vehicle attitude will depend to a large extent on the sling load response to attitude discussed above. Consider this equation for a helicopter where $\beta = 0$. μ is taken to be 0.75 for a typical heavy lift helicopter, the corresponding equation is,

$$\frac{\dot{u}_s}{g} = - \theta + 0.75 \theta_L$$

The attitude term changes sign and is larger than the sling load deflection term. In order to understand further the implications of the above results consider a low frequency motion of the vehicle, in which the angular acceleration terms can be neglected in the sling load equation. In this case, the sling load equation can be solved for sling load amplitude,

$$\theta_L = - \frac{\dot{u}_s}{g} - \theta$$

Substituting, for the AEROCRANE

$$\frac{\dot{u}_s}{g} = - 0.167 \theta$$

For the helicopter with no buoyant lift,

$$\frac{\dot{u}_s}{g} = - \theta$$

Thus, for slow maneuvering of the buoyant vehicle with a sling load only about $\frac{1}{6}$ the acceleration is obtained as compared to the helicopter.

Now the more general case is considered, that is, an expression is derived for the frequency response of translational acceleration to vehicle attitude. The relationship between the sling load motion with respect to space and the vehicle attitude was developed above as

$$\frac{\theta_{AL}}{\theta} = \frac{-\frac{Z_A}{Z_L}\tilde{s}^2 + \frac{(1 - \beta + \mu)}{(1 + \frac{\beta}{2})}}{\tilde{s}^2 + \frac{(1 + \frac{\beta}{2} + \mu)}{(1 + \frac{\beta}{2})}}$$

This expression can be used with the sling load equation to eliminate the sling load deflection giving.

$$-\frac{\dot{u}_s}{g\theta} = \frac{(1 - \beta + \mu)}{(1 + \frac{\beta}{2} + \mu)} \left\{ \frac{\left[1 + \left(\frac{Z_A}{Z_L}\right)\left(\frac{\mu}{1 - \beta + \mu}\right)\right]\tilde{s}^2 + 1}{\left(\frac{1 + \frac{\beta}{2}}{1 + \frac{\beta}{2} + \mu}\right)\tilde{s}^2 + 1} \right\}$$

where, in this expression the Laplace variable has been nondemensionalized by the sling load frequency. Placing the AEROCRANE values of buoyancy ratio and sling load ratio in this expression yields

$$-\frac{\dot{u}_s}{g\theta} = 0.167 \left[\frac{(1 + 2\frac{Z_A}{Z_L})\tilde{s}^2 + 1}{0.67\,\tilde{s}^2 + 1} \right]$$

The coefficient in front of the brackets is the low frequency amplitude found above. If the frequency response is calculated for $\frac{Z_A}{Z_L} = 0$ and 0.472 (the value used in the analog simulation), the resulting characteristic is shown in Figure 6. At low frequencies $\dot{u}_s$ is in phase with $(-\theta)$ indicating the usual result that a nose down pitch gives a forward translation. The corresponding acceleration is small as noted above. If faster inputs are applied, specifically at frequency ratios higher than $\frac{1}{\sqrt{1 + 2\frac{Z_A}{Z_L}}}$ then the phase shifts 180° as indicated in the figure. That is for rapid control motions, in fact due to the sling load dynamics, the vehicle translational acceleration response to attitude changes sign indicating that there will be difficulties in rapidly controlling the vehicle with cyclic pitch through attitude, i.e., the effect may appear to the pilot somewhat like a control reversal when the pilot is primarily concentrating on controlling position over the ground. This effect would tend to be more significant in buoyantly supported vehicles owing to the low static gain of the acceleration - attitude transfer function, which would tend to make the pilot apply more rapid control motions, is discussed further in the section on analog simulation.

Attaching the load at the center of gravity alleviates this effect slightly since it increases the frequency at which phase shift occurs. In fact, this appears to be the major effect of sling load attachment point on the vehicle control. The effect of the pitching moment produced

as a result of the location of the sling load attachment point is small compared to the speed stability effect as noted in the analog simulation section where the response is discussed in more detail.

Figure 7 shows the extent of the frequency band where phase shift occurs as a function of sling load frequency and sling load attachment point. Shortening the sling load cable will of course increase the frequency at which the 180° phase shift occurs.

The corresponding transfer function for a helicopter assuming $\mu = 0.75$ is equal to

$$-\frac{\dot{u}_s}{g\theta} = \left\{ \frac{(1 + 0.43 \frac{Z_A}{Z_L})\, \tilde{s}^2 + 1}{0.571\, \tilde{s}^2 + 1} \right\}$$

Without buoyancy, the low frequency response amplitude is one. The sling load attachment point location has less effect on the frequency at which phase shift occurs as shown also in Figure 7. The frequency response of the helicopter is also shown on Figure 6. Owing to the much larger value of translational acceleration obtained without the buoyant force there is probably less tendency to make rapid control motions and consequently less tendency to operate into the region of 180° phase shift.

The simple model employed here indicates that this low value of translational acceleration is inherent in any hovering vehicle which obtains an appreciable portion of its lift from buoyancy and that further handling qualities studies are highly desirable to fully understand the importance of this marked difference from a helicopter. It

also tends to indicate that short sling load lengths (high sling load frequencies) are desirable, such that, the pilot will not encounter the phase shift region.

With a translational force control such as the winglets, this effect is not present since the control directly produces translational acceleration.

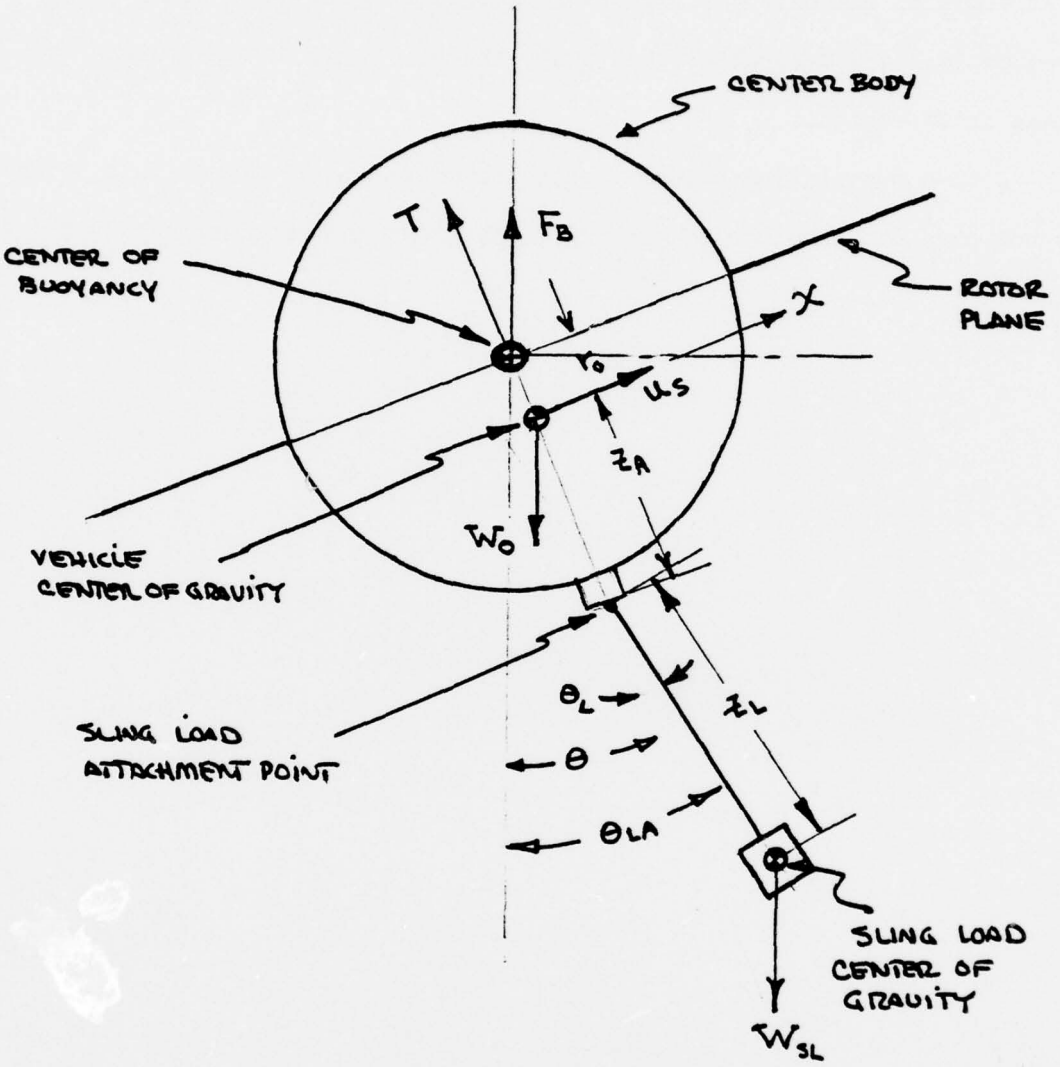

Figure 3: Geometry and Nomenclature for Sling Load Analysis.

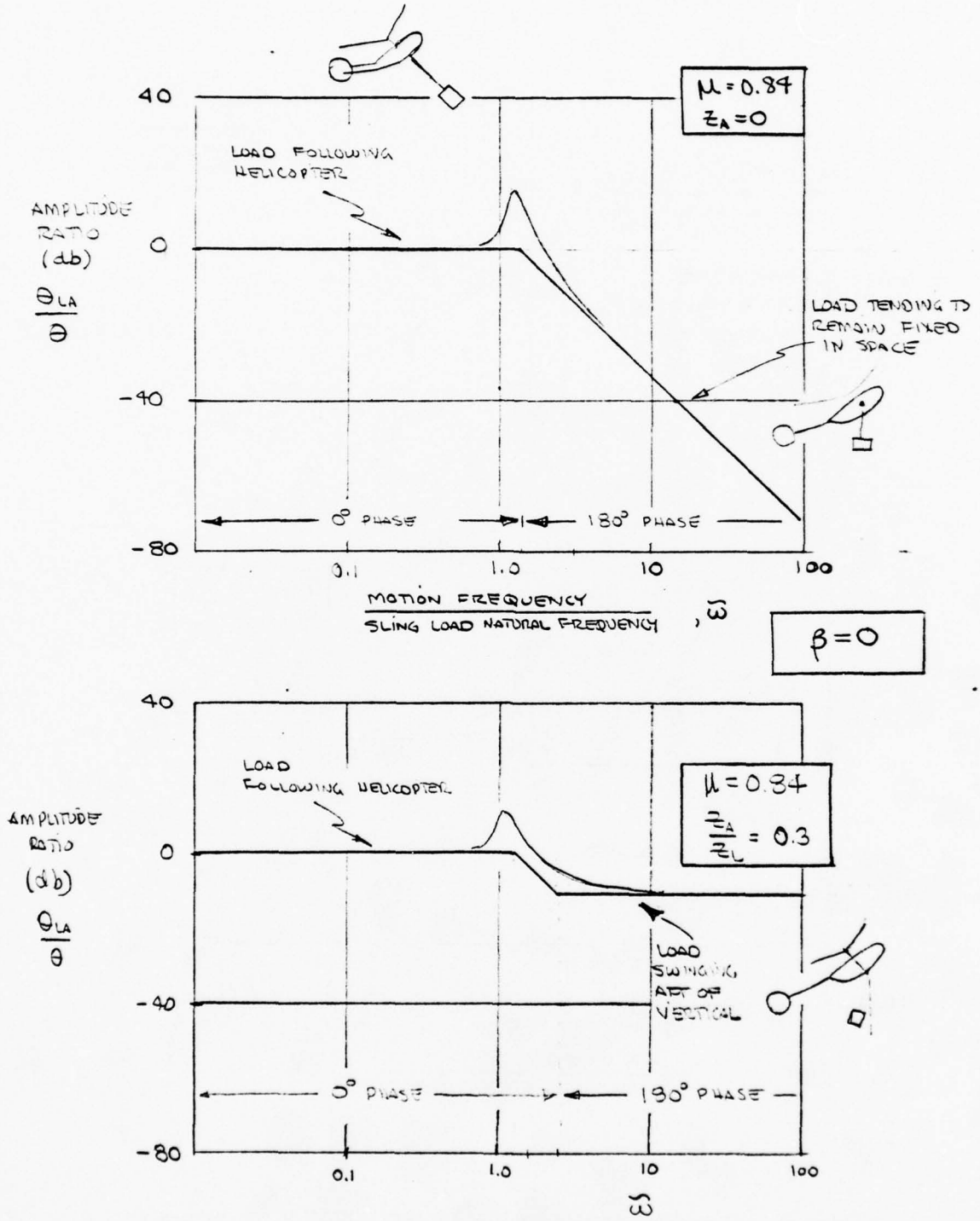

Figure 4: Approximate Motion of Sling Load Without Buoyancy.

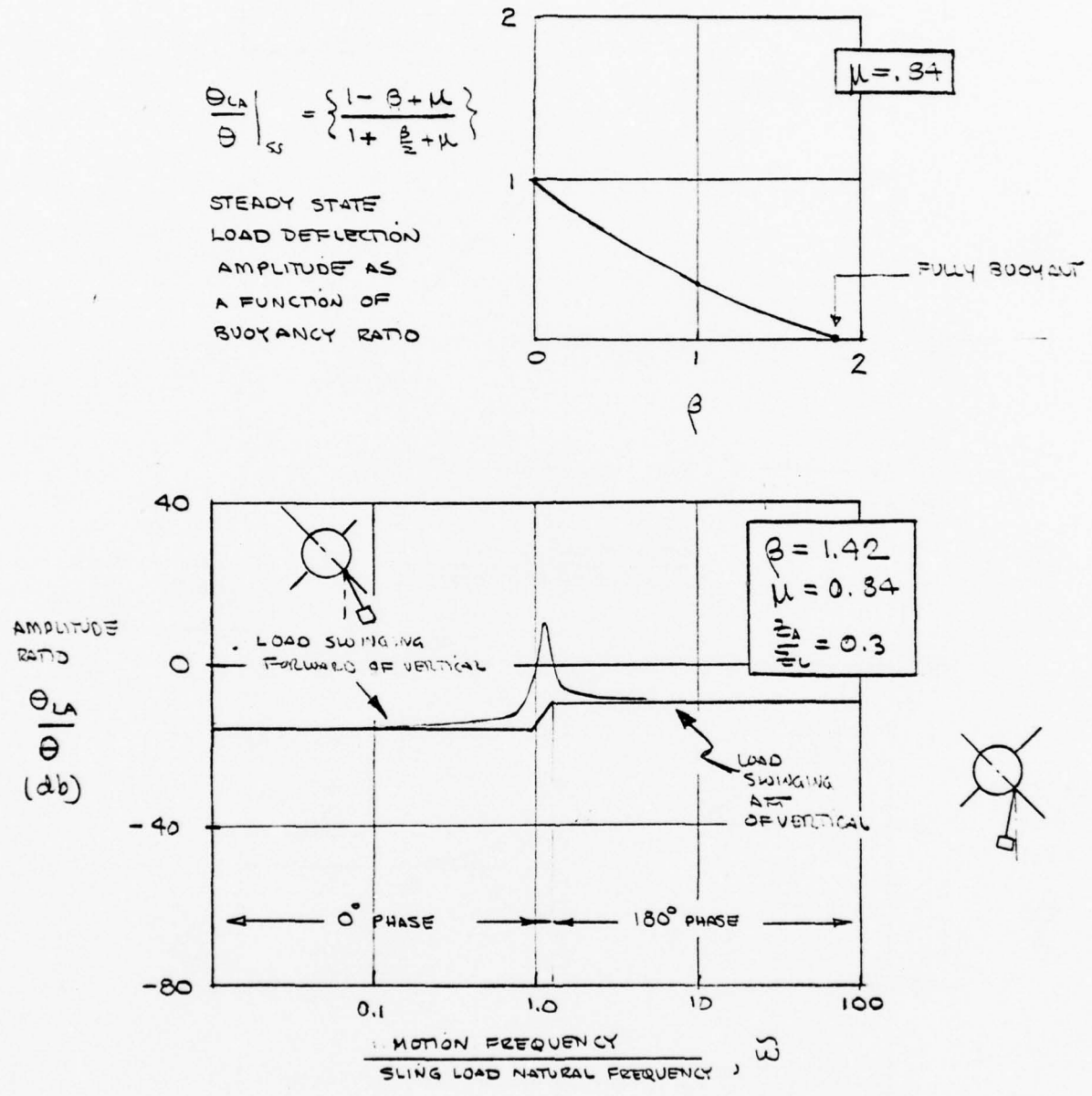

Figure 5: Approximate Motion of Sling Load With Buoyancy.

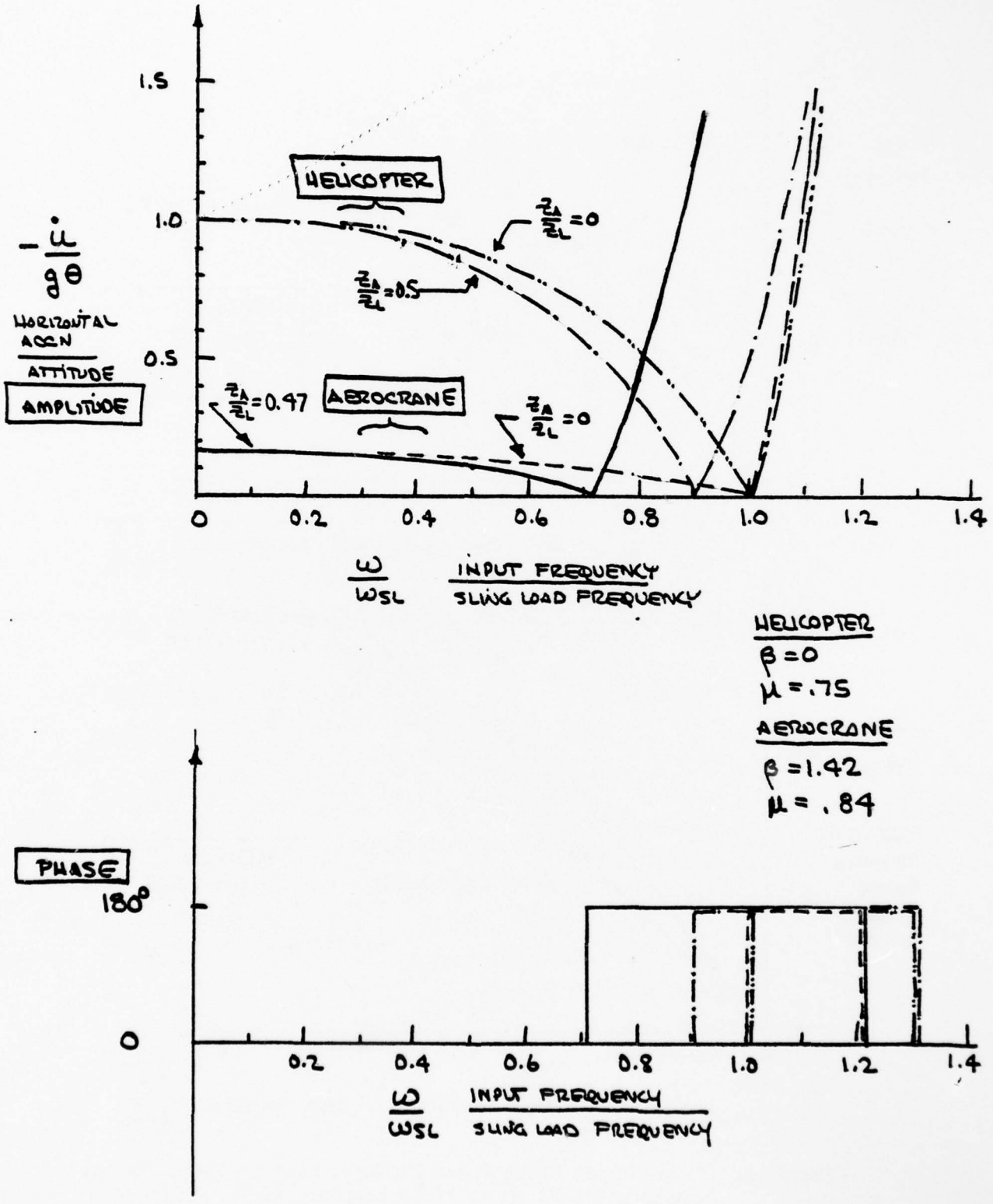

Figure 6: Frequency Response Comparison of Translational Acceleration to Pitch Attitude Response for AEROCRANE and Helicopter.

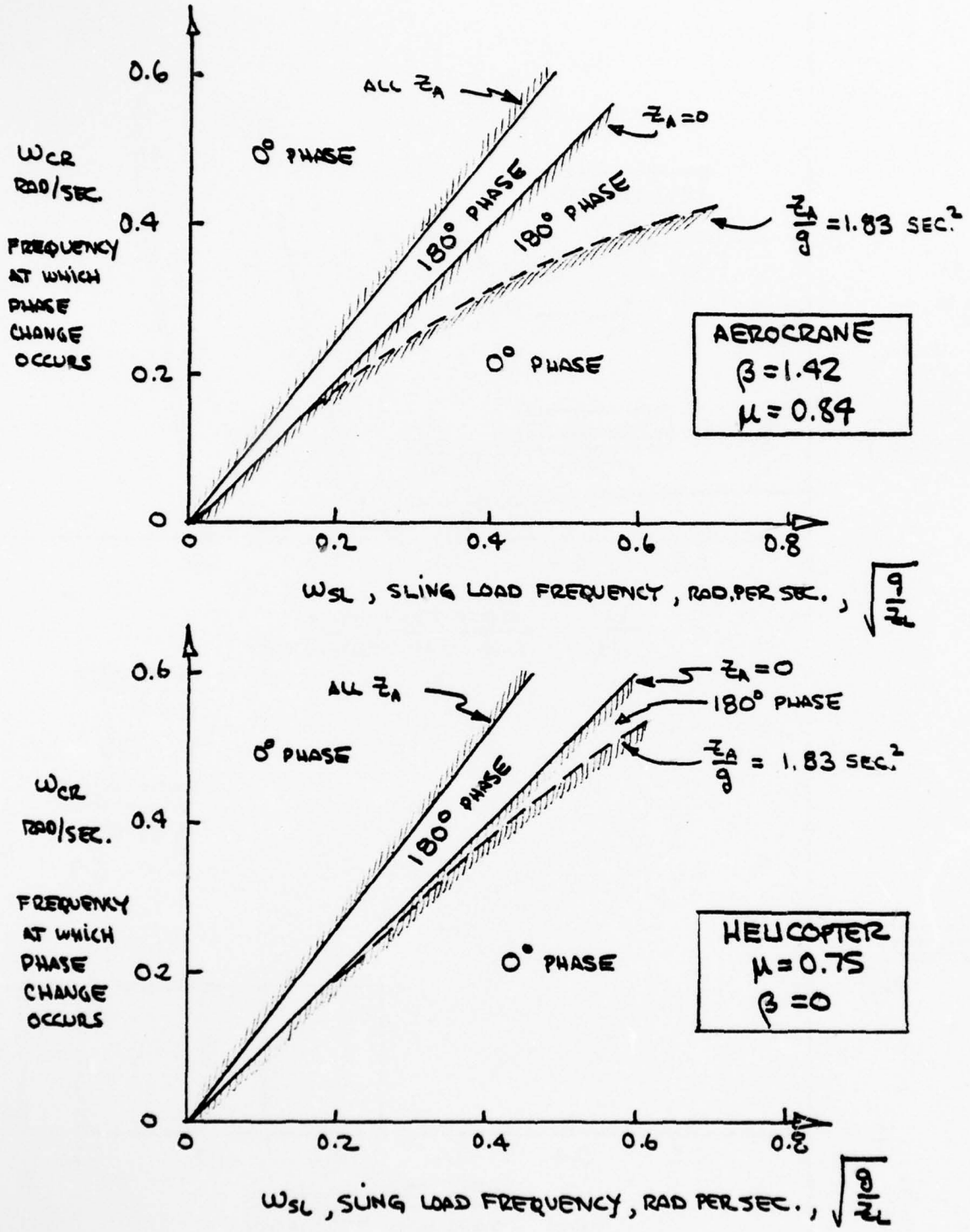

Figure 7: Frequency at Which Phase Change Occurs in Translational Acceleration Pitch Attitude Response as a Function of Sling Load Frequency and Attachment Point.

NON-DIMENSIONAL EQUATIONS OF MOTION

It is convenient to non-dimensionalize the equations of motion of the AEROCRANE in order that the influence of vehicle size on hovering stability and control can be examined. Further, this organization of the equations of motion will make it possible to readily examine the effects of various parameters of interest on the hovering stability and control.

The following non-dimensionalization is employed. Time is nondimensionalized by the rotor rotational velocity in radians per second, Ω, lengths by centerbody radius, R_s, and forces by the vehicle weight W_o. The following notation is used to represent nondimensional quantities:

$( )'$ = differentiation with respect to dimensionless time (Ωt).

$(\bar{\ })$ = length divided by centerbody radius

$\hat{\omega}$ = nondimensional frequency, $\frac{\omega}{\Omega}$

The various force ratios involved in the equations of motion are defined as follows:

β = buoyancy ratio, buoyant force divided by vehicle weight, $\frac{F_B}{W_o}$

μ = sling load weight ratio, sling load weight divided by vehicle weight, $\frac{W_{SL}}{W_o}$

The aerodynamic thrust to weight ratio can be expressed from vertical

equilibrium considerations in terms of the ratios μ and β as

$$\frac{T}{W_o} = (1 + \mu - \beta)$$

The apparent mass of the spherical centerbody is equal to one half of its displaced mass[6] and consequently is equal to

$$\frac{m_a}{m_o} = \frac{\beta}{2}$$

It may be noted that in general, this relationship between the buoyant force ratio and the apparent mass involves the assumption that the centerbody is filled with lifting gas (the vehicle is not equipped with ballonets) and that the mass of the lifting gas is included in the vehicle mass.

With these definitions it is possible to express the equations of motion for the hovering dynamics of the AEROCRANE in terms of the following dimensionless parameters in addition to β and μ defined above:

χ = ratio of centerbody radius to rotor radius, $\frac{R_B}{R}$

F_R = Froude number based on tip speed and rotor radius, $\frac{\Omega^2 R}{g}$

C_{WO} = weight coefficient, $\frac{W_o}{\rho\pi R^2 (\Omega R)^2}$

A = aerodynamic moment factor, $\frac{\rho\pi R^5}{I'}$

$\frac{I_z}{I'}$ = ratio of polar moment of inertia to pitch/roll moment of inertia

$\hat{\omega}_R^2$ = reference frequency, $\frac{W_o R_B}{\Omega^2 I'}$

$\hat{\omega}_{sL}^2$ = uncoupled sling load frequency, $\frac{g}{Z_L \Omega^2}$

$\bar{Z}_A$ = dimensionless location of sling load attachment point, $\frac{Z_A}{R_B}$

$\bar{r}_o$ = dimensionless location of center of gravity with respect to center of buoyancy

In addition to these parameters, the aerodynamic stability derivatives produced by the rotor enter the equations of motion. In non-dimensional form, three of the four moment derivatives are equal (Appendix B). That is,

$$\frac{2C_{M_\mu}}{a\sigma} = \frac{2C_{M_{A_{1s}}}}{a\sigma} = -\frac{2C_{M_{\hat{q}}}}{a\sigma}$$

Expressions for the two derivatives $\frac{2C_{M_\mu}}{a\sigma}$ and $\frac{2C_{L_\mu}}{a\sigma}$ are given in Appendix B. The moments are nondimensionalized by

$$C_{M,L} = \frac{M,L}{\rho\pi R^2 (\Omega R)^2 R}$$

The velocity and pitch rate are nondimensionalized by

$$\mu = \frac{u}{\Omega R}, \quad \hat{q} = \frac{q}{\Omega}$$

These non-dimensional derivatives are a function of aerodynamic thrust coefficient, blade lift curve slope, rotor solidity and centerbody radius to blade radius ratio. Their dependence on thrust coefficient is given in Figure B-1 for a solidity typical of AEROCRANE designs. The theory is developed in Reference 1 and described in Appendix B.

The radius of gyration of the vehicle in pitch, k_y, can be introduced to further reduce the number of dimensionless parameters.

$$k_y = \sqrt{\frac{I'}{m_o}}$$

Consequently two of the parameters given above, A and $\hat{\omega}_R^2$ can be expressed as

$$A = \frac{\rho \pi R^5}{I'} = \frac{3}{4} \frac{\beta}{\chi^5 \bar{k}_y^2}$$

$$\hat{\omega}_R^2 = \frac{W_o R_B}{\Omega^2 I'} = \frac{1}{F_R \bar{k}_y^2 \chi}$$

Alternate forms of the weight coefficient and the sling load frequency are

$$C_{WO} = \frac{W_o}{\rho \pi R^2 (\Omega R)^2} = \frac{4}{3} \frac{\chi^3}{F_R \beta}$$

$$\hat{\omega}_{SL}^2 = \frac{g}{Z_L \Omega^2} = \frac{1}{F_R \chi \bar{Z}_L}$$

Thus, the hovering dynamic stability characteristics, i.e., the dimensionless natural frequency of the motion, $\hat{\omega}_N$, and the damping ratio, ζ, of the AEROCRANE with sling load can be expressed functionally as

$$\hat{\omega}_N, \zeta = f\left(F_R, \beta, \frac{k_z}{k_y}, \bar{k}_y, \chi, \sigma, \bar{r}_o, \bar{Z}_A, \bar{Z}_L, \mu\right)$$

The first seven parameters are associated with the basic design of the AEROCRANE, and the last three are associated with the sling load and its attachment point.

Consider the influence of size on the dynamics of a series of geometrically similar AEROCRANES, i.e., vehicles with the same values of χ, σ, $\bar{r}_o$, $\bar{Z}_A$, $\bar{Z}_L$. To examine the changes in the dynamics which will occur with full size AEROCRANES in contrast to the model of Reference 1, four parameters must be considered: the buoyancy ratio, β; the radii of gyration $\bar{k}_z$, and $\bar{k}_y$; and the Froude number F_R.

The buoyancy ratio is largely a design choice. Present estimates of the size of this ratio for a large AEROCRANE are of the order of 1.4. This is a somewhat higher value than the dynamic model characteristics of Reference 1 where $1.14 < \beta < 1.19$. This variation would be expected as certain of the components employed in a model, e.g., the power plants tend to have a higher specific weight then the corresponding units on a full size vehicle.

Converting the thrust to weight ratio to a thrust to sling load (or payload) ratio from the equation above,

$$\frac{T}{W_{SL}} = 1 + \frac{1 - \beta}{\mu}$$

Selecting the buoyancy ratio as 1.42 and the sling load ratio as 0.84 gives a thrust to payload ratio of 0.5 as is characteristic of proposed AEROCRANE designs.

The radii of gyration might be expected to vary from the dynamic model characteristic of Reference 1 owing to different construction techniques which would be employed on a full size AEROCRANE. Largely the radii of gyration would depend upon the relative mass and mass

distribution in the blades and propulsion units compared to the center-body mass distribution. For the model of Reference 1, the complete moments of inertia were determined to be

$$I_z = 653 \text{ slug ft}^2$$

$$I' = 521 \text{ slug ft}^2$$

I' includes apparent inertia terms from the blades and center of gravity/center of buoyancy spacing amounting to 71 slug-ft^2. Subtracting this from the above, $I_y = 450$ slug ft^2. About 60 percent of this inertia arises from the nacelles and blades and about 25 percent from the instrumentation package. About 85 percent of the polar moment of inertia I_z is contributed by the blades and nacelles.

The radii of gyration for the model are

$$\bar{k}_y = 1.00 \text{ (without apparent inertia)}$$

$$\bar{k}_y' = 1.08 \text{ (including apparent inertia)}$$

$$\bar{k}_z = 1.21$$

It would be expected that a full size AEROCRANE would have similar inertial characteristics for the following reasons. A large contribution to the pitch/roll inertia would arise from the gondola crew station which would take the place of the instrumentation package on the model. The relative weight of the blades and nacelles would tend to be less than the model, however, the propellers would represent relatively more contribution to the inertia since the wooden propellers

employed on the model were very light. On balance it might be expected that the dimensionless radii of gyration of the model can be considered as a first approximation to the characteristics of a full size AEROCRANE in the absence of a detailed design. For reference, Table 1 shows the various contributions to the inertia of the model of Reference 1. The calculated value of the pitch inertia was verified by experiment.

Thus, the final parameter to be considered is the Froude number

$$F_R = \frac{\Omega^2 R}{g} = \frac{(\Omega R)^2}{Rg}$$

It may be noted that this parameter is a direct measure of the number of g's experienced at the tip of a rotor blade, or in other words, the g field in which the power plant must operate. Taking the radius as a measure of the size of the vehicle, the angular velocity is the remaining parameter. If the tip speed varies with size, i.e., proportional to the radius, what may be considered as a series of Froude scaled vehicles results, and the rotor RPM would vary inversely as the square root of the linear size of the vehicle. Further, the dimensionless dynamic characteristics (natural frequency ratioed to rotor angular velocity and damping ratio) would be invariant with size. Therefore, increasing the size of the AEROCRANE in this fashion would only result in a slower response time with no change in the stability. It is quite reasonable to expect this trend with size, based on the fact that the rotor thrust coefficient with full payload, would be invariant with size. From above

$$\frac{C_T}{C_{W0}} = (1 + \beta - \mu)$$

or

$$\frac{C_T}{\sigma} = \left(\frac{4}{3}\frac{\chi^3}{\sigma}\right)\frac{1}{F_R}\left(1 + \frac{(1-\mu)}{\beta}\right)$$

Thus, if the rotor and centerbody geometry (σ, χ) are invariant with size and the buoyancy ratio and payload ratio have been selected as noted, the average rotor blade lift coefficient[5] (proportional to $\frac{C_T}{\sigma}$) is determined by F_R.

The limitation which could be encountered is the fact that the tip speed increases with size to maintain the Froude number constant. However, this vehicle is designed with a low tip speed so that even for large increases in size from the model of Reference 1, only moderate tip speeds result. The tip speed of the model of Reference 1 was 61.7 feet per second nominally. For a large AEROCRANE ten times the size of this model (rotor radius 196.4 feet) the tip speed to maintain a constant Froude number and consequently the same blade lift coefficient is equal to 195 feet per second, a very moderate value compared to modern helicopter rotors.

Thus, it is considered that the dimensionless parameters of the model described in Reference 1 are reasonably representative of a full size AEROCRANE. Table II lists these dimensionless parameters along with those obtained in a recent design study for a full size AEROCRANE with a 16 ton payload. The dimensionless parameters of the 16 ton vehicle are used for the study of the influence of the sling load geometry on the hovering dynamics discussed in another section of this

report. The influence of the center of gravity position, $\bar{r}_o$, the sling load attachment point, $\bar{Z}_A$, and the sling load length $\bar{Z}_L$ are examined. The other parameters are considered fixed at the values given in Table II. The influence of size of the vehicle on the time scale of the motion is obtained by determining the rotor angular velocity from the Froude number given in Table II and the radius of the rotor for the size AEROCRANE of interest.

If an AEROCRANE equipped with winglets is considered, then an additional parameter is introduced. This is most conveniently expressed as the ratio of winglet area S_W to the product of blade chord and radius (cR). If it is assumed that the chord of the winglet is equal to the chord of the blade then this ratio becomes the ratio of winglet span to blade radius, i.e., the parameter $\bar{\bar{b}}_W$ introduced in Appendix A.

TABLE I

RELATIVE CONTRIBUTIONS OF COMPONENTS OF DYNAMIC MODEL TO WEIGHT AND MOMENT OF INERTIA

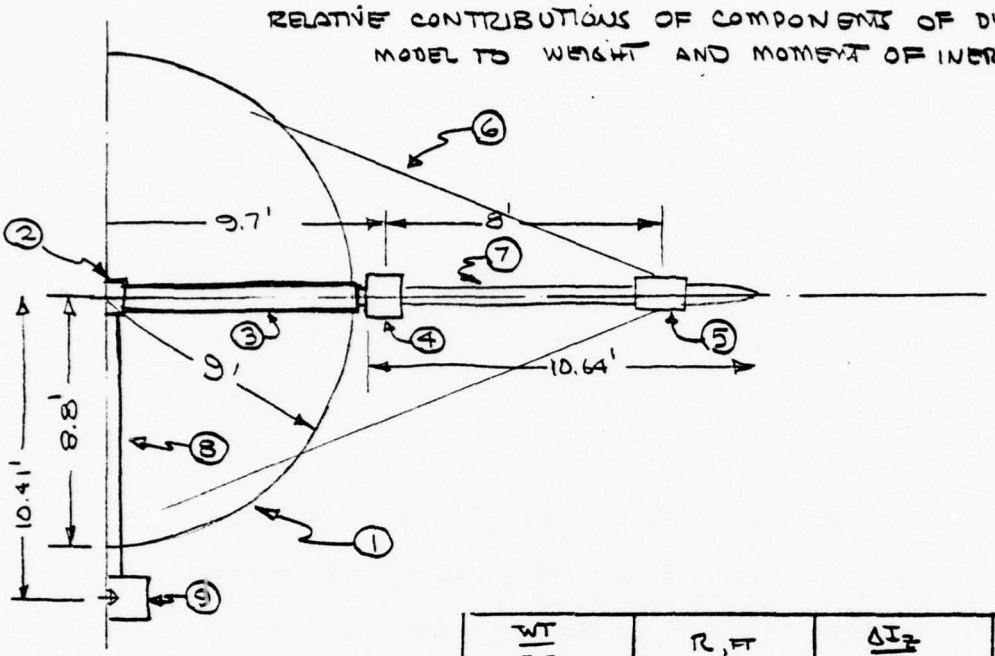

		$\frac{WT}{W_0}$	R, FT	$\frac{\Delta I_z}{I_z}$	$\frac{\Delta I_x^*}{I_x^*}$
①	GAS CONTAINING ENVELOPE	0.18	9 FT $I = \frac{2}{3}MR^2$	.08	.11
②	MANIFOLD	0.01	–	–	–
③	HORIZONTAL RADIALS	0.11	4.8 FT TO CG	.03	.02
④	BLADE PITCH SERVOS	0.05	9.7 FT	.04	.02
⑤	NACELLE ASSEMBLIES	0.16	11.7 FT	.42	.29
⑥	EXTERNAL CABLES	0.03	–	–	–
⑦	ROTATING WINGS	0.21	15 FT TO CG	.43	.30
⑧	SOUTH POLE	0.06	4.8 FT TO CG	0	.02
⑨	GONDOLA/ INST. PACKAGE	0.19	10.4 FT	0	.24

$W_0 = 176.8$ LBS

$I_z = 6532$ SLUG FT^2

$I_x^* = 474.6$ SLUG FT^2 [ABOUT CENTER OF BUOYANCY]

TABLE II

NON-DIMENSIONAL AEROCRANE PARAMETERS

	DYNAMIC MODEL OF REFERENCE 1	PROPOSED 16 TON DESIGN
$\chi = \frac{R_B}{R}$	0.46	0.43
$F_R = \frac{\Omega^2 R}{g}$	6.01	5.61
$\frac{I_z}{I'}$	1.25	1.25
$A = \frac{\rho\pi R^5}{I'}$	41.9	65.6
$B = A \frac{\bar{k}_y^2}{(1 + \frac{\beta}{2})} \chi^2$	6.48	9.20
$\beta = \frac{F_B}{W_o}$	1.14 - 1.19	1.42
$\bar{k}_y = \sqrt{\frac{I'}{m_o}} \frac{1}{R_B}$	1.08	1.14
$C_{W_o} = \frac{W_o}{\rho\pi R^2 (\Omega R)^2}$	0.0159(1)	0.0111
$\sigma = \frac{bc}{\pi R}$	0.138	0.142
$\bar{\omega}_R^2 = \frac{W_o R_B}{\Omega^2 I'}$	0.31(1)	0.31
$\mu = \frac{W_{SL}}{W_o}$	0.50 - 0.69(2)	0.84
$\frac{C_T}{\sigma}$	0.042 - 0.058(2)	0.0328

(1) Parameters shown for W_o = 177 lbs. only.

(2) Umbilical cable weight included as part of sling load.

HOVERING DYNAMIC STABILITY CHARACTERISTICS OF THE AEROCRANE

In this section, the dynamic stability characteristics of the AEROCRANE in hovering are described. The characteristic roots of the AEROCRANE are discussed as a function of the vehicle center of gravity location and sling load geometry. Results are presented based on the dimensionless parameters given in Table II for a 16 ton vehicle. Thus, the characteristic roots are presented divided by rotor angular velocity, Ω. For various size AEROCRANES with the non-dimensional characteristics given in Table II, the influence of size can be evaluated by determining the angular velocity corresponding to the gross weight of the size vehicle of interest.

The formulation of the dynamic model of the AEROCRANE is described in detail in Appendixes B and C. A linearized model with six-degrees-of-freedom (vehicle roll and pitch, horizontal and lateral velocity, sling load pitch and roll) is employed. It has been shown in Reference 1 that this analytical model accurately predicts the measured dynamic stability and response characteristics of a Froude scaled dynamic model, described by the dimensionless parameters given in Table II.

Figure 8, gives the characteristic roots and eigenvectors for the reference configuration. This reference configuration has the center of gravity located below the rotor hub at one-tenth the centerbody radius ($\bar{r}_o = 0.1$), the sling load is attached one centerbody radius below

the center of gravity ($\bar{Z}_A = 1.0$) and the nondimensional sling load frequency $\hat{\omega}_{SL}^2 = 0.195$ corresponding to a sling load length of 125 feet for the proposed 16 ton design. These geometric characteristics were employed for the analog simulation studies described in another section of this report.

There are five oscillatory modes involving significant components of all the variables of motion; one high frequency mode which is primarily an angular motion with negligible contributions from the translational velocities; two intermediate frequencies corresponding essentially to the sling load dynamics; and two low frequency vehicle modes.

All of the modes of motion are stable for the reference configuration. It can be noted from the eigenvector configurations that each lateral variable (e.g., vehicle roll angle and vehicle pitch angle) is 90 degrees out of phase and of equal amplitude indicating that the transient modes are circling motions, and can be identified by the direction of the circling compared to the direction of rotation of the vehicle.

The regressing vehicle and sling load modes are lightly damped compared to the advancing modes. The rapid angular mode and the advancing modes are well damped.

In the two low frequency modes, the sling load amplitudes relative to the vehicle are approximately eight-tenths of the angular motion of the vehicle, indicating that the sling load remains relatively near the vertical. In the rapid angular mode, the sling load amplitude is

approximately one and one half times the vehicle angular motion, indicating excitation of the sling load in rapid maneuvering. In the sling load modes the angular motion of the vehicle is approximately one quarter of the sling load motion indicating relatively weak coupling to the vehicle motion.

The influence of vehicle geometry variations on the characteristic roots are shown in Figures 9 through 10. In these complex plane graphs the modes of motion are shown only in the upper or lower half plane depending upon whether they are regressing (upper half plane) or advancing (lower half plane) modes for clarity.

Figure 9 shows the influence of vehicle center of gravity position. The sling load attachment point is maintained at a distance of one centerbody radius below the reference center of gravity position. It can be seen that lowering the center of gravity has a stabilizing effect on the low frequency modes as earlier studies indicated. The center of gravity position has a negligible influence on the sling load modes and a small effect on the rapid angular mode.

Figure 10 shows the influence of sling load attachment point ($\bar{Z}_A$) and sling load length (or sling load natural frequency) on the dynamics. Sling load natural frequency has only a minor influence on the low frequency modes and the rapid angular modes, but of course, causes marked changes in the sling load modes as would be expected. With the sling load attached at one centerbody radius below the center of gravity ($\bar{Z}_A = 1.0$) the modes of motion are stable for all sling load frequencies

investigated. Attaching the sling load at the vehicle center of gravity ($\bar{Z}_A = 0$) produces a destabilizing effect. The regressing low frequency mode is unstable. This is a result of a loss in effective pendulosity arising from placing the sling load attachment point at the center of gravity of the vehicle. In addition, as might be expected the regressing sling load mode is also mildly unstable. There is only a small influence on the rapid angular mode in either case.

The instability which arises is very mild. These analytical results assume no sling load damping. It would be expected that if a small amount of sling load damping were included these modes would be stable. Thus, from a dynamic stability viewpoint no advantage is to be gained from locating the sling load attachment point at the vehicle center of gravity. This is of course, a difficult configuration to achieve owing to the vehicle geometry.

All of the above results were obtained using a digital computer program. The real time simulation studies described elsewhere were conducted on an analog computer using the vehicle characteristics of the reference configuration described above. In addition, the analog model incorporated terms to account for the nonlinear effects of centerbody drag and Magnus force as well as a small amount of sling load damping relative to the vehicle ($\zeta_{s_L} = 0.1$). Winglets were incorporated in the analog model as well, using the theoretical model for winglet contributions described in Appendix A. Figure 11 shows the transient response of the vehicle to cyclic pitch and winglet deflection as obtained from the analog computer. The cyclic pitch response characteristics agree with the digital computer solutions for the characteristic roots

described above. The responses are shown however in real time (Ω = 1.15 rad/sec) for the 16 ton proposed design. Note that the sling load motion in response to a cyclic pulse is largely a result of the angular response of the vehicle.

The response to a winglet input is shown in Figure 11b. Here the time history exhibits considerably more damping as a result of the winglet contributions to the stability derivatives of the vehicle. In particular the winglet size chosen for the investigation ($\bar{\bar{b}}_W$ = 0.25), based on the considerations described in Appendix A result in a very large drag damping, (X_u = - 0.407) and a small increase in speed stability ($\Delta M_u \cong 0.001$). The large X_u results in a well damped low frequency mode as may be seen by comparing Figure 11b (with winglets) to Figure 11a (without winglets). Two other features of the transient response of the AEROCRANE to a winglet input may be noted. The rapid winglet pulse input results in considerable excitation of the sling load as a result of the initial translational acceleration produced by the winglet. Since the sling load has a significant mass compared to the mass of the vehicle this results in a coupling into the horizontal velocity as may be noted from the time history. Also as the vehicle translates forward in response to the winglet input, a significant pitch up occurs as a result of the speed stability of the rotor resulting in a considerably lower steady-state velocity from the winglet input than would be expected if the vehicle remained level. This result indicates that it would be desirable to incorporate attitude

feedback to cyclic to minimize the coupling arising from translation if the winglet controls are employed.

Gusts inputs were incorporated in the analog simulation as well. Unfortunately, no experimental data are available on the gust response of the AEROCRANE. In the absence of data, a simplified model was employed to estimate the influence of wind gusts on vehicle motion. Gust inputs were treated as equivalent to a change in the translational velocity of the vehicle and no attempt was made to account for the influence of the spatial velocity distribution of a gust field on the response of the vehicle.

Proper modelling of the gust response of AEROCRANE vehicles is a very significant aspect of precision hovering and experimental data are essential for future simulation studies.

Figure 12 shows the response of the 16 ton payload configuration with and without winglets to a step gust of 5 fps and a random gust with an RMS value of 5 fps.

A step gust input, while not physically realistic, does provide a good basis for comparison of the gust response of the vehicle with and without winglets.

It can be seen by reference to Figures 12a and 12b which show the response to a step gust, that with winglets, the initial translational velocity response is considerably faster. There is an initial horizontal acceleration due to the presence of the winglets and the vehicle reaches the steady-state velocity of 5 fps in a somewhat shorter time. With

winglets, the long period dynamics are well damped while in the winglet off case, the lightly damped oscillation persists. Figures 12c and 12d show the uncontrolled response of the vehicle with and without winglets for a random gust disturbance with a 5 fps RMS level. The amplitude of the response of the vehicle is similar in both cases however, with winglets there is a noticeable increase in the high frequency content of the response especially in the horizontal velocity time history. The presence of the winglets results in forces acting on the vehicle which are linearly proportional to velocity and in addition, the large value of X_u noted above results in a comparatively fast time constant in the translational response of the vehicle which is not present when the winglets are absent. This increase in the high frequency response to gusts would indicate that the vehicle equipped with winglets would experience higher structural loads in turbulent air.

The next section of this report describes the results of some real time simulation studies of the AEROCRANE with the vehicle dynamic characteristics illustrated in Figures 11 and 12.

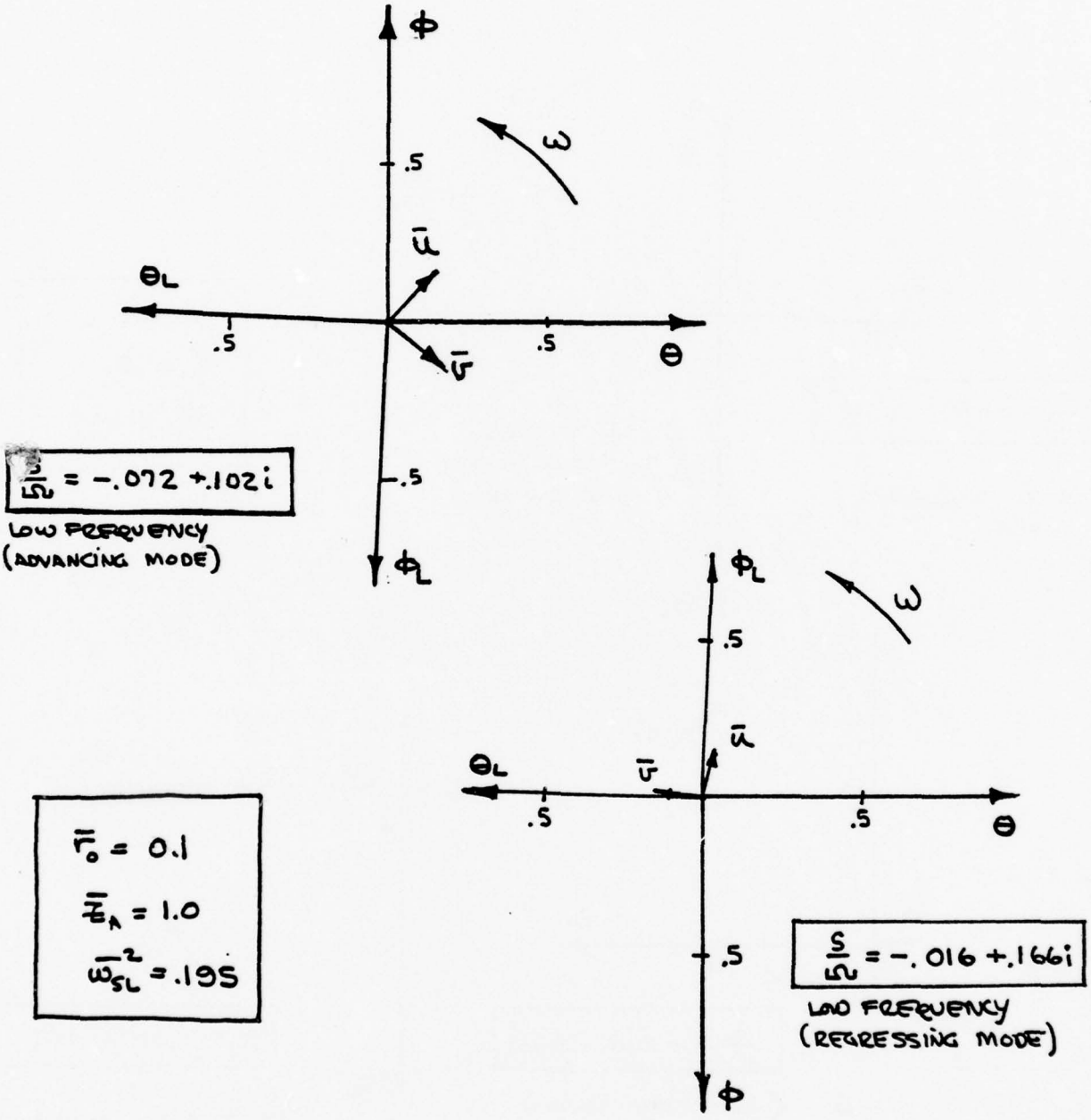

Figure 8a: Eigenvectors for Reference Case. Low Frequency Modes.

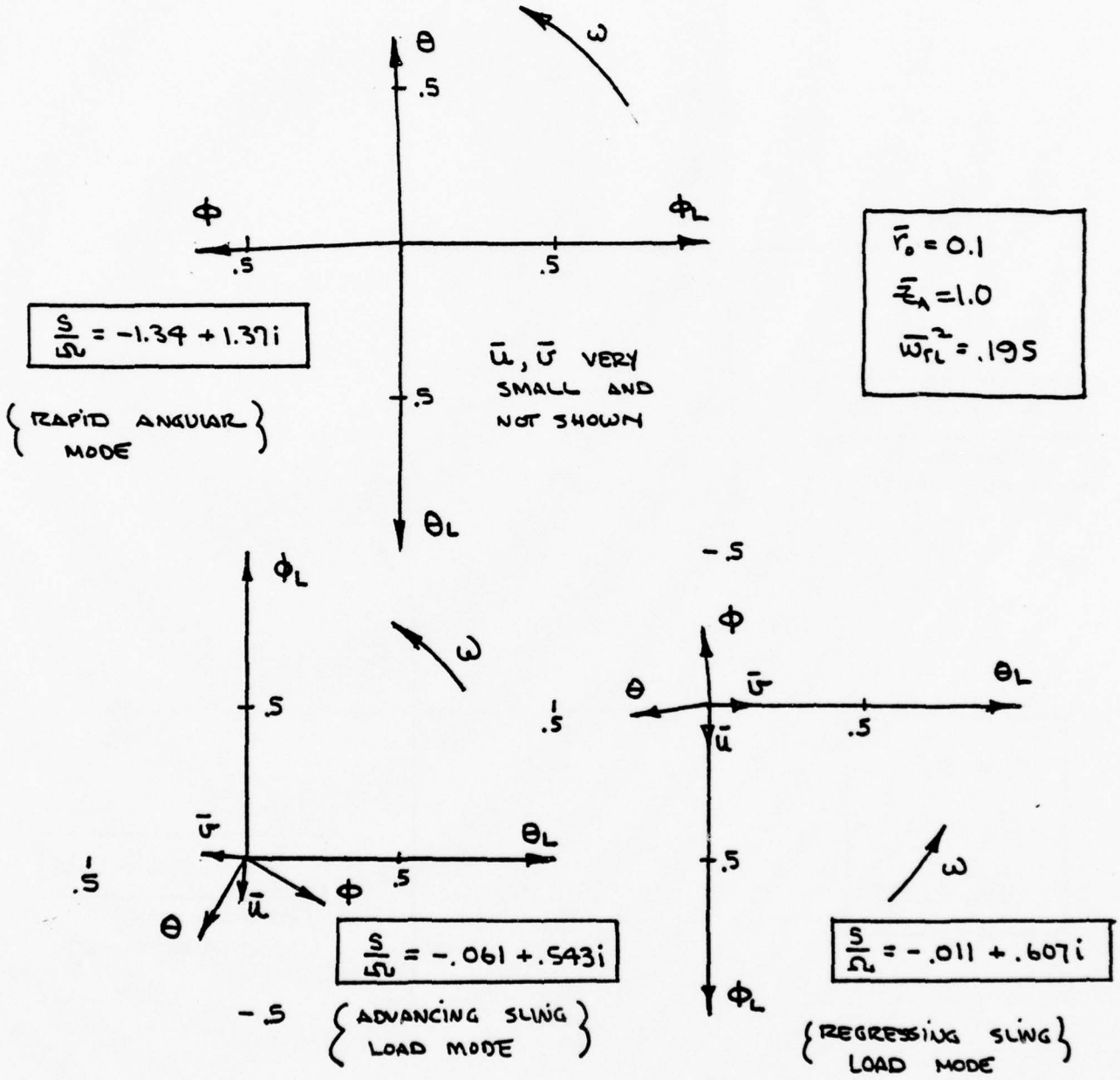

Figure 8b: Eigenvectors for Reference Case. Sling Load and High Frequency Modes.

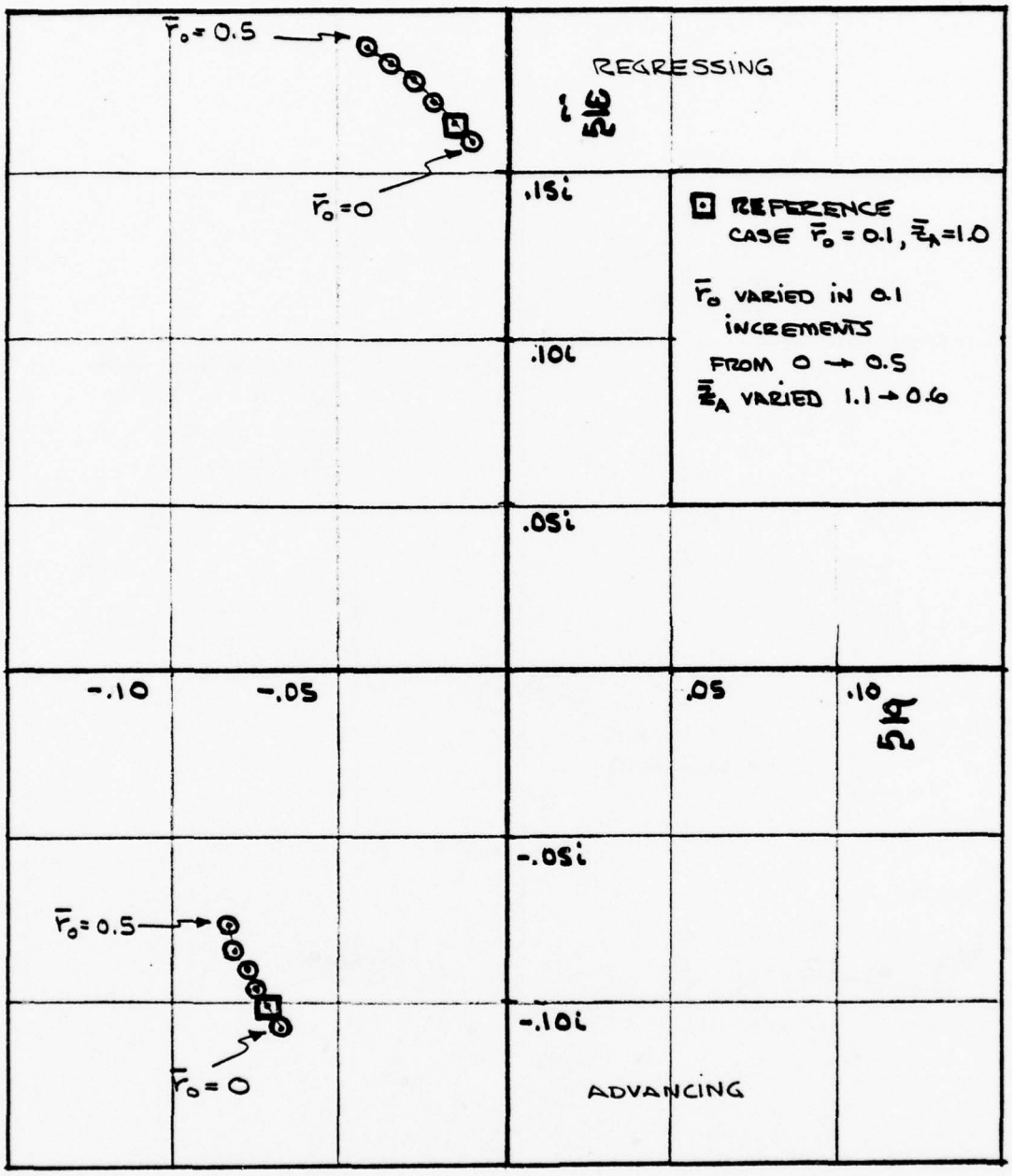

Figure 9a: Influence of Center of Gravity Location.
Low Frequency Modes.

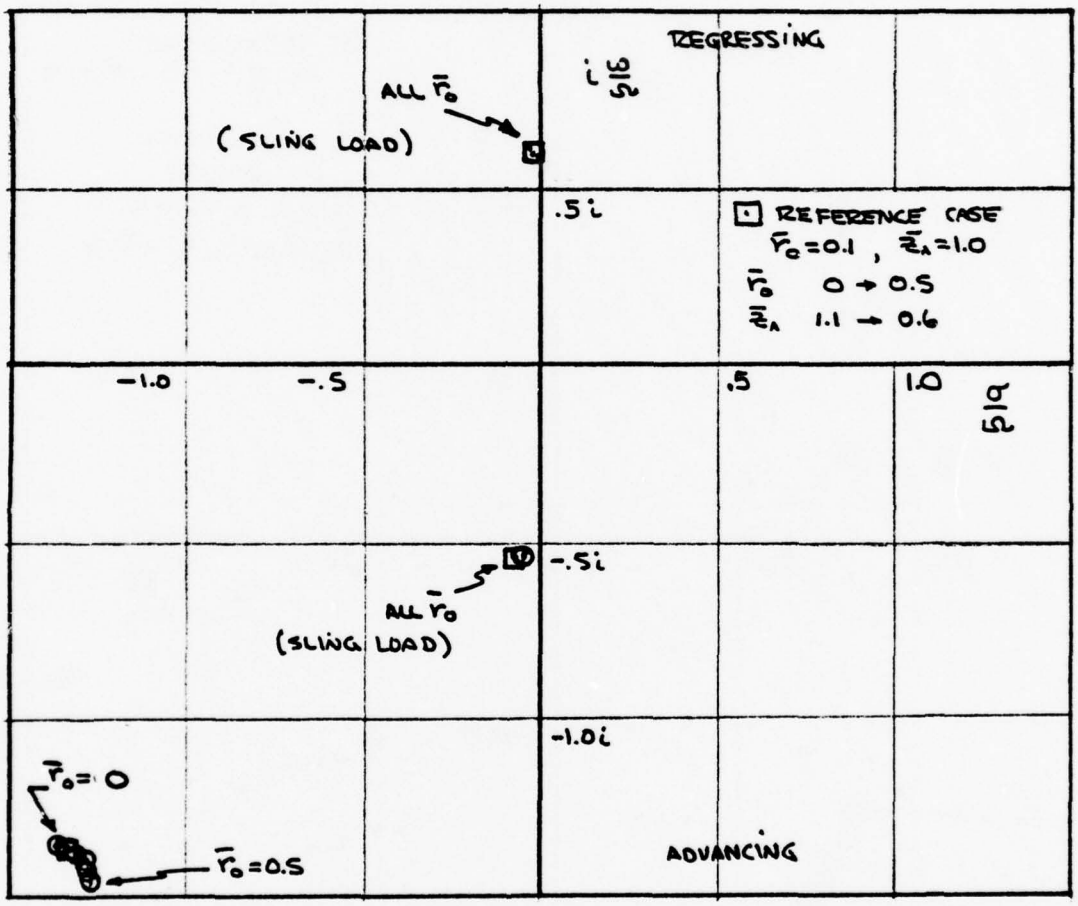

Figure 9b: Influence of Center of Gravity Location. Sling Load and High Frequency Modes.

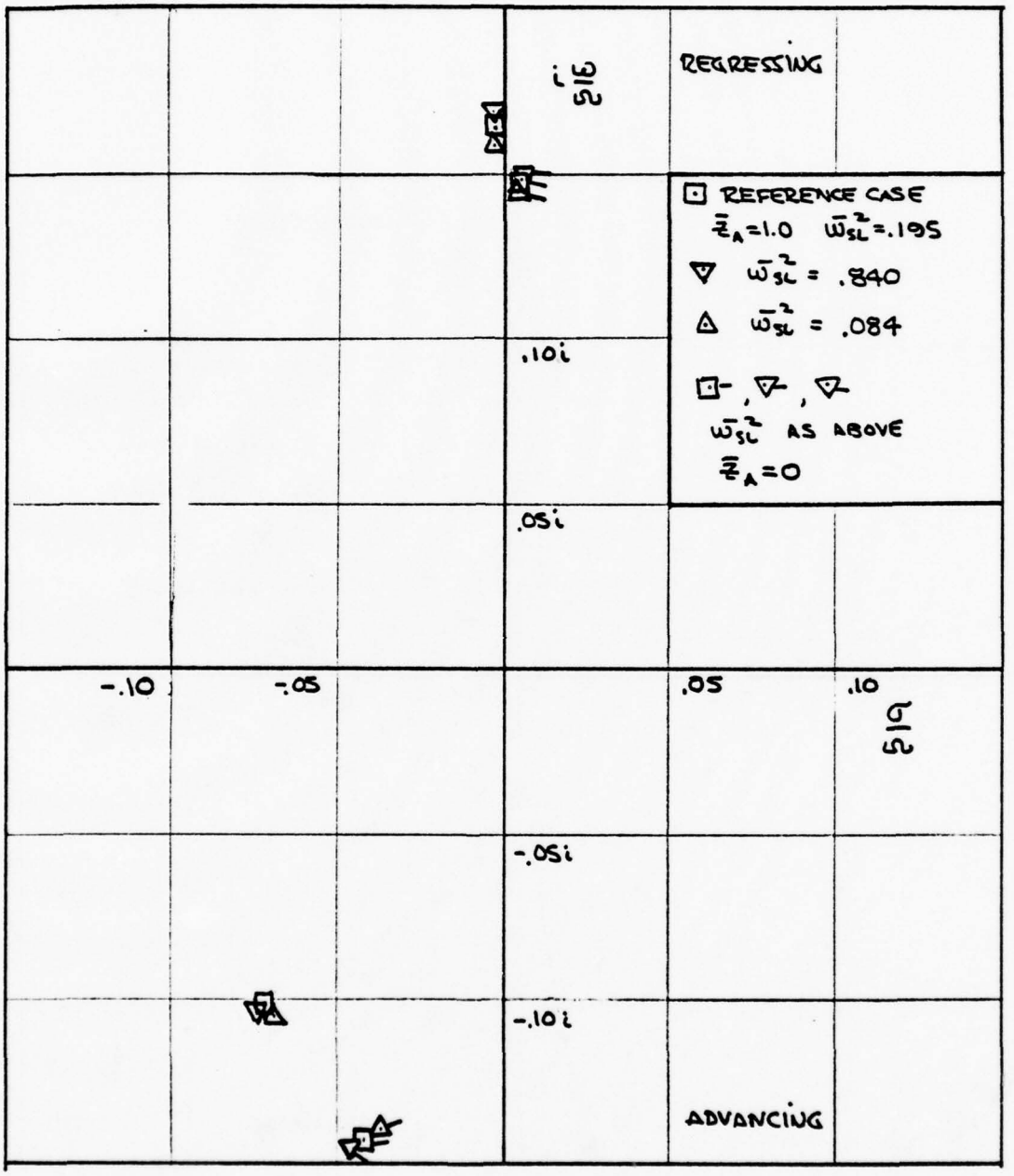

Figure 10a: Influence of Uncoupled Sling Load Frequency and Sling Load Attachment Point on Low Frequency Modes.

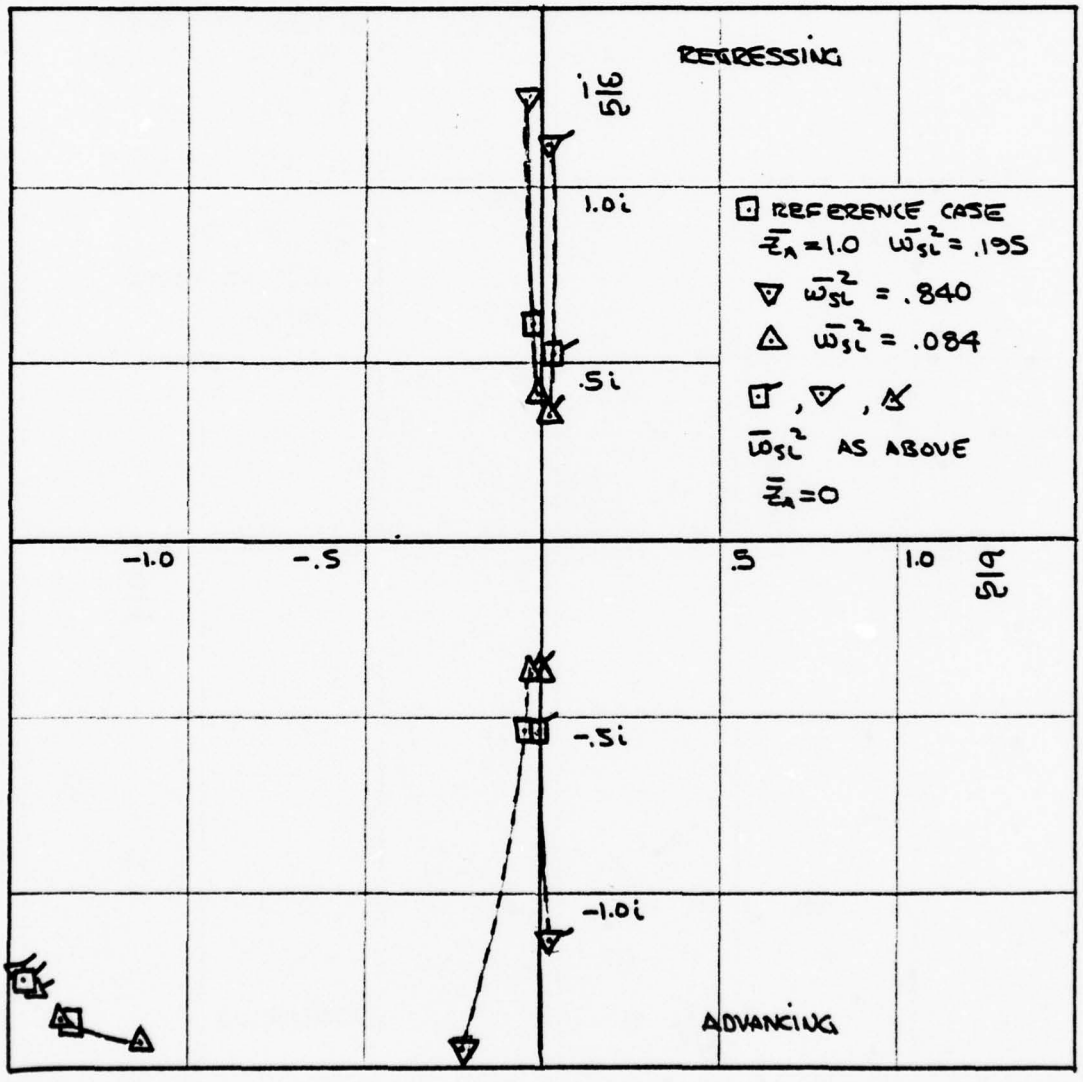

Figure 10b: Influence of Uncoupled Sling Load Frequency and Sling Load Attachment Point on Sling Load and High Frequency Modes.

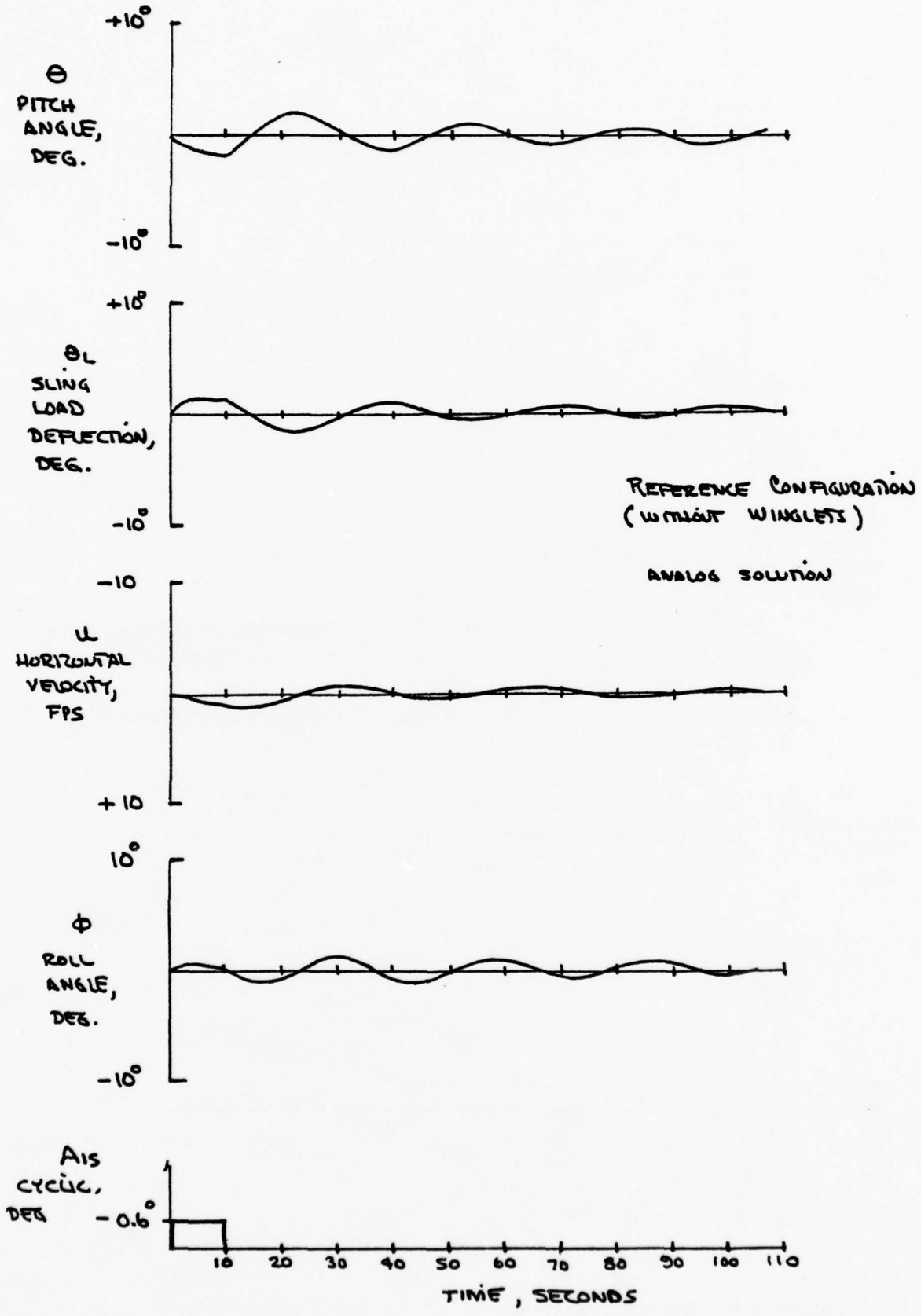

Figure 11a: Transient Response of 16 Ton AEROCRANE to Cyclic Pulse Input.

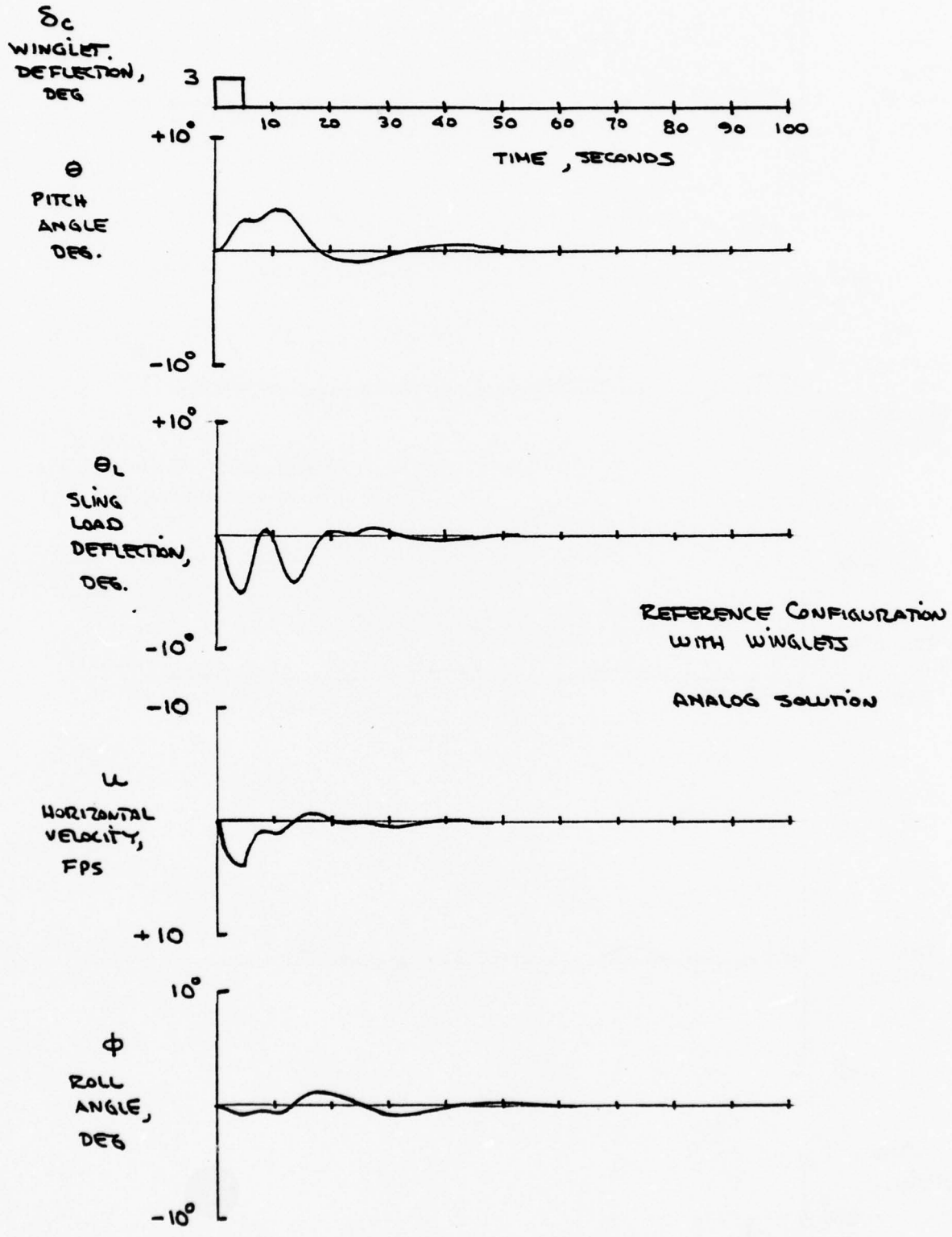

Figure 11b: Transient Response of 16 Ton AEROCRANE to Winglet Pulse Input.

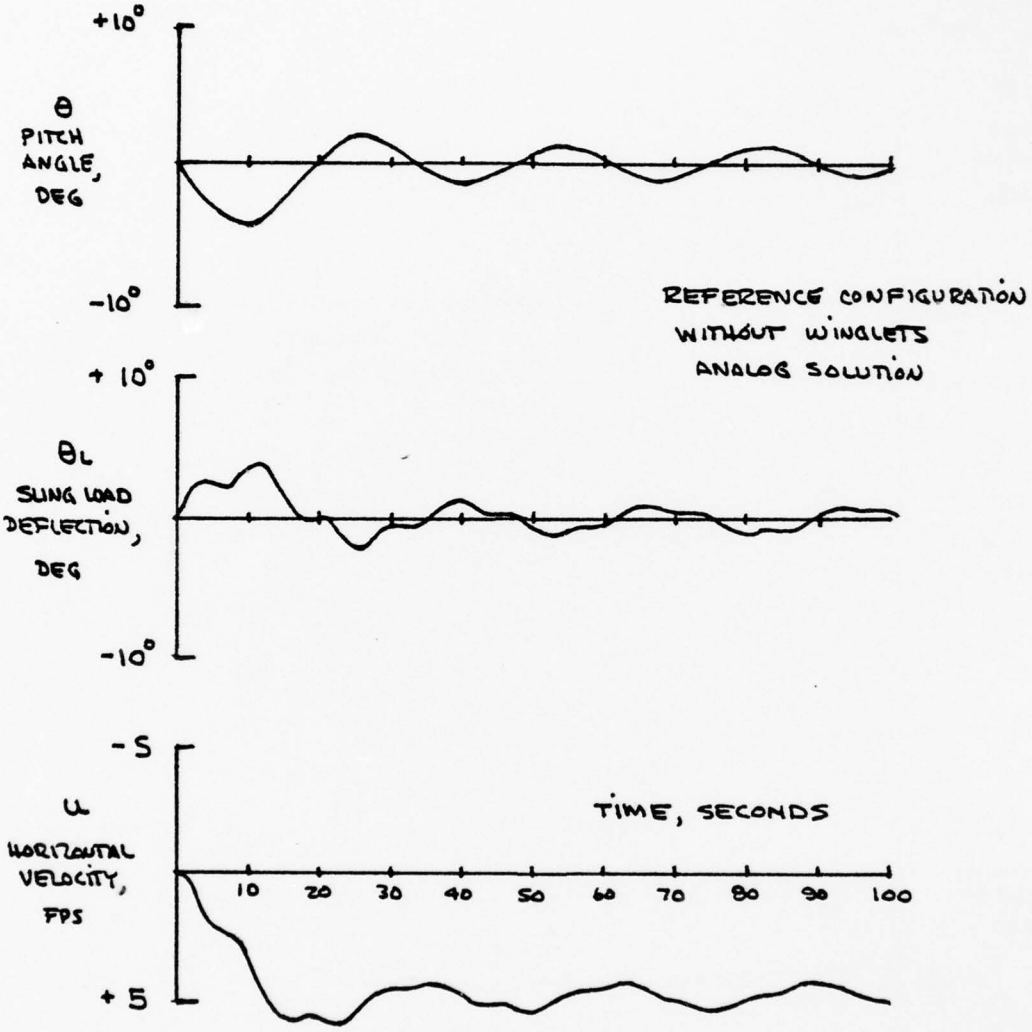

Figure 12a: Gust Response of 16 Ton AEROCRANE. Winglets Off. 5 fps Step Gust.

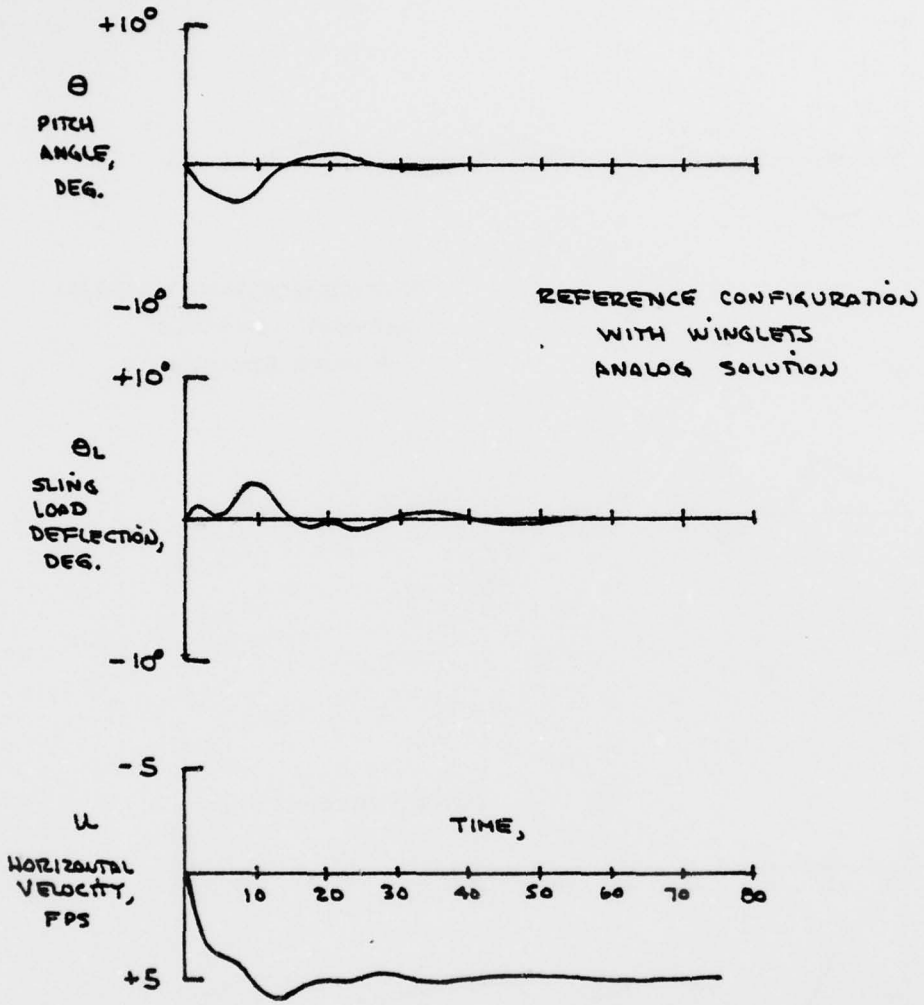

Figure 12b: Gust Response of 16 Ton AEROCRANE. Winglets On. 5 fps Step Gust.

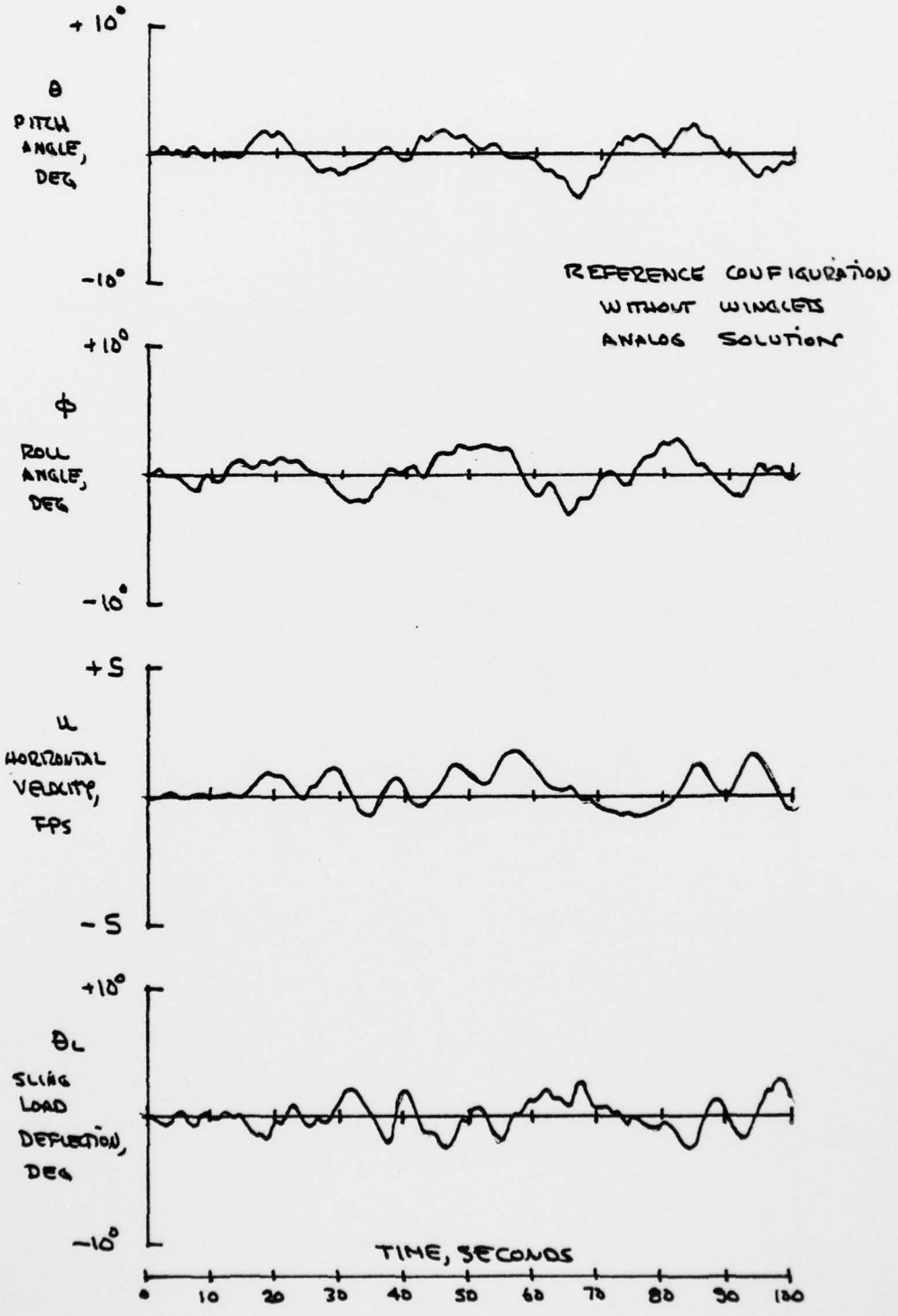

Figure 12c: Gust Response of 16 Ton AEROCRANE. Winglets Off. Random Gust. 5 fps RMS.

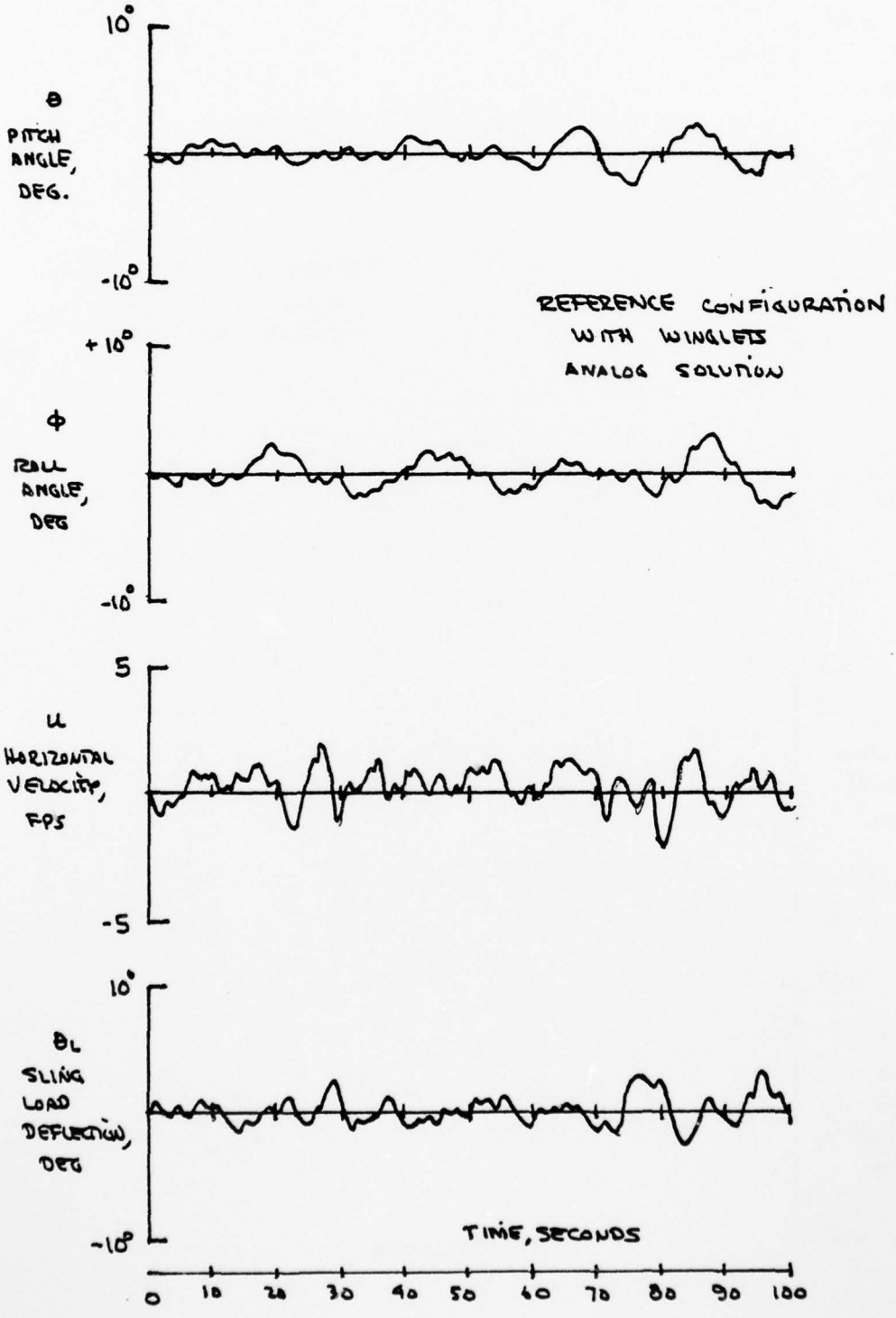

Figure 12d: Gust Response of 16 Ton AEROCRANE. Winglets On. Random Gust. 5 fps RMS.

SIMULATION STUDIES

An investigation of the handling qualities of the AEROCRANE in hovering flight was conducted using an analog computer to model the vehicle dynamics in and near hovering flight. The equations of motion programmed are described in the Appendixes. A six-degree-of-freedom model was employed including four-degrees-of-freedom for the basic vehicle and two-degrees-of-freedom for the sling load. A random gust input was employed to disturb the vehicle for certain of the experiments. Only the reference configuration was examined, and the vehicle parameters employed were those of a 16 ton proposed AEROCRANE design given in Table III.

The basic objective of this investigation was to obtain a comparison of the handling of the AEROCRANE in hover with the heavy lift helicopter (HLH) studies reported in Reference 3, and in addition, to compare the control of the AEROCRANE with cyclic pitch to control with winglets.

Consequently, two tasks were examined: hovering over a spot with the operator attempting to maintain a position in space in the presence of random gusts with an RMS level of 5 fps; and precision maneuvering, that is flying from one location to another.

It should be noted that the set-up involved was a very simple one. The longitudinal and lateral displacements of the vehicle in space were fed into an x-y plotter and the operator attempted to perform the task with only information on the position of the vehicle in space through a

proportional control stick. No simulated cockpit was employed and the operator did not have the benefit of any cues other than the motion of the vehicle as perceived on the x-y plotter. It is felt that this particular experimental set-up tends to make cyclic control in hovering inherently difficult.

In general, with cyclic control it was necessary to employ attitude feedback to be able to achieve any reasonable level of precision control as would be expected given the task. The attitude feedback employed was of a form found to be desirable as a consequence of the experimental results of Reference 1. That is, feedback of the form

$$A_{1s} = - K_A(\theta - \phi)$$

$$B_{1s} = K_A(\theta + \phi)$$

were employed with a gain $K_A = 0.3$ %. Basically it was found that using winglet control either of the tasks was relatively easy to perform, while with cyclic control both tasks were considerably more difficult. The addition of attitude feedback appeared to have only a small effect on the control task with winglet control. However, neither of the tasks could be accomplished with cyclic control without attitude feedback.

First consider the task of hovering over a spot. Figure 13 shows a comparison of the time history of hovering over a spot with winglet control to that with cyclic control. The gust level employed in these two cases was 5 fps RMS. The operator was able to keep the vehicle,

much of the time, within a one foot square using winglet control and only ocassionally was a two foot square exceeded. The total time of the experiment shown was five minutes and no attitude feedback was employed (recall that the vehicle has an inherent attitude feedback due to the center of gravity/center of buoyancy spacing). Thus, using winglet control it appears that the basic vehicle with no automatic stabilization can be very effectively hovered over a spot. In fact, indications from this experiment indicate the the winglets give precision control of a level similar to that achieved with a sophisticated automatic control system in the HLH simulation of Reference 3 as shown in Figure 14.

With cyclic control the situation was quite different. It was not possible to maintain a position within the scale of the x-y plotter (± 5 feet) for any length of time with the basic vehicle. With attitude feedback it was possible to maintain position within a 10 foot square for three minutes as shown in Figure 13. This appears to be somewhat poorer performance than indicated for the HLH with attitude hold as shown in Figure 14.

Now consider the other task, that of precision maneuvering from point to point at low speeds. The operator commenced flying at the center of the x-y plotter and then flew to a one foot square box at one location and then on to the next as shown in Figure 15. No gust inputs were employed in this task. Again with winglet control the task was relatively easy. No significant difference was noted between

the cases with and without attitude feedback. A relatively straight path between boxes was flown and there was no difficulty stopping and remaining within the box as shown in Figure 15. This behavior is quite similar to that indicated in Reference 3 for the HLH with the high gain velocity hold system as shown in Figure 14.

With cyclic control again the task proved impossible without attitude feedback. With attitude feedback a sample trace is shown in Figure 15. The task was still very difficult and a considerable amount of practice was required (approximately 20 minutes) to achieve the result indicated in the figure. It appeared to the operator that precision translation must be accomplished either at a very low speed or a very "high" speed. The operator noticed significant inputs from the sling load motion which complicated the control task. The difficulty with this task is clearly related to the problem area discussed in the section on sling load dynamics where, when low frequency control is attempted only a small translational acceleration is achieved. As higher frequency inputs are employed the translational acceleration decreases due to sling load motion and ultimately the phase of the attitude/acceleration response can reverse. It should be noted that this characteristic appears to be rather fundamental to precision control of vehicles which obtain an appreciable amount of their lift from buoyancy as noted in another section.

In order to ascertain in a simple fashion the importance of the sling load dynamics, the sling load damping ratio was increased to 0.5.

The operator noted that the sling load didn't tend to "throw the vehicle around" as much, and it was considerably easier to achieve the desired result of flying from place to place as shown in Figure 15.

It should also be noted that in all of these experiments the operator was controlling the center of gravity motion of the vehicle. The sling load motions corresponding to two typical runs are shown in Figure 15 indicating that there is considerable sling load motion. In addition, another feature of the hovering control of the AEROCRANE which may be of considerable importance is the influence of the location of the pilot in the actual vehicle with respect to the center of gravity of the vehicle, with respect to the hovering control problem. Some discussion of considerations in this regard can be found in Reference 10. It was not possible with the simple simulator employed in these studies to investigate this point.

TABLE III

PHYSICAL PARAMETERS OF 16 TON AEROCRANE USED IN ANALOG SIMULATION STUDY

1.) Overall Vehicle

W_o = 38,000 lbs.

F_B = 54,000 lbs.

I' = 5.40×10^6 slug ft^2

I_z = 6.75×10^6 slug ft^2

r_o = 5.9 ft.

2.) Rotor

R = 136.5 ft.

c = 15.25 ft.

Ω = 11 rpm (1.15 rad/sec)

a = 5.73

b = 4

T = 16,000 lbs.

3.) Centerbody

R_B = 59 ft.

C_D = 0.78

C_{LM} = 0.30

4.) Sling Load

W_{SL} = 32,000 lbs.

Z_A = 59 ft.

Z_L = 125 ft.

ζ_{SL} = 0.10

5.) Winglet*

C_W = 15.25 ft.

b_W = 34.13 ft.

a_W = 4.6

*Note that for the simulation studies involving cyclic, the winglets are removed from the model.

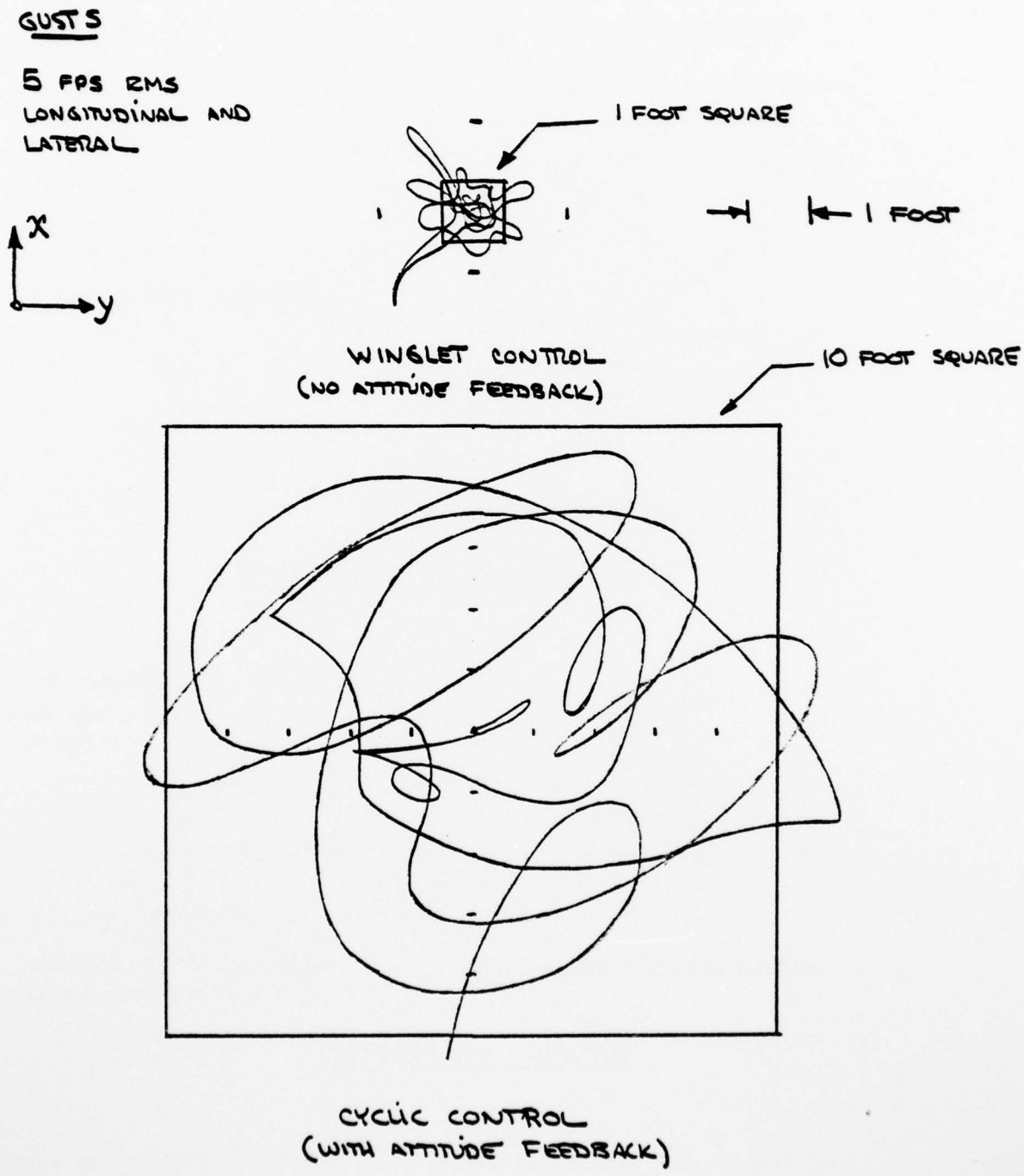

Figure 13: Comparison of Hovering Hold in Gust with Winglet Control and Cyclic Control. 16 Ton AEROCRANE.

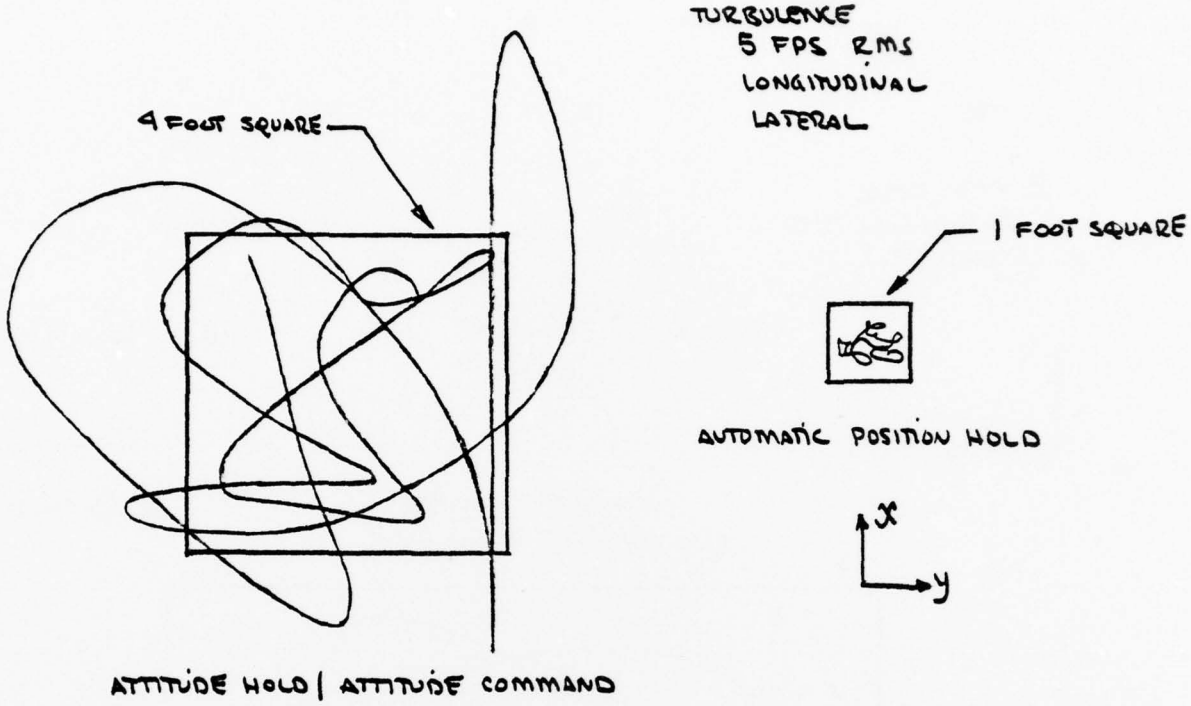

HOVERING HOLD IN TURBULENCE

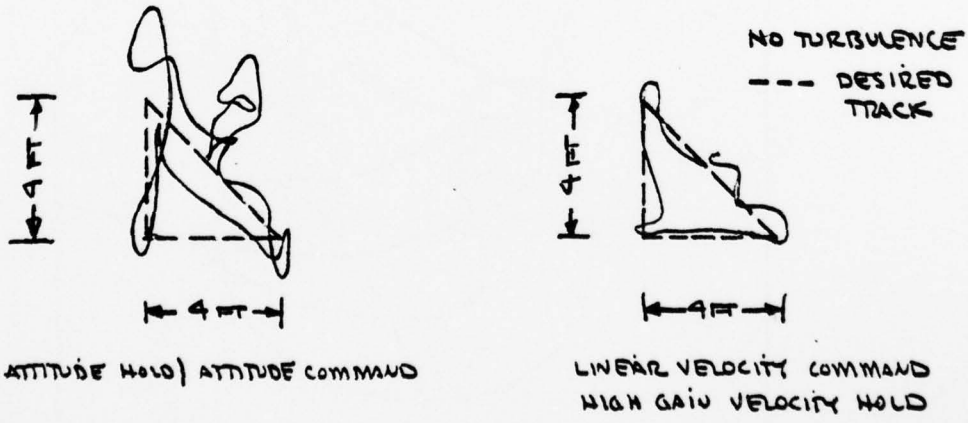

PRECISION MANEUVERING

Figure 14: Simulation Results for Heavy Lift Helicopter (Reference 3).

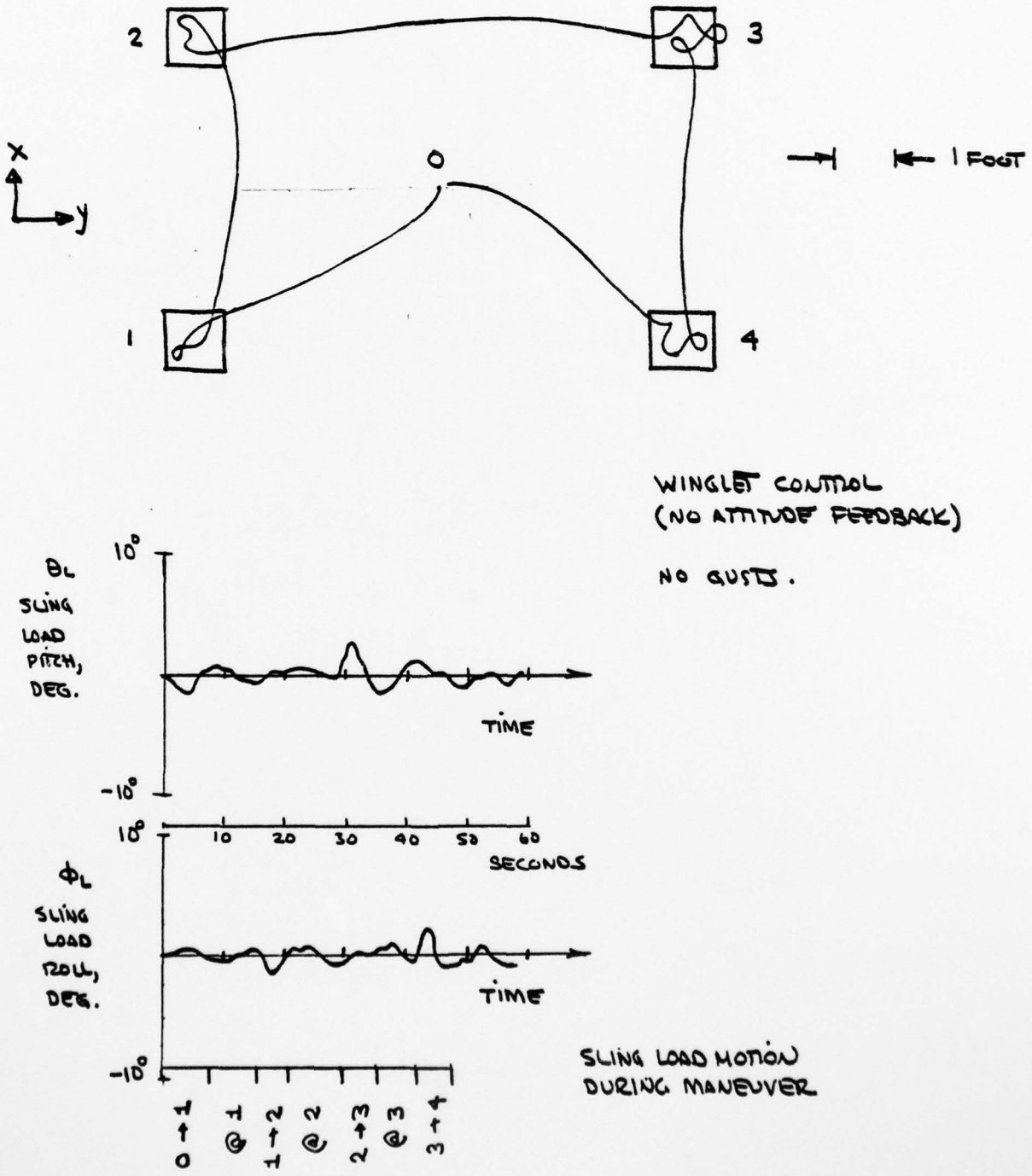

Figure 15a: Precision Maneuvering with Winglet Control. 16 Ton AEROCRANE.

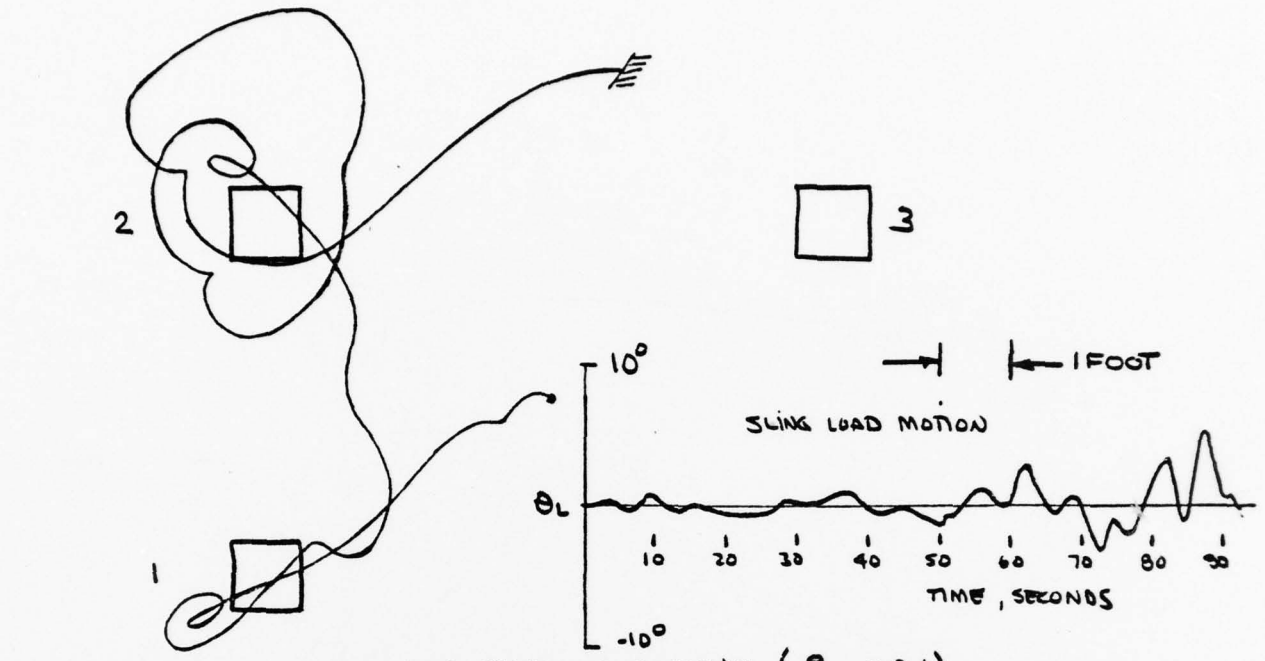

CYCLIC CONTROL
ATTITUDE FEEDBACK
NO GUSTS

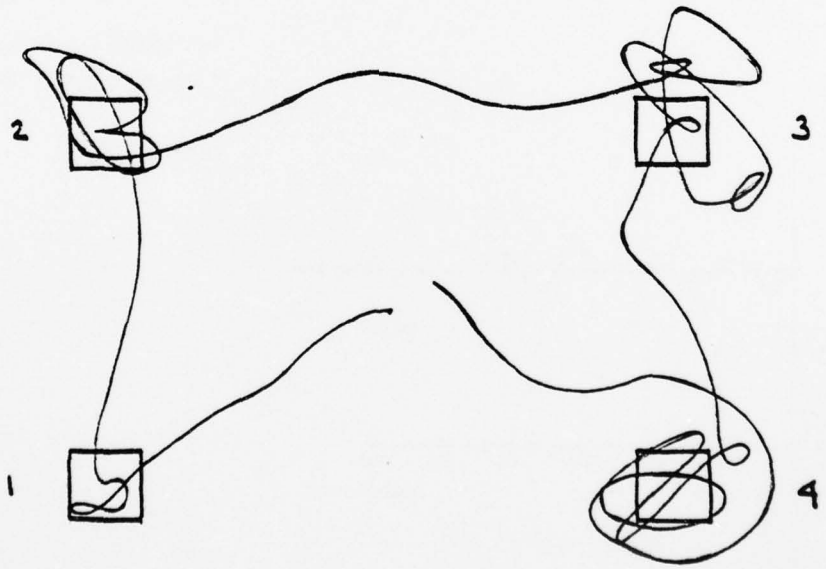

Figure 15b: Precision Maneuvering with Cyclic Control.
16 Ton AEROCRANE.

COMPARISON OF AEROCRANE HOVERING DYNAMICS WITH CONVENTIONAL HELICOPTERS

It is instructive to compare the hovering stability and control characteristics of the AEROCRANE with conventional helicopters of equivalent size. Reference 5 presents estimates of the stability derivatives of various large proposed tandem rotor helicopter designs with gross weights varying from 25 tons to 100 tons. Reference 4 presents the hovering stability and control derivatives for a 20 ton single rotor helicopter. Thus, to include single rotor in this discussion, an estimate of the variation of these derivatives with size of the vehicle must be made. As indicated in Reference 4, the variation of the stability and control derivatives of a conventional helicopter with gross weight, will be somewhat different than the variations indicated for the AEROCRANE primarily as a result of the fact that for various technical reasons all helicopters operate at about the same tip speed and consequently as the vehicle size is increased the tip speed is maintained constant rather than increasing with size as Froude scaling would indicate. The consequence of this on the variation of the important stability derivatives can be determined in the following way. Consider the variation of the three stability derivatives largely responsible for the longitudinal hovering dynamic characteristics of a vehicle; the pitch damping, M_q, the speed stability M_u, and the control effectiveness M_δ. Expressed in non-dimensional form:

AD-A054 281 PRINCETON UNIV N J DEPT OF AEROSPACE AND MECHANICAL--ETC F/G 1/3
A STUDY OF THE PRECISION HOVER CAPABILITIES OF THE AEROCRANE HY--ETC(U)
FEB 78 H C CURTISS, W F PUTMAN, R M MCKILLIP N62269-77-C-0074
UNCLASSIFIED AMS-TR-1363 NADC-76341-30 NL

2 OF 2
AD
A054281

END
DATE
FILMED
6 -78
DDC

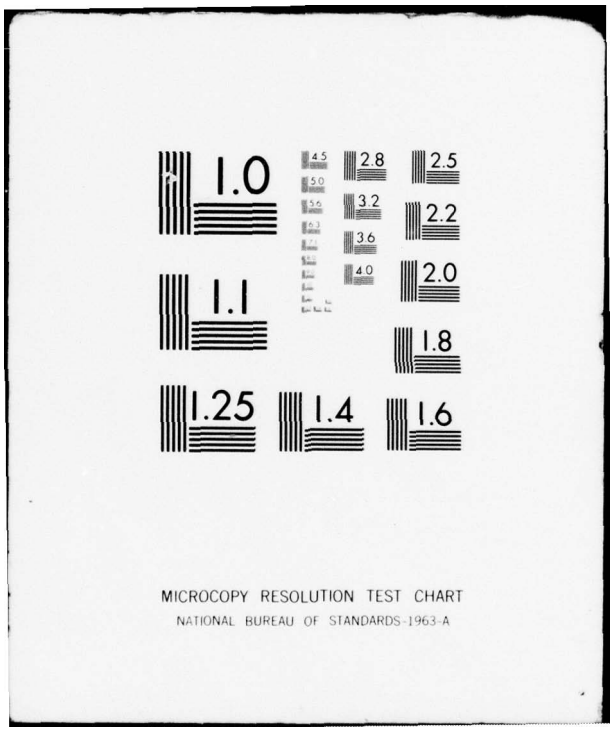
1.0
1.1
1.25
1.4
1.6
1.8
2.0
2.2
2.5
2.8
3.2
3.6
4.0
4.5
5.0
5.6
6.3
MICROCOPY RESOLUTION TEST CHART
NATIONAL BUREAU OF STANDARDS-1963-A

$$M_q = \left(\frac{\rho\pi R^2 (\Omega R)^2 R}{I_y}\right) \frac{1}{\Omega} C_{m_{\hat{q}}}$$

$$M_u = \left(\frac{\rho\pi R^2 (\Omega R)^2 R}{I_y}\right) \frac{1}{\Omega R} C_{m_{\mu}}$$

$$M_\delta = \frac{\rho\pi R^2 (\Omega R)^2 R}{I_y} C_{m_\delta}$$

$C_{m_{\hat{q}}}$, $C_{m_{\mu}}$, and C_{m_δ} will depend only upon the geometry of the helicopter. Thus, if a series of geometrically similar hovering vehicles are considered the variations in the three dimensional derivatives with size can be expressed as

$$M_q \sim \frac{R^4 V_T}{I_y}$$

$$M_u \sim \frac{R^3 V_T}{I_y}$$

$$M_\delta \sim \frac{R^3 V_T^2}{I_y}$$

where $V_T = \Omega R$

For the conventional helicopter it may be assumed that V_T is independent of size (Reference 4), consequently

$$M_q \sim \frac{R^4}{I_y}$$

$$M_u, M_\delta \sim \frac{R^3}{I_y}$$

Defining the ratio of the gross weight of one helicopter to another of similar geometry as

$$w = \frac{W_1}{W_o}$$

Reference 4 indicates that as the helicopter gross weight is increased, the linear dimensions grow as the square root of the weight ratio

$$\frac{R_1}{R_o} = w^{\frac{1}{2}}$$

The moments of inertia increase with gross weight with a power somewhat less than the gross weight ratio squared.

$$\left(\frac{I_1}{I_o}\right)_y \cong w^{1.9} \qquad \left(\frac{I_1}{I_o}\right)_x \cong w^{1.6}$$

Substituting these ratios into the above expressions it is found that

$$\frac{M_{q_1}}{M_{q_o}} \sim w^{.1} \qquad \frac{L_{p_1}}{L_{p_o}} \sim w^{.4}$$

$$\frac{M_{u_1}}{M_{u_o}} \sim \frac{M_{\delta_1}}{M_{\delta_o}} \sim w^{-.4} \qquad \frac{L_{v_1}}{L_{v_o}} \sim \frac{L_{\delta_1}}{L_{\delta_o}} \sim w^{-.1}$$

The pitch damping is approximately independent of size. The speed stability and the pitch control power decrease with increasing gross weight varying approximately as the square root of the gross weight. Table I of Reference 4 indicates that these simple relationships give the dominant trends in the pitch derivatives. The roll derivatives vary somewhat differently owing to the smaller increase in roll inertia with weight.

For the AEROCRANE a somewhat different dependence is obtained. In particular, since the tip speed of the AEROCRANE is low, the variations in these quantities are somewhat different. It has been assumed that a series of Froude scaled vehicles is being considered, such that

$$\frac{R_1}{R_o} = w^{\frac{1}{3}}$$

$$\frac{V_{T2}}{V_{T_o}} = w^{\frac{1}{6}}$$

$$\frac{I_1}{I_o} = w^{\frac{5}{3}}$$

There is no difficulty encountered with increasing the tip speed as required by Froude scaling, and in this case the linear dimensions grow as the cube root of the weight. The average rotor blade lift coefficient $(\frac{C_T}{\sigma})$ is independent of size. Note that if constant tip speed is assumed, the rotor radius grows as the square root of the gross weight to maintain the same blade lift coefficient. In this case the following derivative variations result.

$$\frac{M_{q_1}}{M_{q_o}} = w^{-\frac{1}{6}}$$

$$\frac{M_{u_1}}{M_{u_o}} = w^{-\frac{1}{2}}$$

$$\frac{M_{\delta_1}}{M_{\delta_o}} = w^{-\frac{1}{3}}$$

Thus in Froude scale all of the derivatives are reduced, the largest reduction occurring in the speed stability. It may be recalled that in the Froude scaled case there is no change in the dimensionless vehicle dynamics, that is, only the time scale of the motion changes.

Table IV lists the derivatives for various size vehicles. The values for the tandem helicopter are taken from Reference 4. The values for the single rotor are taken from Reference 10 for a 20 ton vehicle (S-65) and then are scaled to a 100 ton vehicle using the constant tip speed scaling described above. The AEROCRANE derivatives are based on the Froude scaling given above.

There are some other fundamental differences between the AEROCRANE and helicopters to be noted before discussing the influence of these various derivatives on the motion. First it may be noted that the influence of the speed stability on the dynamics will be considerably less for the AEROCRANE than for the helicopter owing to the fact that the vehicle is supported in part by buoyancy. The influence of the speed stability is largely to cause an unstable dynamic motion, however it appears in the equations of motion multiplied by the factor $\frac{T}{m}$ which for a conventional hovering helicopter is equal to g, the acceleration of gravity. Owing to the buoyant force, this multiplying factor is essentially equal to

$$\frac{W_o + W_{sL} - F_B}{m'} = g\left(\frac{1 + \mu - \beta}{1 + \frac{\beta}{2}}\right) .$$

It has been assumed for comparison purposes that the payload is rigidly

attached to the vehicle or in other words, that $\theta = \theta_t$ which is approximately true in the long time dynamics. Consequently this factor, which appears multiplied times M_u in the characteristic equation, is about 25 percent of g for the parameters assumed for the AEROCRANE and consequently there is less influence of M_u on the characteristic roots. Another way of understanding this effect is that with a buoyant force, less translational acceleration is produced by the AEROCRANE as a result of pitch and consequently there is a smaller velocity excursion associated with pitch and consequently less impact of M_u on the dynamics.

One further aspect of the AEROCRANE tends to improve the inherent dynamics of the AEROCRANE compared to hovering helicopter and that is the fact that the center of gravity is located below the center of buoyancy and consequently there is some inherent attitude stability which is no present on a conventional helicopter without attitude feedback.

Certain other considerations also result in differences in the dynamic behavior. Consider the short time steady-state degree-of-freedom motion with a step input in cyclic. Using the dimensionless aerodynamic derivatives for the AEROCRANE from Appendix B

$$- C_{m_{\hat{q}}} = C_{m_{A_{1s}}}$$

Consequently when the vehicle has attained a steady pitch rate

$$M_q \dot{\theta} + M_{A_{1s}} A_{1s} = 0$$

Using the relationships given above for the dimensional derivatives

taken with the equality of the non dimensional derivatives, the equation above becomes

$$\frac{\dot{\theta}}{\Omega} - A_{1s} = 0$$

$$\dot{\theta} = + \Omega A_{1s}$$

that is, the short time angular rate developed by a cyclic input is directly proportional to the rotor angular velocity. Consider now a simple model for the single rotor helicopter. Assuming that the total moment applied to the single rotor helicopter is proportional to longitudinal flapping, the equation for the flap angle can be written as

$$\Delta a_{1s} = - \frac{16}{\gamma\Omega} \dot{\theta} - B_{1s}$$

A steady angular rate implies that there is no moment applied to the helicopter, consequently $\Delta a_{1s} = 0$. Therefore

$$\dot{\theta} \cong - \frac{\gamma \Omega}{16} B_{1s}$$

γ is the order of 10 for the single rotor helicopter discussed in Reference 10, consequently

$$\dot{\theta} \cong - \frac{5}{8} \Omega B_{1s}$$

and a result of similar form to the AEROCRANE is obtained. This approximate result also applies to the single rotor helicopter and the tandem helicopter in roll. For the tandem helicopter in pitch

a somewhat different expression results since both control, which is obtained from differential collective pitch, and damping arise from thrust variations. Assuming a tandem helicopter with the center of gravity located midway between the two rotors, the dimensionless derivatives are approximately given by

$$C_{m_{\hat{q}}} \cong \frac{4}{3} \frac{\ell^2}{R^2} C_{T_{\theta_o}}$$

$$C_{m_{\delta}} = 2 \frac{\ell}{R} C_{T_{\theta_o}}$$

where ℓ is the distance from the rotor hub to the center of gravity. Consequently for equilibrium

$$\frac{1}{\Omega} \frac{4}{3} \left(\frac{\ell}{R}\right)^2 C_{T_{\theta_o}} \dot{\theta} + 2 \frac{\ell}{R} C_{T_{\theta_o}} \Delta\theta_o = 0$$

consequently

$$\dot{\theta} = \frac{3}{2} \frac{\ell}{R} \Omega \Delta\theta_o$$

In Reference 4, $\frac{\ell}{R} = 0.76$ and therefore

$$\dot{\theta} = 1.14 \Omega \Delta\theta_o$$

Thus, it can be seen in all three cases that the fundamental parameter determining the angular steady-state rate for a given control input is the rotor RPM. Consequently the AEROCRANE with its lower tip speed will tend to develop a smaller pitch rate for a given physical control

deflection than the conventional helicopter, i.e., a larger cyclic deflection with stick motion will tend to be desirable.

The 16 ton payload AEROCRANE has a rotor RPM of 11 (1.15 rad per sec) whereas the 40 ton gross weight tandem has a rotor RPM of 19.8 rad per sec indicating a considerably larger pitch rate for a given angular deflection of the control.

The actual derivatives give a steady rate due to cyclic of 7.0 degress per sec/inch. To achieve this value on the AEROCRANE would require for a rotor RPM of 11, a gearing of the order of 6 degrees of cyclic per inch of stick. The implications of this are discussed below in terms of handling qualities.

Comparison of the AEROCRANE damping and control sensitivity in hovering with the tandem helicopter characteristics given in Reference 4 and the single rotor data given in Reference 10 is shown in Figure 16. The single rotor data given in Reference 10 is for a 20 ton vehicle (S-65) for the roll axis only. To obtain pitch axis characteristics it is assumed that the ratio of pitch inertia to roll inertia is 4.5 and that the longitudinal stick gearing is 2.5 times the lateral stick gearing. The characteristics of a 100 ton single rotor were obtained by scaling the 20 ton vehicle using the parameter variations with gross weight given in Reference 4 and described above. Reference 10 indicates a similar variation in roll inertia for the single rotor as Reference 4 indicates for the tandem. For comparison purposes, the control gearing of the AEROCRANE was taken

to be three degrees of cyclic per inch of control deflection. This gearing is chosen for comparison purposes only.

Also shown on Figure 16 are the $3\frac{1}{2}$ pilot rating boundaries determined by the handling qualities experiments reported in Reference 11 for a 15 ton single rotor helicopter.

It should be kept in mind in the following discussion that this is the largest helicopter for which handling qualities data are available. The Military Specification for Helicopter Flying and Ground Handling Characteristics (MIL-H-8501A) indicates a downward trend of damping and control sensitivity with size and it is concluded in Reference 11 that the results presented there generally support the desirable trends indicated in MIL-H-8501A. It should be noted that the criteria of MIL-H-8501A were derived from flight experiments on a 2.5 ton helicopter. It should also be noted that the AEROCRANE differs in two respects from the conventional helicopters:

1.) Center of gravity/center of buoyancy spacing provides an inherent attitude stability (M_θ and L_ϕ) which will influence judgements on handling qualities.

2.) The translational acceleration of an AEROCRANE per degree of tilt is about one-sixth of that of a helicopter.

The presence of some attitude stability is certainly in a favorable direction. It is difficult to assess the impact of the translational

acceleration-attitude relationship.

Figure 16 shows then the comparison of these vehicles. Generally the AEROCRANE characteristics place it on the left of the graphs of damping vs. control sensitivity compared to the helicopters. The AEROCRANE in general has a very high level of angular damping about both axes and a low control sensitivity for the assumed stick gearing. It does however lie quite close to the visual flight $3\frac{1}{2}$ pilot rating boundaries. Its characteristics are essentially on the pilot rating boundary in the roll case and somewhat outside the pitch boundary. The characteristics of the AEROCRANE relative to the helicopters is primarily a result of the low rotor angular velocity described above.

Figure 17 shows a comparison of the AEROCRANE damping and control sensitivity characteristics compared to the boundary given in Reference 11 along with that of Reference 12 (MIL-H-8501A). It can be seen that both AEROCRANE vehicles examined essentially meet the specifications of MIL-H-8501A. The relationships given in MIL-H-8501A were evaluated for a 35 ton gross weight vehicle in the case of the 16 ton payload AEROCRANE and a 109 ton gross weight vehicle for the 50 ton payload configuration. Again it should be emphasized that applying the criteria of Reference 12 to vehicles of this gross weight represents a considerable extrapolation from the vehicle on which the data are based (2.5 ton) as well as the vehicle of Reference 11 (15 ton). As an example, the minimum values of the angular damping derivatives given by Reference 12 are

$$M_q = -8\, I_y^{-.3} \qquad\qquad L_p = -18\, I_x^{-.3}$$

For the 16 ton and 50 ton AEROCRANE these expressions give:

for the 16 ton payload vehicle

M_q = - 0.076 per sec $\qquad$ L_p = - 0.172 per sec

and for the 50 ton payload vehicle

M_q = - 0.043 per sec $\qquad$ L_p = - 0.097 per sec

These required levels of damping indicated in Reference 12 are essentially more than a factor of 10 less than the values estimated for the AEROCRANE. As can be seen by this comparison as well as from the Figures, the AEROCRANE possesses a very high level of angular damping and so it appears difficult to draw detailed conclusions from this comparison with other vehicles as well as with the specifications. Increasing the stick gearing above the value assumed for the AEROCRANE will place the vehicle well within the criteria of Reference 12, however there is a significant extrapolation involved both as a result of the very large size of the vehicle and the two unique characteristics noted above to assume that meeting the specifications of MIL-H-8501A will produce satisfactory handling qualities in hovering.

The roll and pitch axes of the AEROCRANE are coupled as they are on a single rotor. The tandem essentially has little or no pitch/roll coupling. The coupling levels of the AEROCRANE are similar to those indicated in Table III for the single rotor. In both cases, the coupling derivatives (L_q, M_p) are of a similar size to the damping derivatives (M_q, L_p).

The speed stability and dihedral effect of the AEROCRANE are larger than the values for the tandem indicating a larger gust sensitivity. However, recall that the AEROCRANE will have less translation as a result of pitching so that it is difficult to completely compare the implications of this difference. The speed stability of the AEROCRANE is about three times that of the tandem, however pitch of the AEROCRANE gives about one-sixth the translational acceleration of the tandem so the net effect of a horizontal gust acting through the speed stability on the translational acceleration is of a similar size.

In the case where winglet control is used it is more difficult to find criteria regarding handling qualities. Reference 13 indicates that for aircraft which use direct side force as a primary lateral positioning device, the direct side force control should be sufficiently powerful to obtain lateral acceleration values between 0.08 and 0.12 g in wings-level flight. The winglet size employed in the analog simulation studies, had a control sensitivity of X_{δ} = 1.16 ft per second squared per degree, indicating that a winglet deflection of 3° would produce a satisfactory level of translational acceleration. Again, it should be noted that this value was derived from handling qualities studies on a 2 ton aircraft. It is also noted in Reference 13 that "information is needed for side-force controls on attitude-stabilized aircraft before generalizations to other aircraft can be made".

The analog simulation studies reported here used a total winglet deflection of 3° resulting in a maximum acceleration equal to the value

indicated in Reference 13. The simulation studies indicate that this level of acceleration is quite satisfactory and therefore, considerably smaller winglets could be employed for maneuvering in hover. The winglet required for level trim in forward flight with a spherical centerbody appears to result in larger size winglets than are necessary for maneuvering around hover.

TABLE IV

HOVERING STABILITY AND CONTROL DERIVATIVES FOR TANDEM, SINGLE ROTOR HELICOPTERS AND FULL SCALE AEROCRANE

TANDEM HELICOPTER (Ref. 4)

DESIGN GROSS WEIGHT		25T	100T
M_u	1/Ft-Sec	0.0049	0.0027
M_q	1/Sec	-0.77	-0.89
M_δ	$1/Sec^2$-In	0.27	0.16
L_v	1/Ft-Sec	-0.0076	-0.0054
L_p	1/Sec	-0.57	-0.92
L_δ	$1/Sec^2$-In	0.54	0.39

NOTE:

Tandem has no significant Pitch-Roll coupling.

SINGLE ROTOR (Ref. 10)

DESIGN GROSS WEIGHT		20T	100T(2)
M_q	1/Sec	-0.31(1)	-0.36
M_δ	$1/Sec^2$-In	0.21(1)	0.11
M_p	1/Sec	0.21(1)	0.25
L_p	1/Sec	-1.4	-2.7
L_δ	$1/Sec^2$-In	0.38	0.32
L_q	1/Sec	-0.96(1)	-1.86

NOTE:

Speed stability and dihedral effect not given in Ref. 10. Coupling derivatives (M_p, L_q) estimated.

(1) Estimated assuming $\frac{I_y}{I_x} = 4.5$, $\gamma = 11$.

(2) Estimated using scaling laws of Ref. 4; $I_y \sim w^{1.9}$; $I_x \sim w^{1.6}$, $R \sim w^{0.5}$

TABLE IV Continued

AEROCRANE

PAYLOAD	16T	50T[1]
M_u 1/Ft-Sec	0.013	0.0074
M_q 1/Sec	-1.76	-1.46
$M_{A_{1s}}$[2] 1/Sec²-Deg	0.035	0.024
M_p 1/Sec	-1.44	-1.19
L_v 1/Ft-Sec	-0.013	-0.0074
L_p 1/Sec	-1.76	-1.46
$L_{B_{1s}}$[2] 1/Sec²-Deg	0.035	0.024
L_q 1/Sec	1.44	1.19

(1) Froude scaled from 16T vehicle parameters.

(2) NOTE: Given per degree of cyclic. No stick gearing assumed.

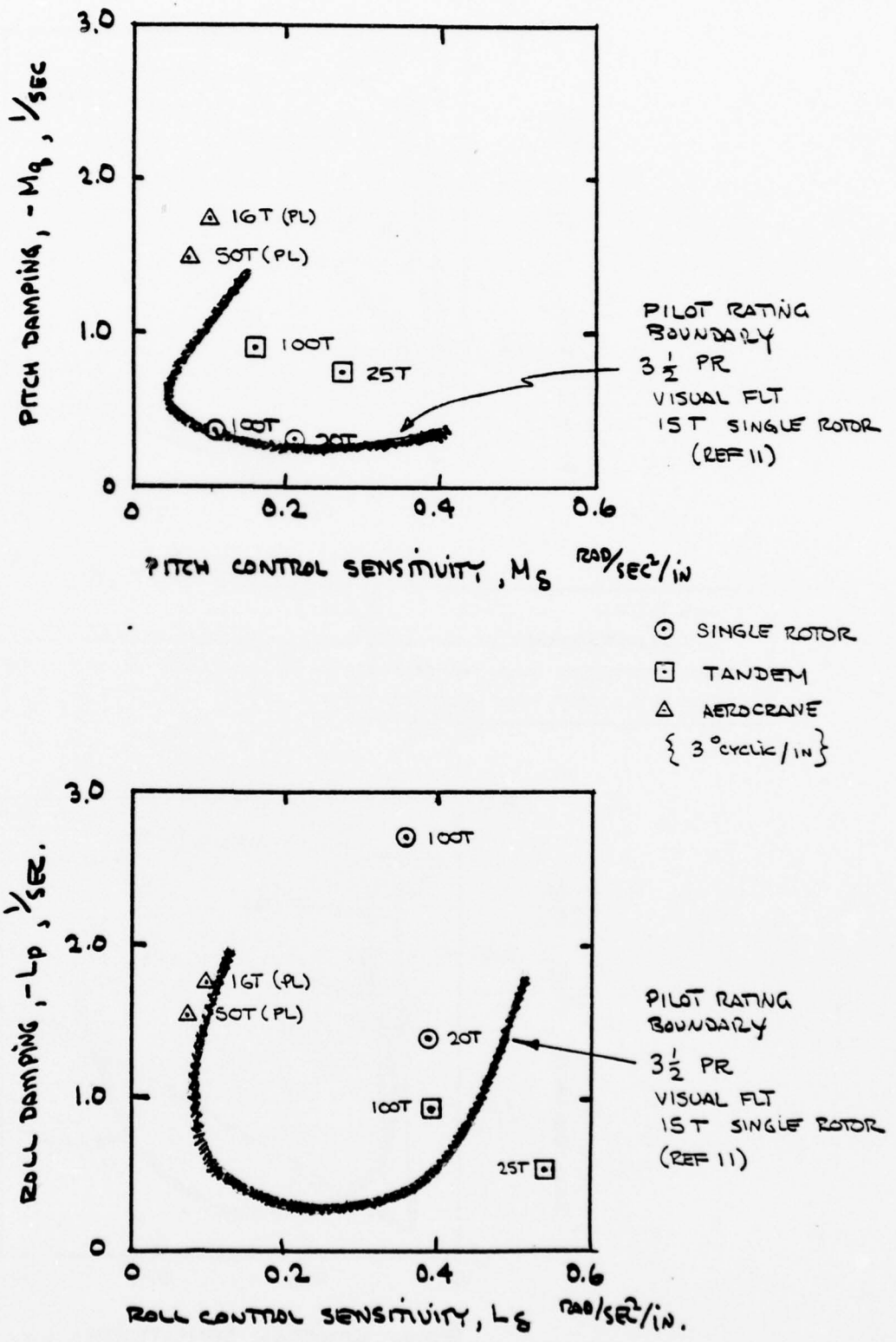

Figure 16: Comparison of Damping and Control Sensitivity of Single Rotor, Tandem and AEROCRANE.

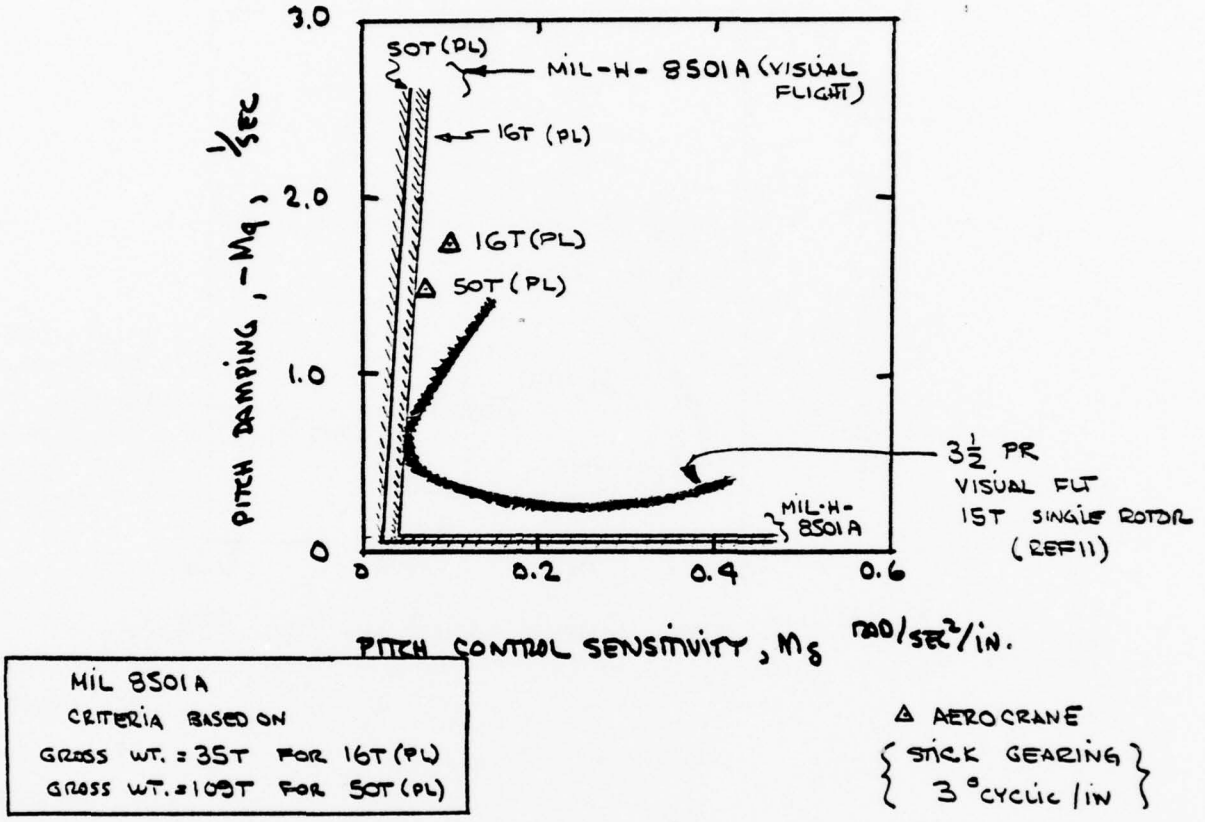

MIL 8501A
CRITERIA BASED ON
GROSS WT. = 35T FOR 16T (PL)
GROSS WT. = 10ST FOR 50T (PL)

△ AEROCRANE
{ STICK GEARING
3° CYCLIC / IN }

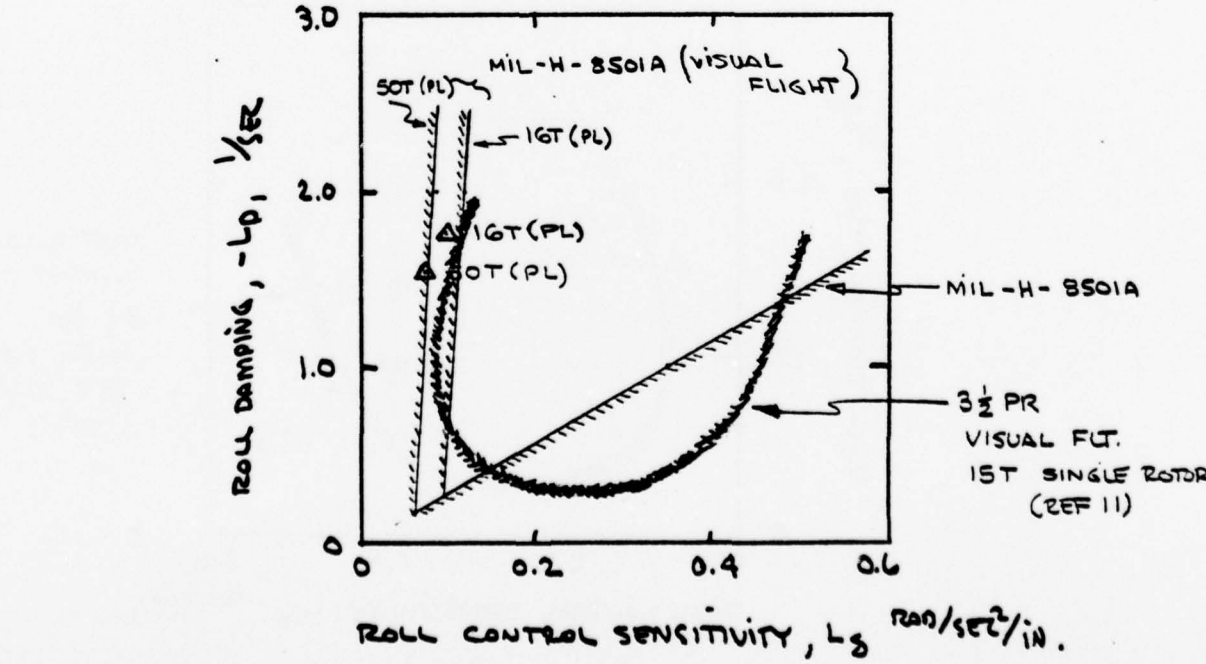

Figure 17: Comparison of AEROCRANE Damping and Control Sensitivity with Handling Qualities Data and MIL-H-8501A.

CONCLUSIONS

1.) The AEROCRANE configurations examined in this report with one minor exception (with the sling load attached at the center of gravity) are dynamically stable in hovering flight. The sling load configuration has only a small influence on the dynamic stability.

2.) Compared to large proposed helicopter designs, the AEROCRANE configuration studied has very high levels of angular damping and low control power. The high levels of angular damping result from the rigid rotor configuration and the low control power results from low rotor angular velocity. The pitch/roll coupling of the AEROCRANE is similar to a single rotor helicopter.

3.) The AEROCRANE configurations investigated meet the visual flight handling qualities specifications of MIL H-8501-A in terms of damping and control sensitivity. It should be noted however that application of MIL H-8501-A to large AEROCRANES requires extrapolation to gross weights well beyond the region where experimental flight test data are available.

4.) A simulation study of the precision control characteristics of the AEROCRANE in hovering flight indicates that with cyclic control, the task of hovering the AEROCRANE over a spot in the presence of gusts or translating from point to point is difficult. The results obtained were similar in many respects to results obtained in simulation studies of conventional large helicopters.

Somewhat larger displacements were noted in the study reported here for these tasks in contrast to the conventional large helicopter. However, in both cases the displacements were comparatively large. It should be noted that a simple simulation was employed here and the operator controlled the vehicle from a presentation of translational displacements only.

5.) The simulation study also examined the precision control characteristics of the AEROCRANE with winglets which provide direct translational force control in hovering flight. Both of the tasks, hovering over a spot in the presence of gusts and translating from point to point become quite simple to perform. It was possible to hover over a spot in the presence of 5 fps RMS gusts within a one foot square, using the winglets with the basic vehicle (no feedback). This performance approaches that obtained in the Heavy Lift Helicopter studies with a very sophisticated automatic control system.

6.) Comparatively large winglets are required to trim the AEROCRANE with a spherical centerbody in level flight at an advance ratio of 0.3. The simulation studies indicated that considerably smaller winglets could be employed if the winglets are employed for maneuvering in hover only.

7.) Sling load dynamics must be carefully considered in the control of any hovering vehicle which obtains an appreciable portion of its lift from buoyant force and carries a sling load which is an

appreciable fraction of the gross weight. This is particularly true when hovering control is obtained by applying moments to the vehicle (e.g. cyclic pitch). The presence of the buoyant force reduces the translational acceleration obtained from pitch attitude. There is a range of control input frequencies in the vicinity of the sling load frequency where as a result of the sling load motions the translational acceleration arising from pitch attitude reverses sign. That is, a nose down attitude produces a rearward acceleration. There is strong coupling between the translational acceleration and sling load motion. The effect of the sling load may be approximately treated as a forced response problem rather than dynamically coupled to the vehicle.

REFERENCES

1.) Putman, W. F. and Curtiss, H. C., Jr.: "An Experimental and Analytical Investigation of the Hovering and Forward Flight Characteristics of the AEROCRANE Hybrid Heavy Lift Vehicle", Princeton University, AMS Technical Report No. 1351, Naval Air Development Center Report No. 76201-30, Sept. 1977.

2.) Hutto, A. J.: "Flight-Test Report on the Heavy Lift Helicopter Flight Control System", Journal of the American Helicopter Society, Vol. 21, No. 1, Jan. 1976.

3.) Davis, J. M., Landis, K. H. and Leet, J. R.: "Development of Heavy Lift Helicopter Handling Qualities for Precision Hover", American Helicopter Society Preprint 940, May 1975.

4.) Lytwyn, R. T., et al: "Analysis and Simulation of Piloted Performance in Crane-Type Helicopters in Hover", American Helicopter Society Preprint 943, May 1974.

5.) Gessow and Myers: AERODYNAMICS OF THE HELICOPTER, Macmillan Company, New York, 1952.

6.) Kochin, N. E., Kibel, I. A. and Roze, N. W.: THEORETICAL HYDROMECHANICS, Interscience, 1964.

7.) Vertol Division of the Boeing Company: "Experimental Programs Conducted Under the U. S. Army Cart Loan Agreement, Vol. I. Static Tests on a Full Scale Boeing Vertol 76 Rigid Propeller", Boeing-Vertol Report R-339, June 1965.

8.) Crews, S. T., et al: "An Unsteady Wake Model for a Hingeless Rotor", Journal of Aircraft, Vol. 10, No. 12, Dec. 1973.

9.) Banerjee, D., et al: "Identification of State Variables and Dynamic Inflow From Rotor Model Dynamic Tests", Journal of the American Helicoper Society, Vol. 22, No. 2, April 1977.

10.) Carter, E. S., Jr. and Cooper, D. E.: "Survey of Rotary Wing Handling Qualities". International Congress on Subsonic Aeronautics, Annals of the New York Academy of Sciences, Vol. 152, Art. 2, Nov. 22, 1968.

11.) Tapscott, R. J. and Sommer, R. W.: "A Flight Study with a Large Helicopter Showing Trends of Lateral and Longitudinal Control Response with Size", NASA TN D-3600, Sept. 1966.

12.) Anon., Military Specification Helicopter Flying and Ground Handling Qualities; General Requirements for, MIL-H-8501A, 7 September 1961.

13.) Anon., V/STOL Handling I-Criteria and Discussion, II-Documentation. AGARD Report No. 577, Dec. 1970 to June 1973.

14.) Elias, A. L.: "Wing-Tip-Winglet Propulsion for AEROCRANE-Type Hybrid Lift Vehicles", AIAA Paper No. 75-944, July 1975.

APPENDIX A

WINGLET CONTRIBUTIONS TO CONTROL AND STABILITY OF THE AEROCRANE

An alternate means of controlling the AEROCRANE has been proposed which involves the use of winglets. Winglets are vertical surfaces mounted at the tips of each rotor blade as illustrated in Figure A-1. The winglets are of interest for two reasons. First it is possible to fly forward producing a net translational force by suitably varying the winglet deflection angle, δ_W, such that forward flight can be achieved without tilting the vehicle. Second, the winglet can be employed for maneuvering the vehicle as well, by providing translational forces directly through winglet deflection rather than through the tilting of the thrust vector with cyclic pitch. This method of control looks particularly attractive for precision hovering control as discussed elsewhere in this report. Reference 14 has examined the use of winglets for control of the AEROCRANE and indicates the desirable control characteristics which can be obtained with winglets.

The contributions of the winglets to the stability and control characteristics of the AEROCRANE are developed in this Appendix. From Figure A-1 the lift and the drag forces on a winglet can be expressed as

$$L_W = \tfrac{1}{2} \rho V_R^2 S_W a_W(\delta_W + \epsilon)$$
$$D_W = \tfrac{1}{2} \rho V_R^2 S_W C_{DW} \qquad \text{(A-1)}$$

The resultant forces applied to the vehicle by a single winglet in the

rotor axis system is from Figure A-1,

$$X_{RW} = - L_W \sin (\epsilon + \psi) - D_W \cos (\epsilon + \psi)$$
$$Y_{RW} = - L_W \cos (\epsilon + \psi) + D_W \sin (\epsilon + \psi) \qquad \text{(A-2)}$$

The angle between the resultant velocity experienced by the winglet, V_R, and the velocity due to rotation, ΩR, is given by

$$\tan \epsilon = \frac{\mu \cos \psi}{1 + \mu \cos \psi}$$

or (A-3)

$$\sin \epsilon = \frac{\mu}{\mu_R} \cos \psi \quad \text{and} \quad \cos \epsilon = \frac{1 + \mu \sin \psi}{\mu_R}$$

These relationships can be used to give

$$\sin (\psi + \epsilon) = \frac{\cos \psi}{\mu_R}$$
$$\cos (\psi + \epsilon) = \frac{\sin \psi + \mu}{\mu_R} \qquad \text{(A-4)}$$

and

$$\mu_R = \frac{1 + \mu \sin \psi}{\cos \epsilon}$$

The velocities have been nondimensionalized by the tip speed, ΩR, such that,

$$\mu = \frac{V}{\Omega R} \quad \text{and} \quad \mu_R = \frac{V_R}{\Omega R} \ .$$

Since the primary interest is to develop the contributions of the winglet to stability and control, the winglet drag force will be neglected in the succeeding development, as it will not be a primary contributor to the forces and moments influencing the stability and control characteristics.

It is, of course, important in estimating the power consumption of the winglets to include the winglet drag force.

Neglecting the winglet drag and introducing equations (A-1) and (A-4) into (A-2), the resultant forces applied to the vehicle can be expressed as

$$X_{RW} = -\tfrac{1}{2}\rho\,(\Omega R)^2\, S_W\, a_W \mu_R\, (\delta_W + \epsilon)\cos\psi$$

$$Y_{RW} = -\tfrac{1}{2}\rho\,(\Omega R)^2\, S_W\, a_W \mu_R (\delta_W + \epsilon)\,(\sin\psi + \mu) \qquad \text{(A-5)}$$

It is further assumed that ϵ is a small angle. This is a very satisfactory assumption particularly for studies near hovering flight, and probably up to an advance ratio $\mu = 0.3$, where the maximum value of ϵ is 23° as given by equation (A-3). It is further assumed that the angular control motion of the winglet is sinusoidal such that the angle δ_W is given by

$$\delta_W = \delta_c \cos\psi + \delta_s \sin\psi \qquad \text{(A-6)}$$

With the assumption that ϵ is small and using equation (A-6), equation (A-5) can be expressed as

$$X_{RW} = -\tfrac{1}{2}\rho\,(\Omega R)^2\, S_W\, a_W \left\{ \left(\frac{\delta_c + \mu}{2}\right) + \frac{\delta_c \mu}{4} \sin\psi \right.$$

$$+ \frac{\delta_s \mu}{4}\cos\psi + \left(\frac{\delta_c + \mu}{2}\right)\cos 2\psi$$

$$\left. + \frac{\delta_c \mu}{4}\sin 3\psi - \frac{\delta_s \mu}{4}\cos 3\psi \right\} \qquad \text{(A-7)}$$

$$Y_{RW} = -\tfrac{1}{2}\rho\,(\Omega R)^2\,\delta_W\,a_W \left\{ \frac{\delta_s(1+\mu^2)}{2} + (\mu^2 + \tfrac{5}{4}\delta_c\mu)\cos\psi \right.$$

$$+ \tfrac{7}{4}\delta_s\mu\,\sin\psi + \tfrac{1}{2}\left(\mu + \delta_c(1+\mu^2)\right)\sin 2\psi$$

$$\left. - \tfrac{1}{4}\delta_c\mu\,\cos 3\psi - \tfrac{1}{4}\delta_s\mu\,\sin 3\psi \right\}$$

Equations (A-7) give the resultant forces produced by a single winglet. It can be seen that control deflections δ_s and δ_c produce constant forces as well as fluctuating forces up to the third harmonic.

If four winglets are employed, the resultant forces applied to the vehicle can be calculated by summing the contributions of the four winglets using equations (A-7) for each winglet with the azimuth angle, ψ, suitably adjusted to account for the azimuth location of each winglet, i.e.,

$$\begin{aligned} \psi_2 &= \psi_1 + 90^\circ \\ \psi_3 &= \psi_1 + 180^\circ \\ \psi_4 &= \psi_1 + 270^\circ \end{aligned} \qquad \text{(A-8)}$$

All of the harmonic components cancel leaving for four winglets

$$\begin{aligned} X_{RW} &= -\rho\,(\Omega R)^2\,S_W\,a_W(\delta_c + \mu) \\ Y_{RW} &= -\rho\,(\Omega R)^2\,S_W\,a_W(\delta_s)\,(1+\mu^2) \end{aligned} \qquad \text{(A-9)}$$

It should be noted that while the harmonics cancel in an overall sense, the winglets individually do apply oscillating forces to the individual blades as given by equations (A-7)

Thus equations (A-9) give the forces applied to the AEROCRANE as a function of control deflection and advance ratio. It should be noted that the winglets will produce moments as well as forces since the center of gravity of the vehicle is in general not located in the plane of the rotor.

The size of the winglet can be related to the requirement to trim the vehicle in forward flight in level attitude equilibrium. Thus, neglecting the rotor in plane force, the longitudinal winglet force can be equated to the drag of the centerbody to give an estimate of winglet size required

$$- \rho (\Omega R)^2 S_W a_W (\delta_c + \mu) - \tfrac{1}{2} \rho V^2 \pi R_B^2 C_D = 0$$

Solving for winglet deflection,

$$\delta_c = - \mu - 2 \mu^2 s \qquad \text{(A-10)}$$

where

$$s = \frac{\pi R_B^2 C_D}{4 S_W a_W}$$

Taking the winglet to be of rectangular planform with a chord equal to the blade chord, c

$$s = \frac{C_D \chi^2}{\sigma a \bar{\bar{b}}_W}$$

where $\bar{\bar{b}}_W$ is the winglet span nondimensionalized by rotor radius.

In a similar fashion the sine component of winglet deflection must balance the Magnus force. Equating the side force produced by the winglet to the Magnus force gives

$$\delta_s = \left(\frac{2 \mu^2}{1 + \mu^2}\right) s \frac{C_{LM}}{C_D} \qquad \text{(A-11)}$$

and therefore, the relationship between the two components of winglet deflection is given by equation (A-10) and (A-11) as

$$\frac{(\delta_c + \mu)}{\delta_s (1 + \mu^2)} = - \frac{C_D}{C_{LM}} = - \frac{1}{C_R} \qquad \text{(A-12)}$$

The area of the winglet should be selected such that winglet stall is not encountered. The winglet angle-of-attack is given by

$$\alpha_W = \epsilon + \delta_W = (\delta_c \cos \psi + \delta_s \sin \psi + \frac{\mu \cos \psi}{1 + \mu \sin \psi}) \qquad \text{(A-13)}$$

Substituting the required winglet control deflections required for trim, equation (A-13) can be expressed as

$$\alpha_W = - \mu^2 \left\{ \frac{\sin \psi \cos \psi}{1 + \mu \sin \psi} + 2s \left(1 + (\frac{C_R}{1 + \mu^2})\right)^{\frac{1}{2}} \cos (\psi + \phi) \right\}$$

where

$$\phi = \tan^{-1} \frac{C_R}{1 + \mu^2} \qquad \text{(A-14)}$$

Figure A-2 shows the winglet angle-of-attack variation with azimuth required for level attitude trim at an advance ratio of 0.3. The sample calculation is based on the following dimensionless parameters.

$C_D = 0.80$ $\qquad$ $\sigma = .138$

$C_{LM} = 0.30$ $\qquad$ $\chi = .46$

$a_W = 4$

This vehicle geometry is based on the configuration described in Reference 1. The drag and Magnus force coefficients were determined experimentally as described in Reference 1. The cyclic amplitudes of

winglet motion required are also shown.

The analysis assumes that the winglet does not stall and so the results of Figure A-2 indicate that the winglet span to radius ratio, $\bar{\bar{b}}_W$, must be larger than 0.25 to maintain the winglet angle-of-attack below 15° and consequently avoid stall. If the winglet is also used for control at forward speed then some additional margin must be available for control in addition to trim. A further characteristic of interest is the acceleration capability of the winglet, particularly with respect to maneuvering near hover. The ratio of the winglet force produced by winglet deflection to the buoyant force can be expressed as

$$\frac{1}{F_B} \frac{\partial X_{RW}}{\partial \delta_c} = \frac{3\sigma a \bar{\bar{b}}_W}{16 g \chi^3} (\Omega^2 R) \qquad \text{(A-15)}$$

Using the dimensionless parameters given above, and expressing (A-15) in terms of vehicle weight and per degree of winglet deflection

$$\frac{1}{W} \frac{\partial X_{RW}}{\partial \delta_c}_o = \frac{\bar{\bar{b}}_W}{1700} \frac{F_B}{W} (\Omega^2 R) \qquad \text{(A-15}$$

Equation (A-15) is an expression for the acceleration in g's produced by one-degree of winglet deflection. Linear acceleration is independent of size, based on Froude scaling. Using the parameters of the dynamic model described in Reference 1 for the rotor rotational speed and radius,

Ω = 30 RPM

R = 19.9 Ft.

equation (A-15) becomes

$$\frac{1}{W} \frac{\partial X_{RW}}{\partial \delta_c}_o = 0.12 \bar{\bar{b}}_W \frac{F_B}{W} \qquad \text{(A-15)}$$

For a buoyant force to weight ratio 0.75, typical of proposed AEROCRANE designs with payload and a $\bar{\bar{b}}_W = 0.25$ the minimum size winglet for trim at an advance ratio of 0.3,

$$\frac{1}{W} \frac{\partial X_{RW}}{\partial \delta_c}_o = 0.023 \text{ g per degree} \qquad \text{(A-16)}$$

The significance of this level in controlling the AEROCRANE near hover is discussed elsewhere in this report.

Examination of equations (A-9) indicates that the addition of winglets will also influence the stability and gust sensitivity of the AEROCRANE from the fact that the longitudinal force depends linearly on the advance ratio. In hovering flight the linearized dependence of the side force on advance ratio is zero. Note that the linearized contributions of the centerbody are also zero so the impact of winglets must be carefully examined not only with respect to control but with respect to gust sensitivity.

Consequently, the following terms must be added to the equations of motion of the AEROCRANE to account for the presence of winglets in near hovering flight.

Equations (A-9) are given in wind axes. Expressing the contributions of the winglet in body axes

$$\Delta X_{BW} = \frac{\partial X_{RW}}{\partial \delta_c} \delta_c + \frac{\partial X_{RW}}{\partial V} u$$

$$\Delta Y_{BW} = \frac{\partial Y_{RW}}{\partial \delta_s} \delta_s + \frac{\partial X_{RW}}{\partial V} v \qquad \text{(A-17)}$$

where δ_c and δ_s are now assumed to be body referenced. The derivatives are equal to

$$\frac{\partial X_{RW}}{\partial \delta_c} = \frac{\partial Y_{RW}}{\partial \delta_s} = - \rho(\Omega R)^2 S_W a_W$$

$$\frac{\partial X_{RW}}{\partial V} = - \rho(\Omega R) S_W a_W \qquad \text{(A-18)}$$

In addition to forces, the winglets also produce moments owing to the fact that the center of gravity of the vehicle is located a distance r_o below the rotor plane. The pitching moment and rolling moment produced are

$$\Delta M_{B_1 W} = - r_o \Delta X_{BW}$$

$$\Delta L_{B_1 W} = r_o \Delta Y_{BW} \qquad \text{(A-19)}$$

Thus control moments and contributions to the speed stability and dihedral effect are produced. Using equations (A-17), (A-18) and (A-19) these are

$$\frac{\partial \Delta M_{BW}}{\partial \delta_c} = \rho(\Omega R)^2 S_W r_o a_W$$

$$\frac{\partial \Delta M_{BW}}{\partial u} = \rho(\Omega R) S_W r_o a_W \qquad \text{(A-20)}$$

$$\frac{\partial \Delta L_{BW}}{\partial \delta_s} = -\rho(\Omega R)^2 S_W r_o a_W$$

$$\frac{\partial \Delta L_{BW}}{\partial v} = -\rho(\Omega R) S_W r_o a_W$$

The influence of these various winglet contributions is discussed in the main body of this report.

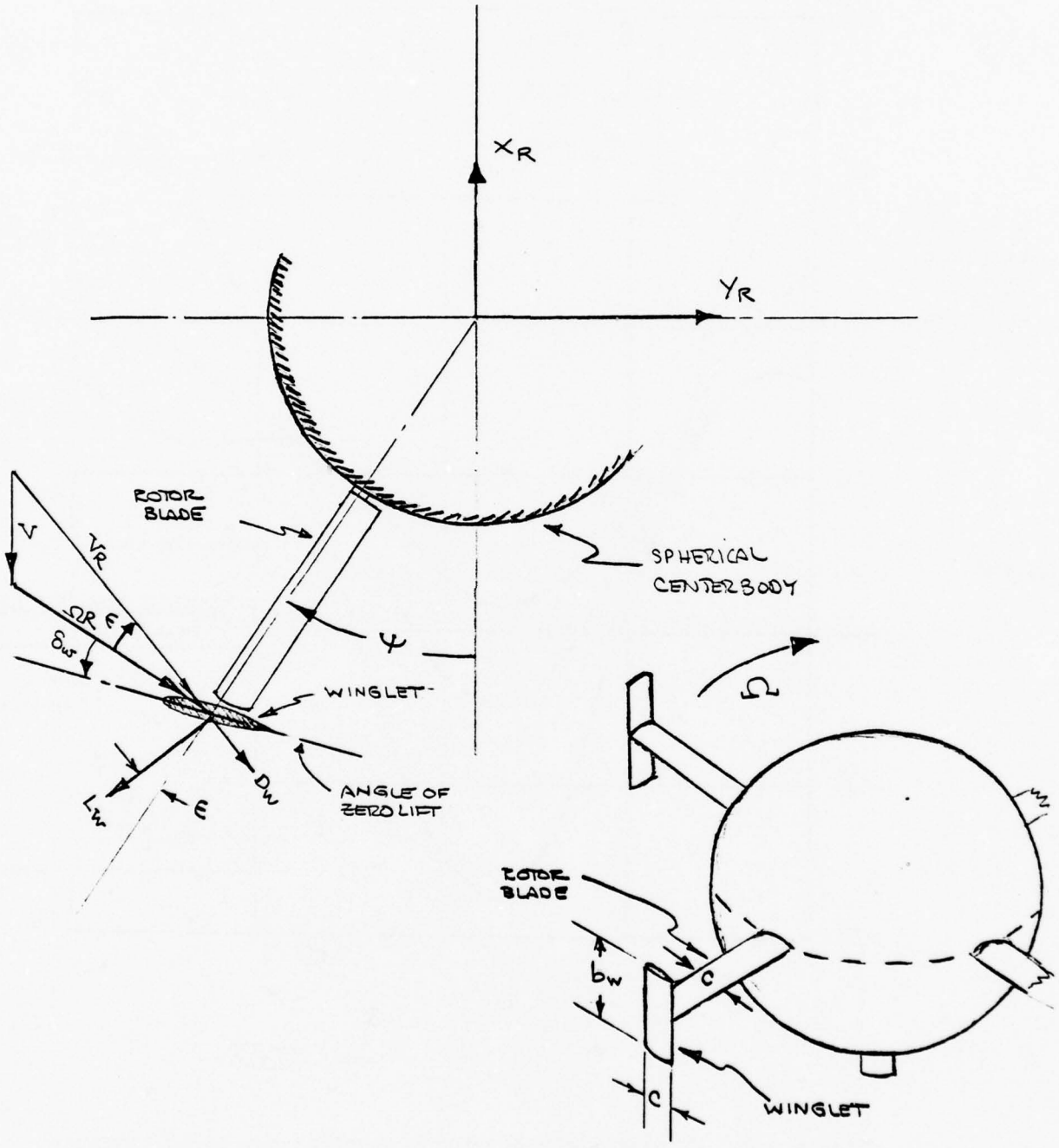

Figure A-1. Geometry for Analysis of Winglet Forces.

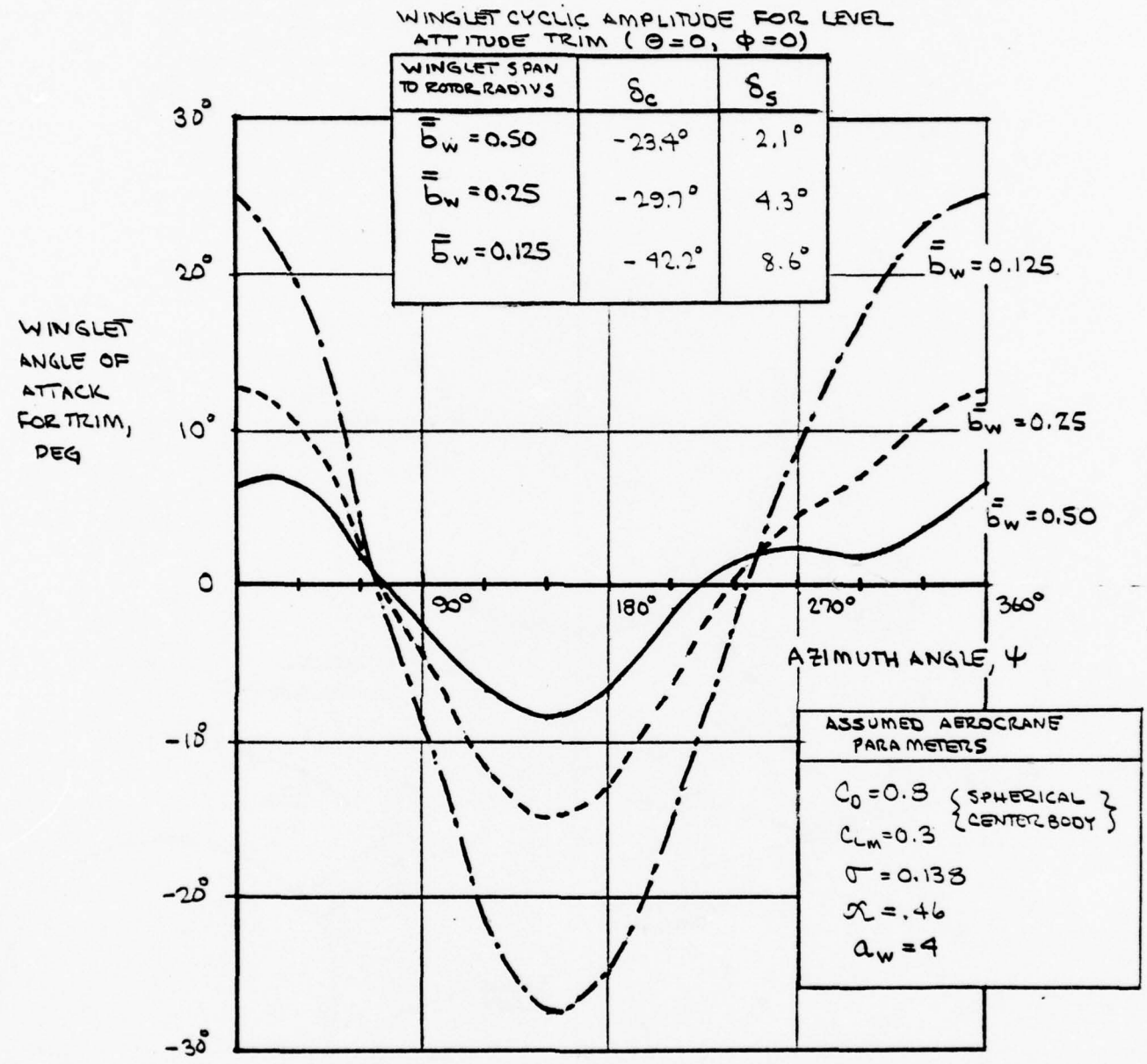

Figure A-2. Winglet Angle-of-Attack Required for Level Attitude Trim ($\theta = 0$, $\phi = 0$) as a Function of Winglet Span to Rotor Radius ($\bar{b}_w$) at an Advance Ratio of $\mu = 0.3$.

APPENDIX B

ROTOR AERODYNAMIC MODEL

The aerodynamic forces and moments produced by the rotor are modelled based on the following assumptions in addition to the usual assumptions that the blade inflow angle is small and the dependence of blade element lift on angle-of-attack is linear:-

1.) The rotor blades are assumed to be rigid so that there is no flapping motion. This assumption is a consequence of the method of blade support as well as the low angular velocity of the rotor. It is possible that for a very large AEROCRANE this assumption may not be valid. However, it is necessary to have detailed designs for the blades and blade support system before the validity of this assumption can be examined further as a function of vehicle size.

2.) The rotor induced velocity is modelled in the following way. The induced velocity is assumed to consist of component independent of azimuth and first harmonic cosine and sine components such that the total inflow velocity can be written as

$$\lambda = \lambda_o + (\lambda_1 x + \lambda_M) \cos \psi + \lambda_L \sin \psi$$

The azimuth independent component, λ_o, is assumed to be given by momentum theory based on an actuator disc area which does not include the spherical centerbody. This component is assumed to be independent of radius. Although this assumption is inconsistant with the fact that the blades are untwisted (Ref. 5) it should be satisfactory for

prediction of stability and control characteristics. A more refined theory is desirable when predicting performance, i.e., power required. Thus,

$$\lambda_o = -\sqrt{\frac{C_T}{2\,(1 - \chi^2)}}$$

The harmonic components of the induced velocity arise from two sources: the blow back of the rotor wake which results from vehicle translation and results in the component $\lambda_1 \times \cos \psi$; and the self induced components λ_M and λ_L which arise from the fact that the non-flapping rotor produces aerodynamic hub moments.

λ_1, the blow back effects is assumed to be given by doubling the value obtained from Coleman's theory. That

$$\lambda_1 = -\,2\,\lambda_o \tan \frac{\chi}{2}$$

where

$$\chi = \tan^{-1}\left(\frac{\mu_s}{-\lambda_s}\right)$$

The doubling of the theoretical value is based on the correlation of experimental results with theory presented in Reference 1 as well as other indications from the literature.

λ_M and λ_L are calculated by assuming that they are proportional to the aerodynamic hub moments produced by the rotor. That is,

$$\lambda_M = j\left(\frac{2C_M}{a\,\sigma}\right)$$

$$\lambda_L = -j\left(\frac{2C_L}{a\,\sigma}\right)$$

The proportionality factor between the aerodynamic hub moments and the harmonic inflow components was assumed to be given by

$$j = \frac{1}{2}\left(\frac{a\sigma}{|\lambda_o|}\right)$$

This result can be derived from momentum theory as shown for example in Reference 8. The constant in this expression depends upon the assumptions employed in the momentum analysis. The value of $\frac{1}{2}$ for the constant in this expression was initially based on the experimental results of Reference 7. It is shown in Reference 1 that this model gave good agreement between the measured and predicted dynamic response characteristics of the AEROCRANE. Reference 9 also presents experimentally determined values of this quantity based on frequency response tests of a model rotor. The results of Reference 9, given in terms of the parameter L, where $j = L\gamma$, agree well with the above expression for j.

The only other feature of the rotor force and moment prediction to be noted is the fact that the rotor blades end at the radius of the spherical centerbody (R_B) and consequently various factors appear in the rotor aerodynamic equations to account for this fact. Define

$$\chi = \frac{R_B}{R}, \quad f_N = 1 - \chi^n$$

The equations for the rotor forces and moments are

$$\frac{2C_T}{a\sigma} = \frac{\theta_o}{3}\left[f_3 + \frac{3\mu_s^2}{2} f_1\right] + \left(\frac{\lambda_s - \mu_s B_{1w}}{2}\right) f_2 + \frac{1}{2}\lambda_i \mu_s f_1$$

$$\frac{2C_H}{a\sigma} = -\frac{\theta_o}{2}\left[\frac{\lambda_L f_2}{2} + \mu_s\lambda_s f_1\right] + \frac{B_{1W}}{4}\left[\lambda_s f_2 + \frac{3}{2}\mu_s \lambda_L f_1\right]$$

$$+ \frac{\mu_s A_{1W}}{8}\left[\lambda_M f_1 + \frac{\lambda_1}{2} f_2\right] - \lambda_s \lambda_L f_1 + \frac{\delta}{2a}\mu f_2$$

$$\frac{2C_Y}{a\sigma} = -\frac{\theta_o}{2}\left[\frac{\lambda_1 f_3}{3} + \frac{\lambda_M f_2}{2}\right] + \frac{A_{1W}}{4}\left[\lambda_s f_2 + \frac{\mu}{2}\lambda_L f_1\right]$$

$$+ \frac{\mu B_{1W}}{8}\left[\lambda_M f_1 + \frac{\lambda_1}{2} f_2\right] - \lambda_s\left[\lambda_M f_1 + \frac{\lambda_1}{2} f_2\right]$$

$$\frac{2C_M}{a\sigma} = \frac{\frac{A_{1W}}{8}\left[f_4 + \frac{\mu_s^2}{2} f_2\right] - \frac{1}{8}\lambda_1 f_4}{1 + \frac{j}{6} f_3} - \frac{\frac{1}{8}\frac{q_w}{\Omega} f_4}{1 + \frac{j}{6} f_3}$$

$$\frac{2C_L}{a\sigma} = \left\{-\frac{B_{1W}}{8}\left[f_4 + \frac{3}{2}\mu_s^2 f_2\right] + \mu_s\left[\frac{\theta_o}{3} f_3 + \frac{\lambda_s}{4} f_2\right]\right\}\left\{\frac{1}{1 + \frac{j}{6} f_3}\right\}$$

$$- \frac{\frac{1}{8}\frac{p_w}{\Omega} f_4}{1 + \frac{j}{6} f_3}$$

The dominant rotor contributions to the vehicle stability and control arise from the hub moment contributions given by $\frac{2C_M}{a\sigma}$ and $\frac{2C_L}{a\sigma}$. It can be noted from the above expressions that a number of the rotor hub moment derivatives are similar in hovering flight. If the blow back effect is approximated at low speeds by assuming the wake angle small

$$\chi \cong -\frac{\mu_s}{\lambda_s} \cong \frac{\mu_s}{|\lambda_o|}$$

and

$$\lambda_1 \cong - \mu_s$$

As a consequence of this assumption it can be seen from the above expression for the pitching moment that

$$\frac{2}{a\sigma} \frac{\partial C_M}{\partial \mu} = - \frac{2}{a\sigma} \frac{\partial C_M}{\partial \hat{q}} = \frac{2}{a\sigma} \frac{\partial C_M}{\partial A_{1s}} = - \frac{2}{a\sigma} \frac{\partial C_L}{\partial \hat{p}} = - \frac{2}{a\sigma} \frac{\partial C_L}{\partial B_{1s}}$$

$\frac{2}{a\sigma} \frac{\partial C_L}{\partial \mu}$ can be expressed in terms of the thrust coefficient as follows. In hovering flight

$$\frac{2C_T}{a\sigma} = \frac{\theta_o}{3} f_3 + \frac{\lambda_s}{2} f_2$$

and

$$\frac{2}{a\sigma} \frac{\partial C_L}{\partial \mu} = \frac{\frac{\theta_o}{3} f_3 + \frac{\lambda_s}{4} f_2}{1 + \frac{j}{6} f_3}$$

Substituting

$$\frac{2}{a\sigma} \frac{\partial C_L}{\partial \mu} = \frac{\frac{2C_T}{a\sigma} - \frac{\lambda_s}{4} f_2}{1 + \frac{j}{6} f_3}$$

Taking $j = \frac{1}{2} \frac{a\sigma}{|\lambda_o|}$ and selecting values for solidity and ratio of centerbody radius to rotor radius typical of AEROCRANE designs, the hub moment derivatives can be calculated as a function of thrust coefficient. These terms are given in Figure B-1.

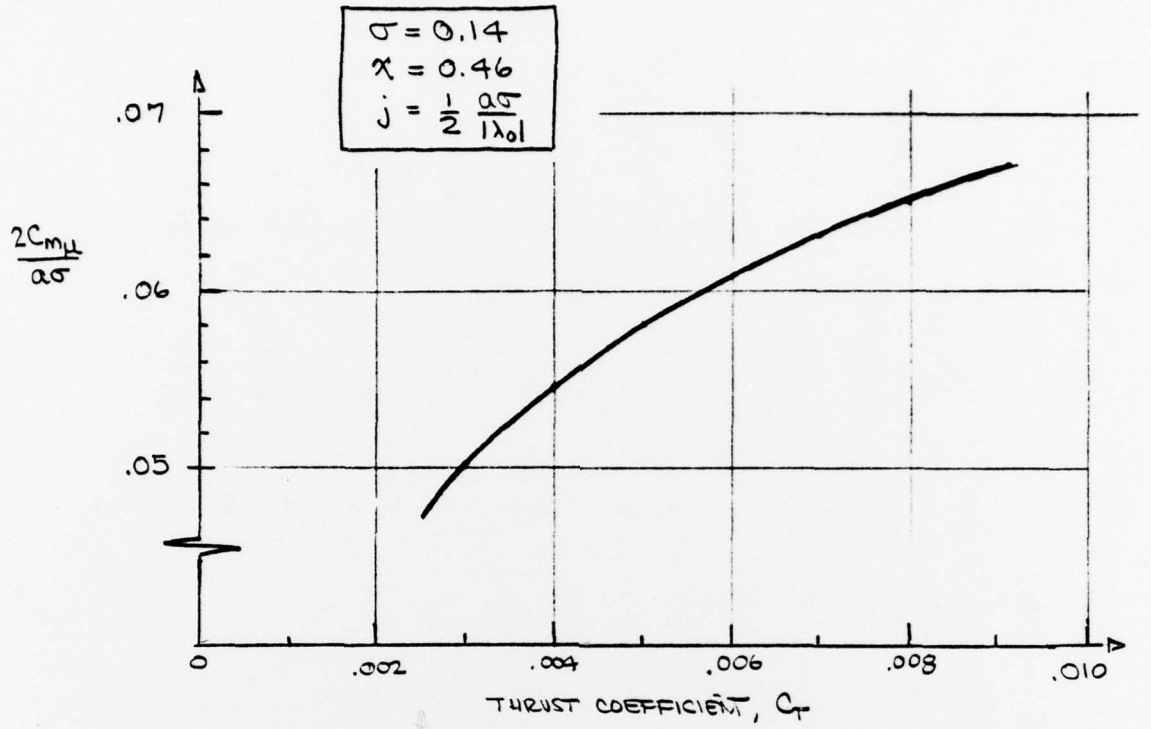

SPEED STABILITY { NOTE THAT $\frac{2C_{m\hat{q}}}{a\sigma} = -\frac{2C_{m_{AIS}}}{a\sigma} = -\frac{2C_{m\mu}}{a\sigma}$ }

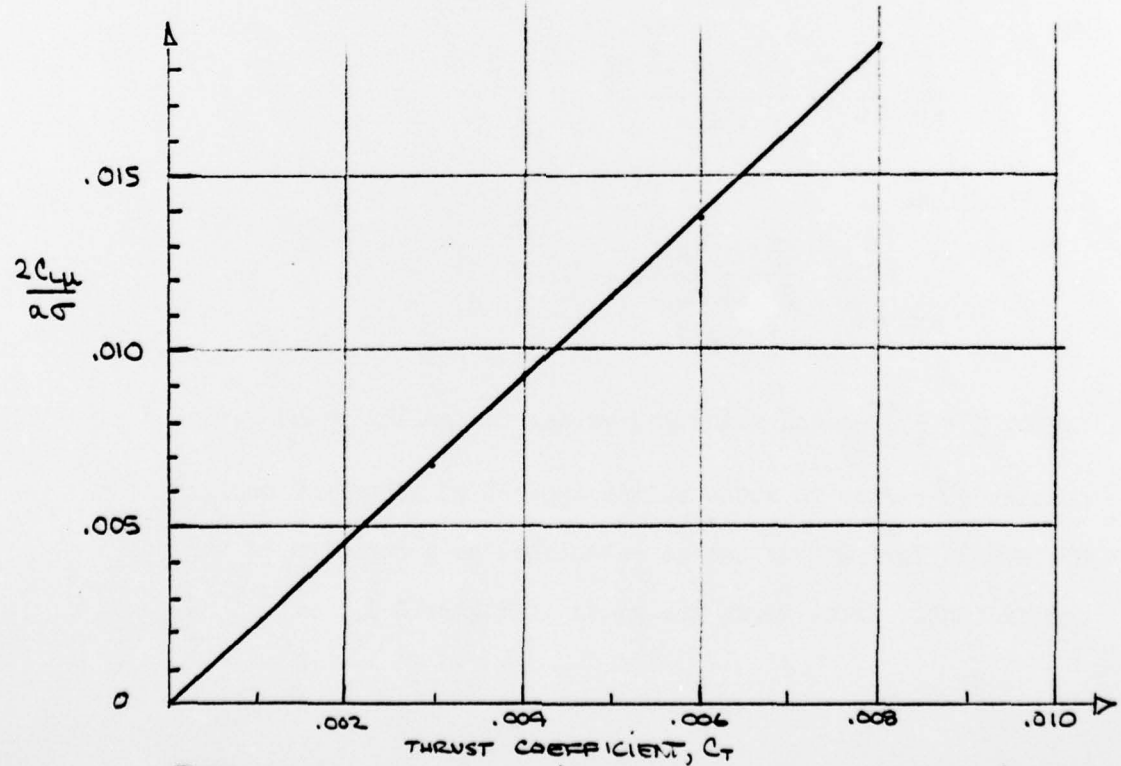

RATE OF CHANGE OF ROLLING MOMENT WITH ADVANCE RATIO

Figure B-1: Rotor Aerodynamic Pitching Moment Derivatives.

APPENDIX C

AEROCRANE EQUATIONS OF MOTION WITH SLING LOAD

Reference 1 presents a detailed derivation of the AEROCRANE equations of motion with a sling load. The sling load is taken to be supported at a distance Z_A below the center of gravity of the vehicle. The sling load is assumed to be a point mass with negligible aerodynamic forces acting on it supported on a cable of length Z_L.

The six equations of motion describing the four degree-of-freedom dynamic motion of the AEROCRANE in hover with a two degree-of-freedom sling load are

$$I' \ddot{\theta} + I_Z \Omega \dot{\theta} + r_o m_A \dot{v}_S + F_B r_o \phi - Z_A m_L g \phi_L = L_{S/A}$$

$$- I_Z \Omega \dot{\phi} + I' \ddot{\theta} - r_o m_A \dot{u}_S + F_B r_o \theta - Z_A m_L g \theta_L = M_{S/A}$$

$$- m_L \dot{u}_S - m_L g (\theta + \theta_L) - m_L (\ddot{\theta} (Z_A + Z_L) + \ddot{\theta}_L Z_L) = 0$$

$$- m_L \dot{v}_S + m_L g (\phi + \phi_L) + m_L (\ddot{\phi} (Z_A + Z_L) + \ddot{\phi} Z_L) = 0$$

$$m' \dot{u}_S - r_o m_A \ddot{\theta} - m_L g \theta_L + (W_o - F_B) \theta = X_{S/A}$$

$$m' \dot{v}_S + r_o m_A \ddot{\phi} + m_L g \phi_L - (W_o - F_B) \phi = Y_{S/A}$$

The terms represented explicitly above include the inertial and gyroscopic terms, buoyancy and gravity terms and aerodynamic acceleration forces and moments ("apparent mass" terms). m' also includes the apparent

mass of the centerbody and I' includes its effect on the pitching and rolling inertia. The right hand side terms include all of the aerodynamic forces and moments. The axes and geometry are shown in Figure C-1.

The aerodynamic forces and moments arise from the rotor centerbody and winglets.

The moments can be expressed as

$$L_{S/A} = L_H + r_o (Y_R + Y_W + F_M)$$

$$M_{S/A} = M_H + r_o (H_R - X_W + D)$$

The forces are

$$X_{S/A} = - H_R + X_W - D$$

$$Y_{S/A} = Y_R + Y_W + F_M$$

where

L_H, M_H are rotor hub moments

Y_R, H_R are rotor inplane forces

X_W, Y_W are winglet forces

F_M, D are centerbody forces, that is, Magnus force and drag.

Appendix B presents expressions for the rotor forces which can be used to determine the rotor derivatives and Appendix A presents the expressions for the winglet contributions. The drag and Magnus forces are given by

$$D = \tfrac{1}{2} \rho \pi R_B^2 \; C_D (u^2 + v^2)$$

$$F_M = \tfrac{1}{2} \rho \pi R_B^2 \; C_{LM} (u^2 + v^2)$$

where C_D and C_{L_M} were determined in Reference 1 by correlation with experiment. Note that if these terms are linearized then their contribution to the linear equations of motion are zero. In the analog computer study discussed elsewhere, these non-linear terms are retained in the computation.

The equations of motion are now non dimensionalized using the approach described elsewhere in this report.

The first two equations, the vehicle moment equations, are divided by $I' \Omega$, and Ω^2 is included in the acceleration terms to nondimensionalize the time. The moment equations become

$$\phi'' + \frac{I_z}{I'}\theta' + \{\tfrac{1}{2}\beta\ \bar{r}_o \hat{\omega}_R^2\ F_R\}\ \bar{v}_s' + \beta\ \bar{r}_o \hat{\omega}_R^2\ \phi - \mu\ \bar{Z}_A \hat{\omega}_R^2\ \phi_L = AC_L$$

$$-\frac{I_z}{I'}\phi' + \theta'' - \{\tfrac{1}{2}\beta\ \bar{r}_o \hat{\omega}_R^2\ F_R\}\ \bar{u}_s' + \beta\ \bar{r}_o \hat{\omega}_R^2\ \theta - \mu\ \bar{Z}_A \hat{\omega}_R^2\ \theta_L = AC_M$$

The vehicle force equations are divided through by $m' \Omega^2 R$ to give

$$\bar{u}_s' - \left\{\frac{\frac{\beta}{2}\bar{r}_o \chi}{1 + \frac{\beta}{2}}\right\}\ \theta'' - \frac{\mu}{F_R\ (1 + \frac{\beta}{2})}\theta_L + \frac{(1 - \beta)}{F_R\ (1 + \frac{\beta}{2})}\ \theta = B\ C_x$$

$$\bar{v}_s' + \left\{\frac{\frac{\beta}{2}\bar{r}_o \chi}{1 + \frac{\beta}{2}}\right\}\ \phi'' + \frac{\mu}{F_R\ (1 + \frac{\beta}{2})}\phi_L - \frac{(1 - \beta)}{F_R\ (1 + \frac{\beta}{2})}\ \phi = B\ C_y$$

where

$$B = \frac{A\ \bar{k}_y^2}{1 + \frac{\beta}{2}}\ \chi^2$$

The sling load equations are divided through by the quantity $m_L g$. The

signs are reversed in the first sling load equation

$$+ F_R \bar{u}_s' + \theta + \theta_L + \frac{1}{\hat{\omega}_{sL}^2}\left(1 + \frac{Z_A}{Z_L}\right)\theta'' + \frac{1}{\hat{\omega}_{sL}^2}\theta_L'' = 0$$

$$- F_R \bar{v}_s' + \phi + \phi_L + \frac{1}{\hat{\omega}_{sL}^2}\left(1 + \frac{Z_A}{Z_L}\right)\phi' + \frac{1}{\hat{\omega}_{sL}^2}\phi_L'' = 0$$

The aerodynamic forces and moments are

$$C_L = \frac{a\sigma}{2}\left\{\frac{2C_L}{a\sigma} + \bar{r}_o \chi \frac{2C_Y}{a\sigma}\right\} + \bar{r}_o \chi \left\{C_{Y_W} + C_{F_M}\left[\frac{\pi R_B^2(\bar{u}_s^2 + \bar{v}_s^2)}{2\pi R^2}\right]\right\}$$

$$C_M = \frac{a\sigma}{2}\left\{\frac{2C_M}{a\sigma} + \bar{r}_o \chi \frac{2C_H}{a\sigma}\right\} + \bar{r}_o \chi \left\{- C_{X_W} + C_D\left[\frac{\pi R_B^2(\bar{u}_s^2 + \bar{v}_s^2)}{2\pi R^2}\right]\right\}$$

$$C_Y = \frac{a\sigma}{2}\left\{\frac{2C_Y}{a\sigma}\right\} + C_{Y_W} + C_{F_M}\left\{\frac{\pi R_B^2(\bar{u}_s^2 + \bar{v}_s^2)}{2\pi R^2}\right\}$$

$$C_X = - \frac{a\sigma}{2}\left\{\frac{2C_H}{a\sigma}\right\} + C_{H_W} - C_D\left\{\frac{\pi R_B^2(\bar{u}_s^2 + \bar{v}_s^2)}{2\pi R^2}\right\}$$

The first grouping of terms are the rotor derivatives given in Appendix B. The winglet terms are given in Appendix A, and they are expressed nondimensionally near hover as

$$C_{X_W} = \frac{S_W a_W}{\pi R^2}(\delta_C + \mu)$$

$$C_{Y_W} = \frac{S_W a_W}{\pi R^2}(\delta_S)$$

As a result of symmetry there are a number of equalities among the rotor derivatives as indicated below in the list of derivatives which are found to be present from the results presented in Appendix B.

$$C_{L_{\hat{p}}} = C_{M_{\hat{q}}}$$

$$C_{L_{\bar{v}_s}} = C_{M_{\bar{u}_s}} = - C_{M_\mu}$$

$$C_{L_{\bar{u}_s}} = C_{M_{\bar{v}_s}} = C_{L_\mu}$$

$$C_{Y_{\bar{u}_s}} = - C_{H_{\bar{v}_s}} = C_{Y_\mu}$$

$$C_{Y_{\bar{v}_s}} = C_{H_{\bar{u}_s}} = C_{H_\mu}$$

$$C_{Y_{\hat{q}}} = - C_{H_{\hat{p}}}$$

$$C_{L_{B_{1s}}} = - C_{M_{A_{1s}}}$$

$$C_{Y_{A_{1s}}} = C_{H_{B_{1s}}}$$

The winglet contributions are given above where in hovering it may be noted that

$$C_{X_{W_{\bar{u}_s}}} = C_{X_{W_\mu}}$$

and

$$C_{Y_{W_{\bar{v}_s}}} = C_{X_{W_\mu}}$$

The complete equations of motion for the hovering AEROCRANE may be written in matrix notation as

$$[M]\{q''\} + [C]\{q'\} + K\{q\} = F\{\delta\}$$

where the motion variables are

$$\{q\} = \begin{Bmatrix} \phi \\ \theta \\ \phi_L \\ \theta_L \\ \bar{u}_s \\ \bar{v}_s \end{Bmatrix}$$

and the control terms are

$$\{\delta\} = \begin{Bmatrix} A_{1s} \\ B_{1s} \\ \delta_c \\ \delta_s \end{Bmatrix}$$

The matrix elements for the dimensionless equations are given on the following pages.

$[M] =$

1					$\frac{1}{2}\beta\bar{r}_0\hat{\omega}_R^2 F_R$
	1			$-\frac{1}{2}\beta\bar{r}_0\hat{\omega}_R^2 F_R$	
$\frac{1}{\hat{\omega}_{SL}^2}\left(1+\frac{r_A}{r_L}\right)$		$\frac{1}{\hat{\omega}_{SL}^2}$			$-F_R$
	$\frac{1}{\hat{\omega}_{SL}^2}\left(1+\frac{r_A}{r_L}\right)$		$\frac{1}{\hat{\omega}_{SL}^2}$	F_R	
	$-\frac{\beta_L\bar{r}_0\chi}{1+\beta_L}$			1	
$\frac{\beta_L\bar{r}_0\chi}{1+\beta_L}$					1

MASS MATRIX

$[C] =$

$-AC_{m\hat{q}}$	$\frac{I_z}{I'}$			$-AC_{\ell\mu}$	$AC_{n\mu}$
$-\frac{I_z}{I'}$	$-AC_{m\hat{q}}$			$-AC_{n\mu}$	$-AC_{\ell\mu}$
$BC_{H\hat{p}}$				$BC_{H\mu}$	$-BC_{Y\mu}$
	$-BC_{H\hat{p}}$			$-BC_{Y\mu}$	$-BC_{H\mu}$

DAMPING MATRIX

$[K] =$

$\beta \bar{r}_0 \hat{\omega}_R^2$		$-\mu \bar{\xi}_1 \hat{\omega}_R^2$			
	$\beta \bar{r}_0 \hat{\omega}_R^2$		$-\mu \bar{\xi}_1 \hat{\omega}_R^2$		
1		1			
	1		1		
	$\frac{(1-\beta)}{F_R(1+\frac{\beta}{2})}$		$\frac{-\mu}{F_R(1+\frac{\beta}{2})}$		
$-\frac{(1-\beta)}{F_R(1+\frac{\beta}{2})}$		$\frac{\mu}{F_R(1+\frac{\beta}{2})}$			

SPRING MATRIX

$[F] =$

$AC_{m_{BIS}}$	$-AC_{m_{AIS}}$		$-AC_{m_{SC}}$
$AC_{m_{AIS}}$	$AC_{m_{BIS}}$	$AC_{m_{SC}}$	
	$-BC_{H_{BIS}}$	$BC_{x_{SC}}$	
$BC_{H_{BIS}}$			$BC_{Y_{SC}}$

CONTROL MATRIX

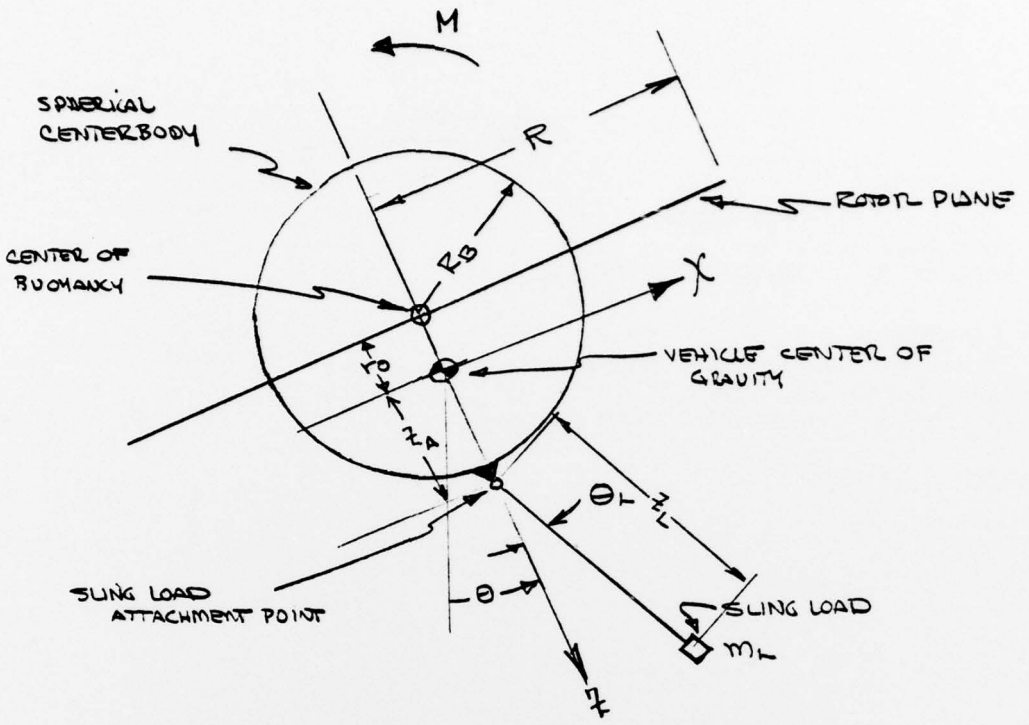

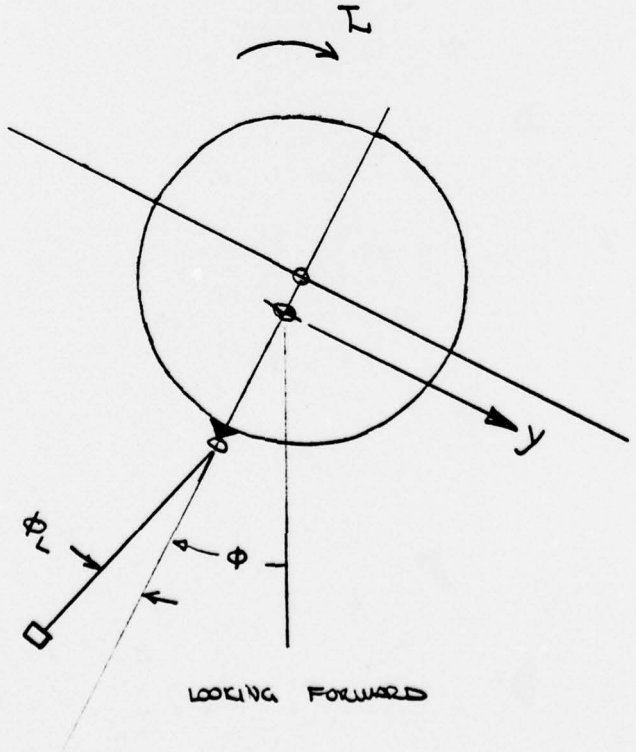

Figure C-1: Axis Systems and Nomenclature.